Implications of D^0-$\bar{D}^0$ mixing for new physics

Eugene Golowich,[1] JoAnne Hewett,[2] Sandip Pakvasa,[3] and Alexey A. Petrov[4]

[1]*Department of Physics, University of Massachusetts, Amherst, Massachusetts 01003, USA*
[2]*Stanford Linear Accelerator Center, Stanford University, Stanford, California 94309, USA*
[3]*Department of Physics and Astronomy, University of Hawaii, Honolulu, Hawaii 96822, USA*
[4]*Department of Physics and Astronomy, Wayne State University, Detroit, Michigan 48201, USA*

(Received 13 September 2007; published 16 November 2007)

We provide a comprehensive, up-to-date analysis of possible new physics contributions to the mass difference ΔM_D in D^0-$\bar{D}^0$ mixing. We consider the most general low-energy effective Hamiltonian and include leading-order QCD running of effective operators. We then explore an extensive list of possible new physics models that can generate these operators, which we organize as including extra fermions, extra gauge bosons, extra scalars, extra space dimensions and extra symmetries. For each model we place restrictions on the allowed parameter space using the recent evidence for observation of D meson mixing. In many scenarios, we find strong constraints that surpass those from other search techniques and provide an important test of flavor-changing neutral currents in the up-quark sector. We also review the recent *BABAR* and Belle findings, and describe the current status of the standard model predictions of D^0-$\bar{D}^0$ mixing.

DOI: 10.1103/PhysRevD.76.095009 PACS numbers: 12.60.−i, 12.15.Ji

I. INTRODUCTION

Meson-antimeson mixing has traditionally been of importance because it is sensitive to heavy degrees of freedom that propagate in the underlying mixing amplitudes. Estimates of the charm-quark and top-quark mass scales were inferred from the observation of mixing in the K^0 and B_d systems, respectively, before these particles were discovered directly.

This success has motivated attempts to indirectly detect new physics (NP) signals by comparing the observed meson mixing with predictions of the standard model (SM). Mixing in the Kaon sector has historically placed stringent constraints on the parameter space of theories beyond the SM and provides an essential hurdle that must be passed in the construction of models with NP. However, anticipated breakthroughs from the B factories and the Tevatron collider have not been borne out—the large mixing signal in the B_d and B_s systems is successfully described in terms of the SM alone (although the parameter spaces of various NP models have become increasingly constrained). Short of awaiting the Large Hadron Collider beauty experiment (LHCb) and the construction of a super-B facility, there is one remaining example for possibly observing indirect signs of NP in meson mixing, the D^0 flavor oscillations. In this case, the SM mixing rate is sufficiently small that the NP component might be able to compete [1]. There has been a flurry of recent experimental activity regarding the detection of D^0-$\bar{D}^0$ mixing [2–5], which marks the first time flavor-changing neutral currents (FCNC) have been observed in the charged $+2/3$ quark sector. With the potential window to discern large NP effects in the charm sector [6,7] and the anticipated improved accuracy for future mixing measurements, the motivation for a comprehensive up-to-date theoretical analysis of new physics contributions to D meson mixing is compelling.

A. Observation of charm mixing

The heightened interest in D^0-$\bar{D}^0$ mixing started with the almost simultaneous observations by the *BABAR* [2] and Belle [3] Collaborations of nonzero mixing signals at about the percent level,[1]

$$y'_{\rm D} = (0.97 \pm 0.44 \pm 0.31) \times 10^{-2} \qquad (BABAR), \quad (1)$$

$$y_{\rm D}^{(CP)} = (1.31 \pm 0.32 \pm 0.25) \times 10^{-2} \qquad (\text{Belle}). \quad (2)$$

This was soon followed by the announcement by the Belle Collaboration of mixing measurements from the Dalitz plot analyses of $D^0 \to K_S \pi^+ \pi^-$ [4],

$$\begin{aligned} x_{\rm D} &= (0.80 \pm 0.29 \pm 0.17) \times 10^{-2}, \\ y_{\rm D} &= (0.33 \pm 0.24 \pm 0.15) \times 10^{-2}. \end{aligned} \quad (3)$$

A preliminary fit to the current database[2] by the Heavy Flavor Averaging Group (HFAG) gives [8]

$$x_{\rm D} = 8.7^{+3.0}_{-3.4} \times 10^{-3}, \qquad y_{\rm D} = (6.6 \pm 2.1) \times 10^{-3}. \quad (4)$$

Since this paper addresses the issue of the mass splitting induced by mixing, our primary concern is with the signal for $x_{\rm D}$, seen here to be a 2.4 sigma effect. This is below the generally accepted threshold for ''evidence'' and is more in the nature of a ''hint.'' However, we note that a 2.4 sigma effect will automatically have a nonzero lower bound at 95% confidence level. For the sake of reference, we cite the one-sigma window for the HFAG value of $x_{\rm D}$,

[1]Our definitions of the mixing parameters $x_{\rm D}$, $y_{\rm D}$, $y'_{\rm D}$, and $y_{\rm D}^{(CP)}$ are standard and are given in Eqs. (11) and (12).

[2]An updated fit [8] gives the values $x_{\rm D} = 8.4^{+3.2}_{-3.4} \times 10^{-3}$, $y_{\rm D} = (6.9 \pm 2.1) \times 10^{-3}$. These are essentially unchanged from the HFAG preliminary results given above and used in our analysis; the difference will not affect our numerical results.

$$5.4 \times 10^{-3} < x_{\rm D} < 11.7 \times 10^{-3} \qquad \text{(one-sigma window)}, \tag{5}$$

or equivalently for $\Delta M_{\rm D}$ itself,

$$8.7 \times 10^{-15}\ \text{GeV} < \Delta M_{\rm D} < 1.9 \times 10^{-14}\ \text{GeV} \quad \text{(one-sigma window)}. \tag{6}$$

Let us briefly describe our strategy for dealing with the above HFAG values in light of both SM and NP contributions. We shall argue in Sec. III that the SM predictions, although indeed compatible with the observed range of values for the D mixing parameters, contain significant hadronic uncertainties. Moreover, we do not know the relative *phase* between the SM contribution and that from any NP model, so that $x_{\rm D}$ will lie between the extreme limiting cases of constructive and destructive interference. In addition, since the observation of D mixing is new, the measurements will fluctuate with future refinements in the analyses and as more data is collected. To best deal with these realities, we will present our results by displaying a given NP prediction as a pure NP signal (i.e. as if there were no SM component) and for comparison, display curves of constant $x_{\rm D}$ for the five values

$$x_{\rm D} = 15.0 \times 10^{-3},\ 11.7 \times 10^{-3},\ 8.0 \times 10^{-3},\ 5.0 \times 10^{-3},\ 3.0 \times 10^{-3}. \tag{7}$$

This (approximately HFAG 2σ) range reveals the sensitivity of $x_{\rm D}$ to variations in the underlying NP parameter space. We will then show the present constraints placed on the NP model parameter space, by assuming that the NP contribution cannot exceed the 1σ upper bound on x_D. This procedure mirrors that which is traditionally employed in obtaining bounds on NP from $K^0 - \bar{K}^0$ mixing.

B. New physics possibilities

D^0-$\bar{D}^0$ mixing at the observed level is much larger than the quark-level (''short-distance'') SM prediction [9] but is in qualitative accord with hadron-level (''long-distance'') SM expectations. However, because the latter are beset with hadronic uncertainties, it cannot be rigorously concluded that only SM physics is being detected. In this paper, we will consider a broad menu of NP possibilities. As the operation of the LHC looms near, the number of potentially viable NP models has never been greater. Our organizational approach to analyzing these is to address NP models with:

(1) Extra fermions (Sec. IV).
  (A) Fourth generation.
  (B) Heavy vectorlike quarks.
    (1) $Q = -1/3$ singlet quarks.
    (2) $Q = +2/3$ singlet quarks.
  (C) Little Higgs models.
(2) Extra gauge bosons (Sec. V).
  (A) Generic Z' models.
  (B) Family symmetries.
  (C) Left-right symmetric model.
  (D) Alternate left-right models from E_6 theories.
  (E) Vector leptoquark bosons.
(3) Extra scalars (Sec. VI).
  (A) Flavor-conserving two-Higgs-doublet models.
  (B) Flavor-changing neutral Higgs models.
  (C) Scalar leptoquark bosons.
  (D) Higgsless models.
(4) Extra space dimensions (Sec. VII).
  (A) Universal extra dimensions.
  (B) Split fermion models.
  (C) Warped geometries.
(5) Extra symmetries (Sec. VIII).
  (A) Minimal supersymmetric standard model.
  (B) Quark-squark alignment models.
  (C) Supersymmetry with R-parity violation.
  (D) Split supersymmetry.

In the above, we have chosen to consider only supersymmetry in Sec. VIII due to its extensive literature and to cover other extended symmetries elsewhere in the paper.

Any NP degree of freedom will generally be associated with a generic heavy mass scale M, at which the NP interaction will be most naturally described. At the scale m_c of the charm mass, this description will have been modified by the effects of QCD. These should not be neglected, so we perform our NP analyses at one-loop level for the strong interactions. The theoretical background for this is presented in Sec. II.

Finally, in order to place the NP discussion within its proper context, it makes sense to first review SM charm mixing. This is done in Sec. III. The remainder of the paper then amounts to considering charm mixing with lots of ''extras.'' The paper concludes in Sec. IX with a summary of our findings.

C. Basic formalism

Let us first review some formal aspects of charm mixing. The mixing arises from $|\Delta C| = 2$ interactions that generate off-diagonal terms in the mass matrix for D^0 and $\bar{D}^0$ mesons. The expansion of the off-diagonal terms in the neutral D mass matrix to second order in the weak interaction is

$$\left(M - \frac{i}{2}\Gamma\right)_{21} = \frac{1}{2M_D}\langle \bar{D}^0 | H_w^{|\Delta C|=2} | D^0 \rangle + \frac{1}{2M_D}\sum_n \frac{\langle \bar{D}^0 | H_w^{|\Delta C|=1} | n \rangle \langle n | H_w^{|\Delta C|=1} | D^0 \rangle}{M_D - E_n + i\epsilon}, \tag{8}$$

where $H_w^{|\Delta C|=2}$ and $H_w^{|\Delta C|=1}$ are the effective $|\Delta C| = 2$ and $|\Delta C| = 1$ Hamiltonians.

The off-diagonal mass-matrix terms induce mass eigenstates D_1 and D_2 that are superpositions of the flavor eigenstates D^0 and $\bar{D}^0$,

$$D_{1,2} = pD^0 \pm q\bar{D}^0, \tag{9}$$

where $|p|^2 + |q|^2 = 1$. The key quantities in D^0 mixing are the mass and width differences,

$$\Delta M_D \equiv M_1 - M_2 \quad \text{and} \quad \Delta\Gamma_D \equiv \Gamma_1 - \Gamma_2, \tag{10}$$

or equivalently their dimensionless equivalents,

$$x_D \equiv \frac{\Delta M_D}{\Gamma_D}, \quad \text{and} \quad y_D \equiv \frac{\Delta\Gamma_D}{2\Gamma_D}, \tag{11}$$

where Γ_D is the average width of the two neutral D meson mass eigenstates. Two quantities, $y_D^{(CP)}$ and y'_D, which are actually measured in most experimental determinations of $\Delta\Gamma_D$, are defined as

$$\begin{aligned} y_D^{(CP)} &\equiv (\Gamma_+ - \Gamma_-)/(\Gamma_+ + \Gamma_-) \\ &= y_D \cos\phi - x_D \sin\phi\left(\frac{A_m}{2} - A_{\text{prod}}\right), \\ y'_D &\equiv y_D \cos\delta_{K\pi} - x_D \sin\delta_{K\pi}, \end{aligned} \tag{12}$$

where the transition rates $\Gamma_\pm$ pertain to decay into final states of definite CP, $A_{\text{prod}} = (N_{D^0} - N_{\bar{D}^0})/(N_{D^0} + N_{\bar{D}^0})$ is the so-called production asymmetry of D^0 and $\bar{D}^0$ (giving the relative weight of D^0 and $\bar{D}^0$ in the sample) and $\delta_{K\pi}$ is the strong phase difference between the Cabibbo favored and double Cabibbo suppressed amplitudes [10]. The quantities A_m and ϕ account for the presence of CP violation in D^0-$\bar{D}^0$ mixing, with A_m being related to the q, p parameters of Eq. (9) as $A_m \equiv |q/p|^2 - 1$ and ϕ a CP-violating phase of M_{21} (if one neglects direct CP violation) [11]. In practice, y_{CP} is measured by comparing decays of D^0 into a state of definite CP, such as K^+K^-, to decays of D^0 into a final state which is not a CP eigenstate (such as $K\pi$) whereas y' is extracted from a time-dependent analysis of the $D \to K\pi$ transition [11].

The states $D_{1,2}$ allow for effects of CP violation. However, CP violation in D^0 mixing is negligible in the standard model and there is no evidence for it experimentally [2,12,13]. Many new physics scenarios contain new phases which can induce sizable CP violation in the D meson sector. Nonetheless, a thorough investigation of such effects is beyond the scope of the present paper. Therefore, we shall work in the limit of CP invariance (so that $p = q$) for the remainder of this paper. Throughout, our phase convention will be

$$\mathcal{C}\mathcal{P}D^0 = +\bar{D}^0. \tag{13}$$

Then $D_{1,2}$ become the CP eigenstates $D_\pm$ with $\mathcal{C}\mathcal{P}D_\pm = \pm D_\pm$.

Keeping in mind the neglect of CP violation and also the phase convention of Eq. (13), we relate the mixing quantities x_D and y_D to the mixing matrix as

$$\begin{aligned} x_D &= \frac{1}{2M_D\Gamma_D}\,\text{Re}\Big[2\langle\bar{D}^0|H^{|\Delta C|=2}|D^0\rangle \\ &\quad + \langle\bar{D}^0|i\int d^4x T\{\mathcal{H}_w^{|\Delta C|=1}(x)\mathcal{H}_w^{|\Delta C|=1}(0)\}|D^0\rangle\Big], \\ y_D &= \frac{1}{2M_D\Gamma_D}\,\text{Im}\langle\bar{D}^0|i\int d^4x T\{\mathcal{H}_w^{|\Delta C|=1}(x) \\ &\quad \times \mathcal{H}_w^{|\Delta C|=1}(0)\}|D^0\rangle, \end{aligned} \tag{14}$$

where $\mathcal{H}_w^{|\Delta C|=1}(x)$ is the weak Hamiltonian density for $|\Delta C| = 1$ transitions and T denotes the time-ordered product. There is no contribution to y_D from the local $|\Delta C| = 2$ term, as it has no absorptive part. New physics contributions to y_D have already been addressed in Ref. [14], so the primary thrust of this paper will be to focus on x_D.

The next step, in Sec. II, is to expand the time-ordered product of Eq. (14) in local operators of increasing dimension (higher dimension operators being suppressed by powers of Λ_{QCD}/m_c).

II. GENERIC OPERATOR ANALYSIS OF D^0-$\bar{D}^0$ MIXING

Though the particles present in models with new physics may not be produced in charm-quark decays, their effects can nonetheless be seen in the form of effective operators generated by the exchanges of these new particles. Even without specifying the form of these new interactions, we know that their effect is to introduce several $|\Delta C| = 2$ effective operators built out of the SM degrees of freedom.

A. Operator product expansion and renormalization group

By integrating out new degrees of freedom associated with new interactions at a scale M, we are left with an effective Hamiltonian written in the form of a series of operators of increasing dimension. Operator power counting then tells us the most important contributions are given by the operators of the lowest possible dimension, $d = 6$ in this case. This means that they must contain only quark degrees of freedom. Realizing this, we can write the complete basis of these effective operators, which can be done most conveniently in terms of chiral quark fields,

$$\langle f|\mathcal{H}_{\text{NP}}|i\rangle = G\sum_{i=1} C_i(\mu)\langle f|Q_i|i\rangle(\mu), \tag{15}$$

where the prefactor G has the dimension of inverse-squared mass, the C_i are dimensionless Wilson coefficients,[3] and the Q_i are the effective operators:

[3]Throughout this paper, we shall denote Wilson coefficients for $|\Delta C| = 1$ operators as $\{c_i\}$ and those for $|\Delta C| = 2$ operators as $\{C_i\}$.

$$
\begin{aligned}
&Q_1 = (\bar{u}_L\gamma_\mu c_L)(\bar{u}_L\gamma^\mu c_L), \qquad Q_2 = (\bar{u}_L\gamma_\mu c_L)(\bar{u}_R\gamma^\mu c_R),\\
&Q_3 = (\bar{u}_L c_R)(\bar{u}_R c_L), \qquad Q_4 = (\bar{u}_R c_L)(\bar{u}_R c_L),\\
&Q_5 = (\bar{u}_R\sigma_{\mu\nu} c_L)(\bar{u}_R\sigma^{\mu\nu} c_L),\\
&Q_6 = (\bar{u}_R\gamma_\mu c_R)(\bar{u}_R\gamma^\mu c_R), \qquad Q_7 = (\bar{u}_L c_R)(\bar{u}_L c_R),\\
&Q_8 = (\bar{u}_L\sigma_{\mu\nu} c_R)(\bar{u}_L\sigma^{\mu\nu} c_R).
\end{aligned} \tag{16}
$$

In total, there are eight possible operator structures that exhaust the list of possible independent contributions to $|\Delta C| = 2$ transitions. Since these operators are generated at the scale M where the new physics is integrated out, a nontrivial operator mixing can occur when we take into account renormalization group running of these operators between the scales M and μ, with μ being the scale where the hadronic matrix elements are computed. We shall work at the renormalization scale $\mu = m_c \simeq 1.3$ GeV. This evolution is determined by solving the renormalization group (RG) equations obeyed by the Wilson coefficients,

$$
\frac{d}{d\log\mu}\vec{C}(\mu) = \hat{\gamma}^T\vec{C}(\mu), \tag{17}
$$

where $\hat{\gamma}$ represents the matrix of anomalous dimensions of the operators in Eq. (16) (note the transposition). Equation (17) can be solved by transforming to the basis where the transpose of the anomalous dimension matrix is diagonal, integrating, and then transferring back to the original basis $\vec{C}_i$. At leading order, we have

$$
\vec{C}(\mu) = \hat{U}(\mu, M)\vec{C}(M), \tag{18}
$$

where $U(\mu, M)$ is the evolution matrix, obtained from Eq. (17) by

$$
\hat{U}(\mu_1, \mu_2) = \hat{V}[r(\mu_1, \mu_2)^{\vec{\gamma}^{(0)}/2\beta_0}]_D\hat{V}^{-1}. \tag{19}
$$

In the above, $\vec{\gamma}^{(0)}$ is the vector containing the diagonal elements of the diagonalized transposed matrix of the anomalous dimensions $\hat{\gamma}^T$, $\hat{V}$ is the matrix that diagonalizes $\hat{\gamma}^T$, and

$$
r(\mu_1, \mu_2) \equiv \frac{\alpha_s(\mu_1)}{\alpha_s(\mu_2)}. \tag{20}
$$

For completeness, we display the matrix of anomalous dimensions at leading order (LO) in QCD [15],

$$
\hat{\gamma} = \begin{pmatrix}
6 - \frac{6}{N_c} & 0 & 0 & 0 & 0 & 0 & 0 & 0\\
0 & \frac{6}{N_c} & 12 & 0 & 0 & 0 & 0 & 0\\
0 & 0 & -6N_c + \frac{6}{N_c} & 0 & 0 & 0 & 0 & 0\\
0 & 0 & 0 & 6 - 6N_c + \frac{6}{N_c} & \frac{1}{2} - \frac{1}{N_c} & 0 & 0 & 0\\
0 & 0 & 0 & -24 - \frac{48}{N_c} & 6 + 2N_c - \frac{2}{N_c} & 0 & 0 & 0\\
0 & 0 & 0 & 0 & 0 & 6 - \frac{6}{N_c} & 0 & 0\\
0 & 0 & 0 & 0 & 0 & 0 & 6 - 6N_c + \frac{6}{N_c} & \frac{1}{2} - \frac{1}{N_c}\\
0 & 0 & 0 & 0 & 0 & 0 & -24 - \frac{48}{N_c} & 6 + 2N_c - \frac{2}{N_c}
\end{pmatrix}
$$

We note that Ref. [15] also includes the next-to-leading-order (NLO) expressions for the elements in the anomalous dimensions matrix. However, we perform our calculations at LO here since the NLO corrections to the matching conditions in the various models of new physics have generally not been computed.

Because of the relatively simple structure of $\hat{\gamma}$, one can easily write the evolution of each Wilson coefficient in Eq. (15) from the new physics scale M down to the hadronic scale μ, taking into account quark thresholds. Corresponding to each of the eight operators $\{Q_i\}$ ($i = 1, \ldots, 8$) is an RG factor $r_i(\mu, M)$. The first of these, $r_1(\mu, M)$, is given explicitly by

$$
r_1(\mu, M) = \left(\frac{\alpha_s(M)}{\alpha_s(m_t)}\right)^{2/7}\left(\frac{\alpha_s(m_t)}{\alpha_s(m_b)}\right)^{6/23}\left(\frac{\alpha_s(m_b)}{\alpha_s(\mu)}\right)^{6/25}, \tag{21}
$$

and the rest can be expressed in terms of $r_1(\mu, M)$ as

$$
\begin{aligned}
r_2(\mu, M) &= [r_1(\mu, M)]^{1/2},\\
r_3(\mu, M) &= [r_1(\mu, M)]^{-4},\\
r_4(\mu, M) &= [r_1(\mu, M)]^{(1+\sqrt{241})/6},\\
r_5(\mu, M) &= [r_1(\mu, M)]^{(1-\sqrt{241})/6},\\
r_6(\mu, M) &= r_1(\mu, M),\\
r_7(\mu, M) &= r_4(\mu, M),\\
r_8(\mu, M) &= r_5(\mu, M).
\end{aligned} \tag{22}
$$

The RG factors are generally only weakly dependent on the NP scale M since it is taken to be larger than the top quark mass, m_t, and the evolution of α_s is slow at these high mass scales. In Table I, we display numerical values for the $r_i(\mu, M)$ with $M = 1$, 2 TeV, and $\mu = m_c \simeq 1.3$ GeV. Here, we compute α_s using the one-loop evolution and matching expressions for perturbative consistency with the RG evolution of the effective Hamiltonian.

TABLE I. Dependence of the RG factors on the heavy mass scale M.

M (TeV)	$r_1(m_c, M)$	$r_2(m_c, M)$	$r_3(m_c, M)$	$r_4(m_c, M)$	$r_5(m_c, M)$
1	0.72	0.85	3.7	0.41	2.2
2	0.71	0.84	4.0	0.39	2.3

B. Operator matrix elements

We will need to evaluate the D^0-to-$\bar{D}^0$ matrix elements of the eight dimension-six basis operators. In general, this implies eight nonperturbative parameters that would have to be evaluated by means of QCD sum rules or on the lattice. We choose those parameters (denoted by $\{B_i\}$) as follows,

$$\begin{aligned}
\langle Q_1\rangle &= \frac{2}{3} f_{\rm D}^2 M_{\rm D}^2 B_1, \qquad \langle Q_2\rangle = -\frac{5}{6} f_{\rm D}^2 M_{\rm D}^2 B_2, \\
\langle Q_3\rangle &= \frac{7}{12} f_{\rm D}^2 M_{\rm D}^2 B_3, \qquad \langle Q_4\rangle = -\frac{5}{12} f_{\rm D}^2 M_{\rm D}^2 B_4, \\
\langle Q_5\rangle &= f_{\rm D}^2 M_{\rm D}^2 B_5, \qquad \langle Q_6\rangle = \frac{2}{3} f_{\rm D}^2 M_{\rm D}^2 B_6, \\
\langle Q_7\rangle &= -\frac{5}{12} f_{\rm D}^2 M_{\rm D}^2 B_7, \qquad \langle Q_8\rangle = f_{\rm D}^2 M_{\rm D}^2 B_8,
\end{aligned} \tag{23}$$

where $\langle Q_i\rangle \equiv \langle \bar{D}^0|Q_i|D^0\rangle$, and f_D represents the D meson decay constant. By and large, the compensatory B factors $\{B_i\}$ are unknown, except in vacuum saturation and in the heavy quark limit; there, one has $B_i \to 1$.

Since most of the matrix elements in Eq. (23) are not known, we will need something more manageable in order to obtain numerical results. The usual approach to computing matrix elements is to employ the vacuum saturation approximation. However, because some of the B parameters are known, we would like to introduce a "modified vacuum saturation" (MVS), where all matrix elements in Eq. (23) are written in terms of (known) matrix elements of $(V-A)\times(V-A)$ and $(S-P)\times(S+P)$ matrix elements $B_{\rm D}$ and $B_{\rm D}^{(\rm S)}$,

$$\begin{aligned}
\langle Q_1\rangle &= \frac{2}{3} f_{\rm D}^2 M_{\rm D}^2 B_D, \\
\langle Q_2\rangle &= -\frac{1}{2} f_{\rm D}^2 M_{\rm D}^2 B_D - \frac{1}{N_c} f_{\rm D}^2 M_{\rm D}^2 \bar{B}_{\rm D}^{(\rm S)}, \\
\langle Q_3\rangle &= \frac{1}{4N_c} f_{\rm D}^2 M_{\rm D}^2 B_D + \frac{1}{2} f_{\rm D}^2 M_{\rm D}^2 \bar{B}_{\rm D}^{(\rm S)}, \\
\langle Q_4\rangle &= -\frac{2N_c - 1}{4N_c} f_{\rm D}^2 M_{\rm D}^2 \bar{B}_{\rm D}^{(\rm S)}, \qquad \langle Q_5\rangle = \frac{3}{N_c} f_{\rm D}^2 M_{\rm D}^2 \bar{B}_{\rm D}^{(\rm S)}, \\
\langle Q_6\rangle &= \langle Q_1\rangle, \qquad \langle Q_7\rangle = \langle Q_4\rangle, \qquad \langle Q_8\rangle = \langle Q_5\rangle,
\end{aligned} \tag{24}$$

where we denote $N_c = 3$ as the number of colors and, as in Ref. [9], define

$$\bar{B}_{\rm D}^{(S)} \equiv B_{\rm D}^{(\rm S)} \cdot \frac{M_{\rm D}^2}{(m_c + m_u)^2} \tag{25}$$

as well as

$$\eta \equiv \frac{\bar{B}_{\rm D}^{(S)}}{B_{\rm D}}. \tag{26}$$

In our numerical work, we take $B_{\rm D}^{(\rm S)} = B_{\rm D} = 0.82$, which is the most recent result from the quenched lattice calculation [16], and use the CLEO-c determination $f_D = 222.6 \pm 16.7^{+2.3}_{-2.4}$ MeV [17]. We urge the lattice community to perform an evaluation of the $\{B_i\}$ parameters defined in Eq. (23) for the full operator set relevant to D meson mixing.

III. STANDARD MODEL ANALYSIS

Theoretical predictions of $x_{\rm D}$ and $y_{\rm D}$ within the standard model span several orders of magnitude. Roughly, there are two approaches, neither of which give very reliable results because m_c is in some sense intermediate between the heavy-quark and light-quark limits. Consider, for example, $\Delta\Gamma_{\rm D}$ as given in Eq. (14)

$$\Delta\Gamma_{\rm D} = \frac{1}{M_{\rm D}} {\rm Im}\langle \bar{D}^0|i\int {\rm d}^4x T\{\mathcal{H}_w^{|\Delta C|=1}(x)\mathcal{H}_w^{|\Delta C|=1}(0)\}|D^0\rangle.$$

To utilize this relation, one inserts intermediate states between the $|\Delta C| = 1$ weak Hamiltonian densities $\mathcal{H}_w^{|\Delta C|=1}$. This can be done using either quark or hadron degrees of freedom. Let us consider each of these possibilities in turn.

A. Quark-level analysis

The "inclusive" (or quark-level) approach is based on the operator product expansion (OPE). In the $m_c \gg \Lambda$ limit, where Λ is a scale characteristic of the strong interactions, ΔM and $\Delta\Gamma$ can be expanded in terms of matrix elements of local operators [1,18] of increasing dimensions suppressed by powers of inverse charm-quark mass. An instructive example concerns a recent analysis of the leading dimension $D = 6$ case [9] in which the width difference $y_{\rm D}$ is calculated in terms of quarks (cf. Fig. 1) and the mass difference $x_{\rm D}$ is then found from dispersion relations. The calculation is carried out as an expansion in QCD, including leading-order $\mathcal{O}(\alpha_s^0)$ and next-to-leading-order $\mathcal{O}(\alpha_s^1)$ contributions with

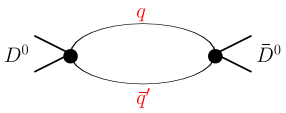

FIG. 1 (color online). Loop diagram for $D^0 \to \bar{D}^0$.

TABLE II. Flavor cancellations in $\Delta\Gamma_D$.

Int. State	$\mathcal{O}(z^0)$	$\mathcal{O}(z^1)$	$\mathcal{O}(z^2)$
$s\bar{s}$	$1/2$	$-3z$	$3z^2$
$d\bar{d}$	$1/2$	0	0
$s\bar{d} + d\bar{s}$	-1	$3z$	$-3z^2$
Total	0	0	0

$$x_D = x_D^{(LO)} + x_D^{(NLO)} \quad \text{and} \quad y_D = y_D^{(LO)} + y_D^{(NLO)}. \quad (27)$$

Here, LO and NLO denote only the corrections at that order and not the full quantity computed to that order. Because $m_b > M_D$, $\Delta\Gamma_D$ experiences no b-quark contribution.[4] This leaves only $s\bar{s}$, $d\bar{d}$, and $s\bar{d} + d\bar{s}$ intermediate states contributing to the mixing diagram of Fig. 1. Taking $m_d = 0$, the mixing loop functions will depend on $z \equiv m_s^2/m_c^2 \simeq 0.006$. Table II examines in detail the loop functions for $\Delta\Gamma_D$ and shows the results of carrying out an expansion in powers of z. We see that the contributions of the individual intermediate states in the mixing diagram are *not* intrinsically small—in fact, they begin to contribute at $\mathcal{O}(z^0)$. However, flavor cancellations remove all contributions through $\mathcal{O}(z^2)$ for $\Delta\Gamma_D$, so the net result is $\mathcal{O}(z^3)$. Charm mixing clearly experiences a remarkable Glashow-Iliopoulos-Maiani (GIM) suppression. The corresponding result for ΔM_D turns out to be $\mathcal{O}(z^2)$. Summarizing, the leading dependences in z for the dimension-six contributions are

$$\begin{aligned} y_D^{(LO)} &\sim z^3 \qquad x_D^{(LO)} \sim z^2 \\ y_D^{(NLO)} &\sim z^2 \qquad x_D^{(NLO)} \sim z^2. \end{aligned} \quad (28)$$

The source of this z dependence is understood as follows. The mixing amplitude is known to vanish in the $m_d = m_s = 0$ limit, so the breaking of chiral symmetry and of $SU(3)$ flavor symmetry play crucial roles. Thus, a factor of m_s^2 comes from an $SU(3)$ violating mass insertion on each internal quark line and another from an additional mass insertion on each line to compensate the chirality flip from the first insertion. This mechanism of chiral suppression accounts for the z^2 dependence of $x_D^{(LO)}$, $y_D^{(NLO)}$, and $x_D^{(NLO)}$. The case of $y_D^{(LO)}$ requires yet another factor of m_s^2 to lift the helicity suppression for the decay of a pseudoscalar meson into a massless fermion pair.

Let us next display the LO expressions for y_D and x_D (to leading order also in z) [9],

[4]We ignore here the b-quark contribution to ΔM_D; its numerical contribution is subleading ($|V_{ud}V_{cd}| \simeq |V_{us}V_{cs}| \simeq 0.22$ whereas $|V_{ub}V_{cb}| \simeq 1.8 \times 10^{-4}$).

TABLE III. Results at dimension six in the OPE.

	LO	NLO	LO + NLO (central values)
y_D	$-(5.7 \to 9.5) \times 10^{-8}$	$(3.9 \to 9.1) \times 10^{-7}$	$\simeq 6 \times 10^{-7}$
x_D	$-(1.4 \to 2.4) \times 10^{-6}$	$(1.7 \to 3.0) \times 10^{-6}$	$\simeq 6 \times 10^{-7}$

$$\begin{aligned} y_D^{(LO)[z^3]} &= \frac{G_F^2 m_c^2 f_D^2 M_D}{3\pi\Gamma_D} \xi_s^2 z^3 (c_2^2 - 2c_1c_2 - 3c_1^2) \\ &\quad \times \left[B_D - \frac{5}{2}\bar{B}_D^{(S)} \right], \\ x_D^{(LO)[z^2]} &= \frac{G_F^2 m_c^2 f_D^2 M_D}{3\pi^2\Gamma_D} \xi_s^2 z^2 \left[c_2^2 B_D - \frac{5}{4}(c_2^2 - 2c_1c_2 \right. \\ &\quad \left. - 3c_1^2)\bar{B}_D^{(S)} \right], \end{aligned} \quad (29)$$

where $\xi_s \equiv V_{us}V_{cs}^*$, and $c_{1,2}$ are the relevant Wilson coefficients. For our numerical computations, we adopt the values used in Ref. [9],

$$\begin{aligned} m_c &= 1.3 \text{ GeV}, \qquad c_1 = -0.411, \\ c_2 &= 1.208, \qquad \alpha_s = 0.406. \end{aligned} \quad (30)$$

Numerical results for the LO and NLO contributions, where a discussion of the NLO effects can be found in Ref. [9], (cf. Table III) reveal that y_D is given by y_{NLO} to a reasonable approximation (due to the z dependence discussed above) whereas x_D is greatly affected by destructive interference between x_{LO} and x_{NLO}. The net effect is to render y_D and x_D of similar small magnitudes, at least through this order of analysis.

The quark-level prediction of x_D and y_D just described is a result of expanding in terms of *three* "small" quantities, z, Λ/m_c, and α_s. As a consequence, the use of an OPE to describe charm mixing is not entirely straightforward because terms suppressed by higher powers of m_c could nevertheless be important if they contained relatively fewer powers of m_s. However, at the next orders in the OPE one encounters $\mathcal{O}(z^{3/2})$ corrections multiplied by about a dozen matrix elements of dimension-nine operators and $\mathcal{O}(z)$ corrections with more than 20 matrix elements of dimension-twelve operators. This introduces a multitude of unknown parameters for matrix elements that cannot be computed at this time. Simple dimensional analysis [19] suggests the magnitudes $x_D \sim y_D \sim 10^{-3}$, although order-of-magnitude cancellations or enhancements are possible.[5]

[5]Any effect of higher orders in $1/m_c$ or $\alpha_s(m_c)$ which could produce a z^n contribution in the lowest possible power $n = 1$ could yield a dominant contribution to the prediction of x_D and y_D [20,21]. Although the *BABAR* and Belle observations of $y \sim 10^{-2}$ could be ascribed to a breakdown of the OPE or of duality, it is clear that such a large value of y_D is by no means a generic prediction of OPE analyses.

B. Hadron-level analysis

The D meson mass is not very large, so one might question whether the OPE approach discussed in the previous subsection can successfully describe D^0-$\bar{D}^0$ mixing. This is especially so since the leading contribution in the $SU(3)$-breaking parameter m_s enters only as a Λ^4/m_c^4 suppressed contribution in the $1/m_c$ expansion, which implies that one has to deal with a large number of unknown operator matrix elements.

As an alternative, one might consider saturating the correlation functions of Eq. (14) with exclusive hadronic states, switching to a purely hadronic description. This approach should be valid as the mass of the D meson lies in the middle of a region populated by excited light-quark states. In principle, this "exclusive" (or hadronic) approach should sum over all possible intermediate hadronic multiplets. Since one has to deal with off-shell hadronic states in the calculation of $x_{\rm D}$, some modeling is necessarily involved. By contrast, a calculation of $y_{\rm D}$ in this approach is less model dependent. The usual approach to computing $x_{\rm D}$ is to first calculate $y_{\rm D}$ and then use a dispersion relation to obtain $x_{\rm D}$. This is appropriate, as the contribution due to b-flavored intermediate states (which appears in $x_{\rm D}$ but not $y_{\rm D}$) is negligibly small.

One possible approach would be to select a set of, say, two-body intermediate states,[6] and write their contribution to mixing in terms of charged pseudoscalar (P^+P^-) branching fractions [23,24],

$$y_{\rm D}^{(P^+P^-)} = \mathcal{B}_{[D^0\to K^+K^-]} + \mathcal{B}_{[D^0\to\pi^+\pi^-]} - 2\cos\delta_{K\pi}[\mathcal{B}_{[D^0\to K^-\pi^+]}\mathcal{B}_{[D^0\to K^+\pi^-]}]^{1/2}, \quad (31)$$

where $\delta_{K\pi}$ is as in Eq. (12). One can use available experimental data on two-body branching ratios to estimate their contribution to $y_{\rm D}$. A dispersion relation then relates $y_{\rm D}$ to $x_{\rm D}$. However, the example above explicitly shows the cancellations between states that are present within a given $SU(3)$ multiplet. Such cancellations make this procedure very sensitive to experimental uncertainties. One would need to know the contribution of each decay mode with extremely high precision, and that is simply not feasible at this time. Another possibility is to model $|\Delta C| = 1$ decays theoretically [25]. In this reference, $\Delta\Gamma_{\rm D}$ was determined in this manner and the result $y_{\rm D} \simeq 10^{-3}$ was found. This result is, however, smaller than the recent *BABAR* and Belle observations.

Clearly, D^0 is not sufficiently light for its decays to be dominated by just two-body final states. Multiparticle intermediate states must also be taken into account in D^0-$\bar{D}^0$ mixing calculations. In doing so, it is convenient to calculate the contribution of each $SU(3)$ multiplet separately, as $SU(3)$ symmetry produces substantial cancellations among members of the same multiplet as we saw above. This can be thought of as a long-distance version of the GIM mechanism. The surviving contribution is expected to be of second order in the $SU(3)$-breaking parameter m_s [20]. Denoting by y_{F_R} a value that y would take if elements of the final state F belonging to $SU(3)$ representation R, or F_R, were the only channels open for D decay, one can write $y_{\rm D}$ as a sum over all possible F_R's weighted by the D-decay rate to each representation,

$$y_D = \frac{1}{\Gamma_D}\sum_{F_R} y_{F_R}\Big[\sum_{n\in F_R}\Gamma(D\to n)\Big]. \quad (32)$$

It is possible to show that y_{F_R} can be computed as [20]

$$y_{F_R} = \frac{\sum_{n\in F_R}\langle\bar{D}^0|\mathcal{H}_w|n\rangle\langle n|\mathcal{H}_w|D^0\rangle}{\sum_{n\in F_R}\langle D^0|\mathcal{H}_w|n\rangle\langle n|\mathcal{H}_w|D^0\rangle}. \quad (33)$$

It should be noted that in the limit of CP conservation and retaining phase space differences as the only source of $SU(3)$ breaking [i.e. neglecting $SU(3)$ breaking in the matrix elements], y_{F_R} can be computed without any hadronic parameters. This is an appropriate approximation, as the main contribution comes from the multiparticle (four-particle) intermediate state multiplets. For those states, there are multikaon modes which are kinematically forbidden. In such cases, phase space effects alone can provide enough $SU(3)$ violation to induce $y_D \sim 10^{-2}$ [20]. In other words, such large effects in $y_{\rm D}$ appear for decays near the D threshold, where an analytic expansion in $SU(3)$ violation is no longer possible. It is interesting that such effects from multiparticle states are not reproduced in the OPE calculation, as the resulting contribution does not come from short distances.

The use of a dispersion relation for $x_{\rm D}$ then suggests it would receive contributions of a similar order of magnitude as those for $y_{\rm D}$ [26]. An important difference between the resulting values of $x_{\rm D}$ and $y_{\rm D}$ is that even retaining phase space differences as the sole contributor to $SU(3)$ breaking does not insure cancellation of the hadronic matrix elements. However, with some reasonable model-dependent assumptions, one arrives at the conclusion that $x_{\rm D} \sim y_{\rm D} \sim 1\%$ [26]. It is thus reasonable to believe that the observed D^0-$\bar{D}^0$ mixing is reflecting standard model contributions.

C. Comments

The above discussions show that, contrary to the B system, standard model estimates of $x_{\rm D}$ and $y_{\rm D}$ for the charm system contain significant intrinsic uncertainties. On the other hand, SM values near those found by *BABAR* and Belle cannot be ruled out. Therefore, it will be difficult to attribute a clear indication of new physics to

[6] The simplest intermediate state is a single-particle resonance contribution. Preliminary estimates of resonance contributions to D^0-$\bar{D}^0$ mixing appear to be small [22], although much remains to be learned about the resonance spectrum in the vicinity of the D^0 mass.

D^0-$\bar{D}^0$ mixing measurements alone. This means that the only robust signal of new physics in the charm system would be the observation of large CP violation, which we will not consider here. Nonetheless, a thorough analysis of indirect new physics contributions is of value, and we find that large regions of parameter space can be excluded in many models, placing additional restrictions on model building. This will be useful in conjunction with corresponding direct searches for new physics at the LHC.

In what follows, we will take the approach that the new physics contributions cannot exceed the 1σ experimental upper bound for $x_{\rm D}$. Keeping in mind that this upper limit is likely to change as data samples increase and analyses mature, we also display the effects of $x_{\rm D} < (15.0, 8.0, 5.0, 3.0) \times 10^{-3}$ on the parameter space of new physics scenarios. These values are to be used as a guide for how our resulting constraints may change in the future. In addition, we will neglect the errors on the determinations of the D meson decay constant and B factors; this will have a small effect on our results given the present large uncertainty in the experimental determination of D^0-$\bar{D}^0$ mixing. In all cases, we will neglect the possibility of interference between the SM and new physics contributions. We now turn to the examination of various scenarios for physics beyond the SM.

IV. EXTRA FERMIONS

The quark sector of the standard model can be modified in several ways, and new fermions are predicted to exist in many extensions of the SM. They can be classified according to their electroweak quantum number assignments; here we consider the possibilities of a sequential fourth generation quark doublet (Sec. IV A), heavy-quark isosinglets (Sec. IV B) and non-SM quarks associated with little Higgs models (Sec. IV C). The contributions of such heavy quarks can remove the efficient GIM cancellation inherent in the short-distance SM computation and can give rise to D^0-$\bar{D}^0$ mixing at the level of the current experimental limit.

A. Fourth generation quark doublet

A simple extension to the standard model is the addition of a fourth family of fermions. Precision electroweak data severely constrains this possibility. The Particle Data Group [13] quotes a restriction on the number of families to be $N_F = 2.81 \pm 0.24$ from the oblique S parameter [27] alone. We note, however, that the LEP Electroweak Working Group [28] allows for a more generous range of the S parameter from their electroweak fit. In either case, this restriction can be relaxed by allowing the T parameter to vary as well, or by adding other sources of new physics which would participate in the electroweak fit such as an extended Higgs sector [29]. The requirement of anomaly cancellation implies the existence of a fourth lepton family as well (almost degenerate to satisfy the $\Delta\rho$ constraint with $m_{\nu_4} > M_Z/2$) or an extra right-handed quark doublet. Direct collider searches by the CDF and D0 Collaborations at the Tevatron currently place a bound [13] on the mass of a charged $-1/3$ fourth generation quark b' of $m_{b'} > 128$, 190, 199 GeV if the b'-quark decays, respectively, via charged current interactions into leptons + jets, via FCNC with $b' \to bZ$, or is quasistable. We recall that perturbative unitarity considerations [30] in $FF \to FF$ scattering restricts the mass of sequential heavy flavors to be $m_F \lesssim 500$ GeV.

Here, we review the contribution of a fourth generation of quarks to D mixing, keeping in mind that some other new physics may also be present in order to evade the precision electroweak constraints and that it also may or may not contribute to the mixing. The primary motivation for this discussion is to set up the formalism that will be used in the following sections.

The $Q = -1/3$ fourth generation quark contributes to D mixing via a box diagram which also contains the SM $W^\pm$ bosons. Note that since the b' quark is not kinematically accessible in charm-quark decay, it will not contribute to the dispersive amplitude for $x_{\rm D}$ in Eq. (14). The $|\Delta C| = 2$ Hamiltonian at the b' mass scale in the fourth generation model is [31]

$$\mathcal{H}_{\rm 4th} = \frac{G_F^2 M_W^2}{4\pi^2} \sum_{i,j} \lambda_i \lambda_j S(x_i, x_j) Q_1, \tag{34}$$

where $S(x_i, x_j)$ are the well-known Inami-Lim functions [32] (given in the appendix), $x_i = (m_{q_i}/M_W)^2$, $\lambda_i \equiv V_{ci}^* V_{ui}$, and the sum runs over the internal quark flavors. As discussed in the previous section, there is a strong GIM cancellation in D meson mixing, which leaves a sizable contribution only from the heavy b' quark and sets $i = j = b'$ in the above sum. Performing the RG evolution, we obtain at the scale m_c

$$\mathcal{H}_{\rm 4th} = \frac{G_F^2 M_W^2}{4\pi^2} \lambda_{b'}^2 S(x_{b'}, x_{b'}) r_1(m_c, M_W) Q_1, \tag{35}$$

which in turn gives

$$x_{\rm D}^{\rm (4th)} = \frac{G_F^2 M_W^2 f_D^2 M_D}{6\pi^2 \Gamma_D} B_D \lambda_{b'}^2 r_1(m_c, M_W) S(x_{b'}, x_{b'}). \tag{36}$$

It should be noted that for $r_1(m_c, M_W)$, only contributions below M_W are required.

The value of $x_{\rm D}^{\rm (4th)}$ as a function of the Cabibbo-Kobayashi-Maskawa (CKM) mixing elements is displayed in Fig. 2 for various values of the b'-quark mass. We see that the 1σ experimental limit of $x_{\rm D} < 11.7 \times 10^{-3}$ places sizable constraints in the b'-quark mixing-mass parameter space. We also show the exclusion contours for possible future experimental bounds of $x_{\rm D} < (15.0, 8.0, 5.0, 3.0) \times 10^{-3}$ (corresponding to the blue (dark gray) dashed, red (gray) dashed, cyan (lightest gray) dotted, and green (light gray) dot-dashed curves, respectively) as discussed in the

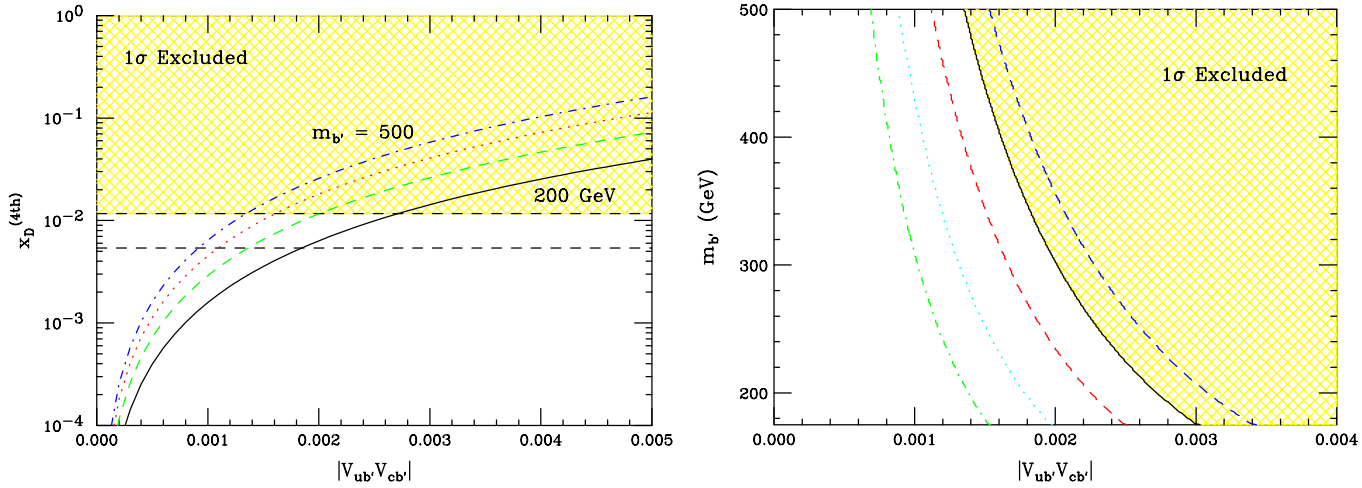

FIG. 2 (color online). Left: $x_{\rm D}$ in the four generation model as a function of the CKM mixing factor $|V^*_{cb'}V_{ub'}|$ for b'-quark masses of 200, 300, 400, and 500 GeV from bottom to top. The 1σ experimental bounds are as indicated, with the yellow shaded area depicting the region that is excluded. Right: The present 1σ excluded region in the mass-mixing parameter plane, as well as possible future contours taking $x_{\rm D} < (15.0, 8.0, 5.0, 3.0) \times 10^{-3}$, corresponding to the blue (dark gray) dashed, red (gray) dashed, cyan (lightest gray) dotted, and green (light gray) dot-dashed curves, respectively.

Introduction. We note that the present constraints on the CKM mixing parameters $|V_{ub'}V^*_{cb'}| \lesssim 0.002$ are an order of magnitude stronger than those obtained from unitarity considerations [13] of the CKM matrix.

B. Heavy vectorlike quarks

The next possibility of interest is the presence of heavy quarks which are $SU(2)_L$ singlets (so-called *vectorlike* quarks) [33]. We will consider both charge assignments $Q = +2/3$ and $Q = -1/3$ for the heavy quarks. Both choices are well motivated, as such fermions appear explicitly in several models of physics beyond the standard model. For example, weak isosinglets with $Q = -1/3$ appear in E_6 grand unified theories (GUTs) [34,35], with one for each of the three generations (D, S, and B). Weak isosinglets with $Q = +2/3$ occur in little Higgs theories [36,37] in which the standard model Higgs boson is a pseudo-Goldstone boson, and the heavy isosinglet T quark cancels the quadratic divergences generated by the top quark in the mass of the Higgs boson.

1. $Q = -1/3$ *singlet quarks*

We first consider the class of models with $Q = -1/3$ down-type singlet quarks. For this case, the down-quark mass matrix is a 4×4 array if there is just one heavy singlet (or 6×6 for three heavy singlets as in E_6 models). As a consequence, the standard 3×3 CKM matrix is no longer unitary. Moreover, the weak charged current will now contain terms that couple up-quarks to the heavy singlet quarks. For three heavy singlets, we have

$$\mathcal{L}^{\rm (ch)}_{\rm int} = \frac{g}{\sqrt{2}} V_{i\alpha} W^\mu \bar{u}_{i,L} \gamma_\mu D_\alpha, \tag{37}$$

where $u_{i,L} \equiv (u, c, t)_L$ and $D_\alpha \equiv (D, S, B)$ refer to the standard up-quark and heavy isosinglet down-quark sectors. The $\{V_{i\alpha}\}$ are elements of a 3×6 matrix, which is the product of the 3×3 and 6×6 unitary matrices that diagonalize the $Q = +2/3$ and $Q = -1/3$ quark sectors, respectively. The resulting box diagram contribution to $\Delta M_{\rm D}$ from these new quarks is displayed in Fig. 3. Assuming that the contribution of one of the heavy quarks (say the S quark) dominates, one can write an expression [similar to that in Eq. (36)] for $x_{\rm D}$ [31],

$$x_{\rm D}^{(-1/3)} \simeq \frac{G_F^2 M_W^2 f_D^2 M_D}{6\pi^2 \Gamma_D} B_D (V^*_{cS} V_{uS})^2 r_1(m_c, M_W) f(x_S), \tag{38}$$

where $x_S \equiv (m_S/M_W)^2$ and $f(x_S) \to x_S(1 + 6\ln(x_S))$ for large x_S. The light-heavy mixing angles $|V^*_{cS}V_{uS}|^2$ should go as $1/m_S$ for large m_S to keep the contribution under control. The current bound on $|V^*_{cS}V_{uS}|^2$ from unitarity of the CKM matrix is not very stringent, $|V^*_{cS}V_{uS}|^2 < 4 \times 10^{-4}$ [13]. An S-quark mass in the range 0.2 to 1 TeV gives rise to a mixing contribution that can exceed the current experimental limit in Eq. (4). Hence a singlet heavy quark

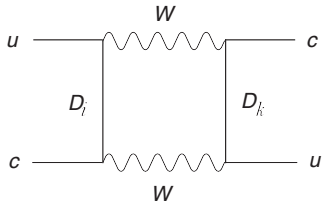

FIG. 3. Box contribution from heavy weak-isosinglet quarks.

of charge $-1/3$ can give rise to x_D near the current experimental limit.

In the E_6-based model proposed by Bjorken *et al.* [38], the 6×6 mass matrix has an especially simple form. The resulting 6×6 mass matrix has a pseudo-orthogonality property which implies that the 3×3 CKM matrix, although not unitary, satisfies

$$\sum_{i=1}^{3} (V_{\rm CKM})^*_{bi} (V_{\rm CKM})_{is} = 0. \tag{39}$$

The analog of this condition in the up-quark sector does not hold, and as a result, there are no new FCNC effects in the down-quark sector. For D^0-$\bar{D}^0$ mixing, the prediction is now that (recall capital lettering is used to denote the heavy quark)

$$|V^*_{cS} V_{uS}|^2 = s_2^2 |V^*_{cs} V_{us}|^2 \simeq s_2^2 \lambda^2, \tag{40}$$

where $|V^*_{cs} V_{us}| \simeq \lambda \simeq 0.22$ and s_2 is the (small) mixing parameter describing the mixing between the light s quark and the heavy S quark. Using the experimental values in Eq. (4), we can place bounds on s_2 for a given mass m_S, e.g. $s_2 \simeq 0.0009$ for $m_S \simeq 0.5$ TeV. We present the constraints on s_2 vs m_S in Fig. 4.

2. $Q = +2/3$ *singlet quarks*

Next, consider the possibility of weak isosinglet quarks having charge $Q = +2/3$. These are present in some theories beyond the SM, including, for example, little Higgs models which will be discussed in more detail in the following section. Here, we present the general formalism for this scenario.

The presence of such quarks violate the Glashow-Weinberg-Paschos naturalness conditions for neutral currents [39]. Since their electroweak quantum number assignments are different than those for the SM fermions, flavor-changing neutral current interactions are generated in the left-handed up-quark sector. Thus, in addition to the charged current interaction

$$\mathcal{L}^{\rm (ch)}_{\rm int} = \frac{g}{\sqrt{2}} V_{\alpha i} \bar{u}_{\alpha,L} \gamma_\mu d_{i,L} W^\mu, \tag{41}$$

there are also FCNC couplings with the Z^0 boson [33],

$$\mathcal{L}^{\rm (ntl)}_{\rm int} = \frac{g}{2\sqrt{2}\cos\theta_w} \lambda_{ij} \bar{u}_{i,L} \gamma_\mu u_{j,L} Z^{0\mu}. \tag{42}$$

Here, $V_{\alpha i}$ is a 4×3 mixing matrix with α running over $1 \to 4$, $i = 1 \to 3$, and with the CKM matrix comprising the first 3×3 block. In this case, a tree-level contribution to ΔM_D is generated from Z^0 exchange as shown in Fig. 5. This is represented by an effective Hamiltonian of the form

$$\mathcal{H}_{2/3} = \frac{g^2}{8\cos^2\theta_w M_Z^2} (\lambda_{uc})^2 \bar{u}_L \gamma_\mu c_L \bar{u}_L \gamma^\mu c_L, \tag{43}$$

where unitarity demands

$$\lambda_{uc} \equiv -(V^*_{ud} V_{cd} + V^*_{us} V_{cs} + V^*_{ub} V_{cb}). \tag{44}$$

Taking the 1σ ranges for the experimentally determined values of the CKM elements [13] yields the constraint $\lambda_{uc} < 0.02$. This Hamiltonian is just a particular case of a more general relation [Eq. (49)] appearing in the follow-

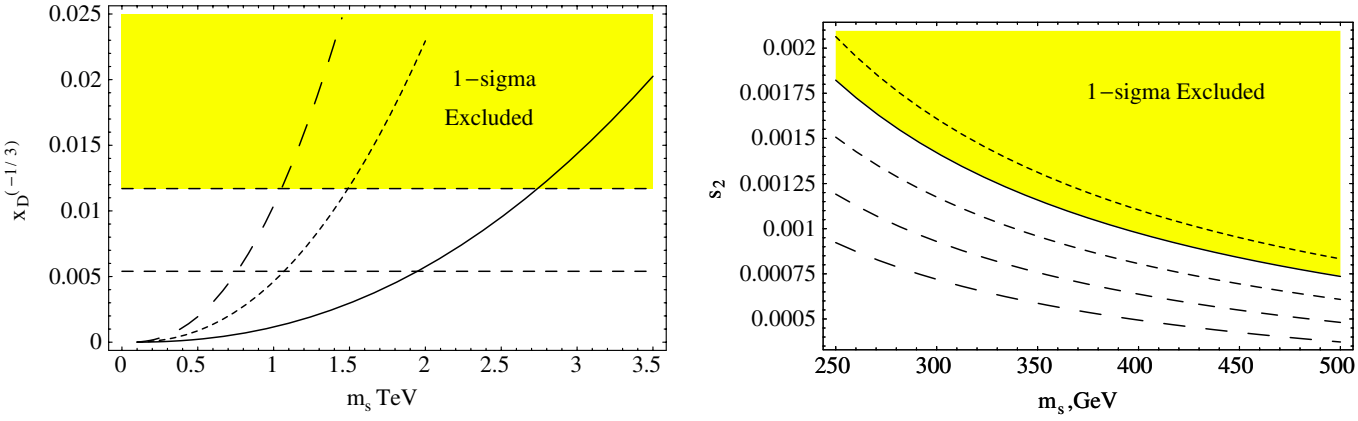

FIG. 4 (color online). Left: x_D in the singlet $Q = -1/3$ quark model as a function of the singlet quark mass for various values of the mixing angle $s_2 = 0.0001, 0.0002, 0.0003$ corresponding to the solid, dotted, and dashed curves, respectively. The 1σ experimental bounds are as indicated, with the yellow shaded area depicting the region that is excluded. Right: The present 1σ excluded region (short-dashed curve) in the mass m_S and mixing angle s_2 parameter plane for the singlet $Q = -1/3$ quark in the model of Bjorken *et al.* [38] described in the text. Possible future contours are also shown, taking $x_D < (15.0, 8.0, 5.0, 3.0) \times 10^{-3}$ from top to bottom, corresponding to the solid, medium-dashed, long-dashed, and longer-dashed curves, respectively.

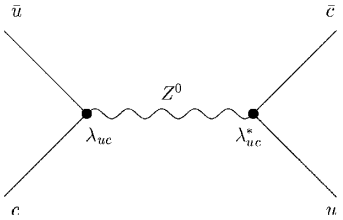

FIG. 5. Tree-level contribution from Z^0 exchange.

ing section.[7] The QCD running from $\mu = M_Z$ to $\mu = m_c$ for this effective Hamiltonian is trivial, leading to

$$\mathcal{H}_{2/3} = \frac{g^2}{8\cos^2\theta_w M_Z^2}(\lambda_{uc})^2 r_1(m_c, M_Z) Q_1, \tag{45}$$

where it should be noted that for $r_1(m_c, M_Z)$, only contributions below M_Z are required. This Hamiltonian leads to

$$x_{\mathrm{D}}^{(2/3)} = \frac{2G_F f_{\mathrm{D}}^2 M_{\mathrm{D}}}{3\sqrt{2}\Gamma_D} B_D(\lambda_{uc})^2 r_1(m_c, M_Z). \tag{46}$$

We present this contribution to x_{D} from models with a singlet $Q = 2/3$ quark in Fig. 6. Note that the bound on the mixing λ_{uc} from D^0-$\bar{D}^0$ mixing is roughly 2 orders of magnitude better than that from unitarity constraints of the CKM matrix.

C. Little Higgs models

Little Higgs models [36,37,40] feature the Higgs as a pseudo Nambu-Goldstone boson of an approximate global symmetry that is broken by a vacuum expectation value (vev hereafter) at a scale of a few TeV. This approximate symmetry protects the Higgs vev through one-loop order relative to the ultraviolet (uv) cutoff of the theory which appears at a higher scale. The breaking of this symmetry is realized in such a way that the Higgs mass only receives quantum corrections at two loops. In these models the one-loop quadratic divergent contributions to the Higgs mass in the SM are canceled by a new particle of the same spin. These models thus predict the existence of new charged $Q = +2/3$ vectorlike quarks, gauge bosons, and scalars at the TeV scale.

The most economical model of this type, in that it introduces the minimal number of new fields, is known as the littlest Higgs [36,37]. It is based on a nonlinear sigma model with $SU(5)$ global symmetry that is broken to the subgroup $SO(5)$ by a vev f. f is generated by strongly coupled physics at the uv scale $\lambda \sim 4\pi f \sim 10$ TeV. The 14 Goldstone bosons remaining after this symmetry breaking yield a physical doublet and complex

[7]The specific correspondence is $C_R = 0$, $C_L^2 \equiv C_{2/3}^2 = g^2\lambda_{uc}^2/(4\cos^2\theta_w)$, and $M_{Z'} = M_Z$.

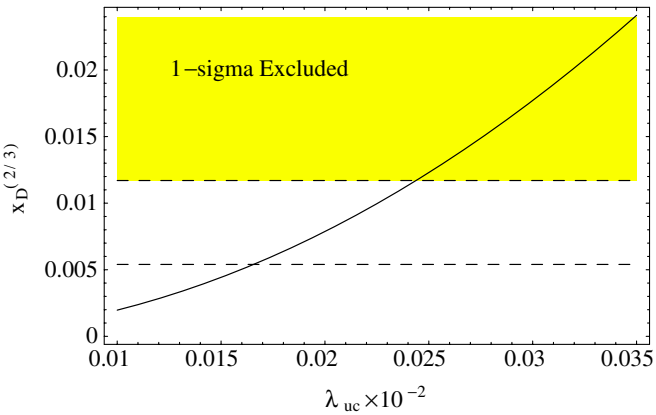

FIG. 6 (color online). Value of x_{D} as a function of the mixing parameter λ_{uc} in units of 10^{-2} in the $Q = +2/3$ quark singlet model. The 1σ experimental bounds are as indicated, with the yellow shaded area depicting the region that is excluded.

triplet under $SU(2)$, which remain massless at this stage. The $SU(5)$ contains a gauged subgroup $[SU(2) \times U(1)]^2$ which is also broken by f to the SM electroweak gauge group. The remaining four Goldstone bosons are then eaten by a Higgs-like mechanism and give mass, of order $f \sim 1$ TeV, to the gauge fields of the broken subgroups. Masses for the complex triplet are generated at the TeV scale by one-loop gauge interactions. The neutral component of the complex doublet plays the role of the SM Higgs, which receives its mass at two-loops from a Coleman-Weinberg potential, giving $\mu^2 \sim f^2/16\pi^2$. Thus the natural scale for f is around a TeV; if f is much higher, the Higgs mass must again be finely tuned and this model no longer addresses the hierarchy problem.

The minimum physical spectrum of this model below a TeV is thus that of the SM with a single light Higgs. At the TeV scale, there are four new gauge bosons (an electroweak triplet and singlet), the scalar triplet, and a single $Q = +2/3$ vectorlike quark T. Other variants of little Higgs models may expand this particle content at the TeV scale.

In general, the new vectorlike T quark can contribute to D^0-$\bar{D}^0$ mixing. Since it has different electroweak quantum numbers from the $Q = +2/3$ quarks in the SM, FCNC interactions will be induced in the left-handed up-quark sector. This generates a tree-level Z boson exchange contribution to D mixing as depicted in Fig. 5. This was considered in Ref. [41], where a specific ansatz for the 4×4 up-quark mass matrix was employed, leading to a quite small contribution to ΔM_D. In general, however, one expects the quark mixing to be of order v/f and the contribution of the flavor-changing Z interaction induced by the existence of the T quark can be sizable, as discussed in the previous section. Current data can be used to constrain the mass and mixing of the T quark, and the results in Fig. 6 are applicable in this case. Tree-level contributions to D mixing with the exchange of the new heavy neutral gauge

bosons will likewise be generated, as the fermionic coupling for these fields is also proportional to the fermion's third component of weak isospin. The operator structure is exactly the same as that given in the previous section, but the magnitude of these contributions will be suppressed relative to the SM Z boson exchange by the heavy mass of the new neutral gauge bosons. In addition, there could also be new contributions to rare D meson decays, as discussed recently in the work of Chen *et al.* [42].

It has been shown [43] that a global fit to the precision electroweak data set places a significant limit, which is roughly parameter independent, on the vev f in the littlest Higgs model of $f \gtrsim 4$ TeV. Variants of this model, employing different global symmetries, can reduce this constraint somewhat [44]. In addition, a discrete symmetry, called T parity, can be introduced [45] to alleviate the electroweak bounds. This symmetry is analogous to R parity in supersymmetry and has the consequence that T parity is conserved in interactions and that the lightest T-odd particle is stable. This provides a natural dark matter candidate in these models. Recent work by Hill and Hill [46] has shown that anomalies in topological interactions can break this discrete symmetry and thus T parity is no longer an exact symmetry; the resulting phenomenology has yet to be worked out. However, the uv completion of the theory may or may not allow for the terms which break T parity, and thus a general statement on the presence of this discrete symmetry in the low-energy theory cannot be made.

In addition to the tree-level contribution discussed above, little Higgs models with T parity can give rise to a loop contribution to D^0-$\bar{D}^0$ mixing involving the exchange of the heavy gauge bosons and new mirror fermions, which are present in this form of the model. In fact, three vectorlike doublets of mirror fermions are introduced in little Higgs models with T parity in order to evade compositeness constraints [45]. The effective Hamiltonian relevant to D^0-$\bar{D}^0$ mixing for this contribution is [47]

$$\mathcal{H}_{\mathrm{LH}} = \frac{G_F^2 M_W^2}{16\pi^2}\frac{v^2}{f^2}\sum_{i,j}\xi_i^{(D)}\xi_j^{(D)}F_{\mathrm{LH}}(z_i, z_j)Q_1. \qquad (47)$$

Here, $\xi^{(D)}$ corresponds to the relevant elements of the weak mixing matrix in the mirror fermion sector which parametrizes the flavor interactions between the SM and mirror fermions. The quantity F_H (given in the appendix) is the loop function computed in Ref. [47]; it depends on $z_i \equiv m_{Mi}^2/M_{W_H}^2$, where m_{Mi} is the mass of the ith mirror quark doublet and W_H represents the heavy charged gauge boson mass. The Q_1 operator appears since the heavy gauge bosons W_H have purely left-handed interactions. The RG running of this Hamiltonian is trivial and leads to a factor of $r_1(m_c, M)$. The resulting contribution to the mass difference is

$$x_{\mathrm{D}}^{(\mathrm{LH})} = \frac{G_F^2 M_W^2 f_D^2 M_D}{24\pi^2\Gamma_D}B_D\frac{v^2}{f^2}\sum_{i,j}\xi_i^{(D)}\xi_j^{(D)}F_H(z_i, z_j)r_1(m_c, M). \qquad (48)$$

This has recently been computed in Ref. [48] in light of the recent experimental measurement of D^0-$\bar{D}^0$ mixing, where it is found that this contribution can saturate the experimental bounds.

In little Higgs models with T parity, there is an additional tree-level contribution arising from the interaction vertex $Z_H\bar{q}T^{(-)}$ where Z_H represents either of the heavy neutral gauge fields and $T^{(-)}$ is the odd T-parity quark. $T^{(-)}$ couples to the weak eigenstate of the T-parity even quark $T^{(+)}$, which receives its mass from the same $Q = +2/3$ Yukawa term that is responsible for the up-quark masses. This induces mixing between the quarks in the up-quark sector, resulting in FCNC interactions of the SM quarks with the exchange of the new heavy neutral gauge fields. The generic formalism for this contribution will be discussed in the next section, however this particular contribution is thought to be small [47].

V. EXTRA GAUGE BOSONS

Many theories with physics beyond the SM have extended electroweak gauge symmetries, whose hallmark are the existence of new heavy neutral and charged gauge bosons. We note that scenarios with extended gauge symmetries also generally contain new fermions which are required for anomaly cancellation, as well as an extended Higgs sector to facilitate the extended symmetry breaking. The additional heavy gauge bosons are produced directly at hadron colliders via the Drell-Yan mechanism, and the search limit on the masses of new W', Z' gauge bosons with SM couplings is approaching 1 TeV from Run II data at the Tevatron. The lower bound on the mass of a SM-coupled $Z'(W')$ is 923(965) GeV from CDF(D0) [49]. The LHC will be able to search for these particles with masses up to 5 TeV [50]. There are many such models that yield large FCNC effects in the up-quark sector.

A. Generic Z' models

It is possible that a new heavy Z' boson has flavor-changing couplings in the up-quark sector. Here, we examine a generic tree-level FCNC interaction that mediates D mixing via Z' exchange, analogous to the transition depicted in Fig. 5. While the discussion presented here is quite general, many string-inspired models have extra $U(1)$ gauge symmetries that lead to extra Z' bosons with possible flavor-changing couplings [35,51,52].

The effective four-fermion Hamiltonian just below the Z' scale is

$$\mathcal{H}_{Z'} = \frac{1}{2M_{Z'}^2}[\mathrm{C_L}^2 Q_1 + 2\mathrm{C_L}\mathrm{C_R}Q_2 + \mathrm{C_R}^2 Q_6], \qquad (49)$$

where the dimensionless flavor-changing couplings $C_{L,R}$ are the model-dependent inputs to the calculation. This is the most general effective Hamiltonian and assumes flavor-changing interactions occur in both the left- and right-handed sectors. We first perform a general analysis and will then consider some particular occurrences of a Z' in the Sections below.

We introduce the Wilson coefficients $C_{1,2,6}(M_{Z'})$ by matching at the Z' mass scale,

$$C_1(M_{Z'}) = C_L^2, \qquad C_2(M_{Z'}) = 2C_L C_R, \qquad C_6(M_{Z'}) = C_R^2, \tag{50}$$

with all other Wilson coefficients being zero at this scale. Assuming that $M_{Z'} > m_t$ and performing the RG running of Eq. (49), we obtain the effective Hamiltonian at the scale $\mu = m_c$,

$$\mathcal{H}_{Z'} = \frac{1}{2M_{Z'}^2}[C_1(m_c)Q_1 + C_2(m_c)Q_2 + C_3(m_c)Q_3 + C_6(m_c)Q_6], \tag{51}$$

with

$$\begin{aligned} C_1(m_c) &= r_1(m_c, M_{Z'})C_1(M_{Z'}), \\ C_2(m_c) &= r_2(m_c, M_{Z'})C_2(M_{Z'}), \\ C_3(m_c) &= \frac{2}{3}[r_2(m_c, M_{Z'}) - r_3(m_c, M_{Z'})]C_2(M_{Z'}), \\ C_6(m_c) &= r_6(m_c, M_{Z'})C_6(M_{Z'}). \end{aligned} \tag{52}$$

The presence of Q_3 in Eq. (51) is due to operator mixing in the RG running. Finally, as a check note that for the case of no evolution ($r_i \to 1$) we obtain the expected behavior $C_i(\mu) \to C_i(M_{Z'})$.

Upon evaluating the D^0-to-$\bar{D}^0$ matrix elements, we obtain the Z' tree contribution to x_D,

$$x_D^{(Z')} = \frac{f_D^2 M_D}{2M_{Z'}^2\Gamma_D} B_D \left[\frac{2}{3}(C_1(m_c) + C_6(m_c)) - C_2(m_c)\left(\frac{1}{2} + \frac{\eta}{3}\right) + C_3(m_c)\left(\frac{1}{12} + \frac{\eta}{2}\right)\right], \tag{53}$$

where we have made use of Eqs. (24) and (26).

Equation (53) can be used to relate the input parameters of Z' models (C_L and C_R) to some value of x_D. Taking $x_D < 11.7 \times 10^{-3}$, particularly simple expressions are obtained for the limiting cases:

(1) $C_R = 0$ (the case with C_L replaced by C_R yields identical limits):

$$\frac{M_{Z'}}{C_L} = \left(\frac{f_D^2 M_D B_D r_1(m_c, M_{Z'})}{3x_D\Gamma_D}\right)^{1/2} > 8.9 \times 10^5 \text{ GeV}, \tag{54}$$

(2) $C_L = C_R \equiv C$:

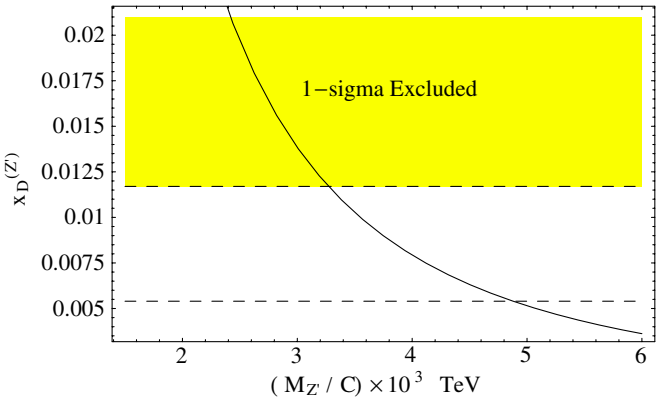

FIG. 7 (color online). x_D in a generic Z' model as a function of the Z' boson mass (normalized by the flavor-changing coupling constant) for the case $C_L = C_R = C$. The 1σ experimental bounds are as indicated, with the yellow shaded area depicting the region that is excluded.

$$\frac{M_{Z'}}{C} = \left(\frac{f_D^2 M_D B_D \kappa}{2x_D\Gamma_D}\right)^{1/2} > 3.4 \times 10^6 \text{ GeV}, \tag{55}$$

where $\kappa \equiv |4r_1(m_c, M_{Z'})/3 - 8r_2(m_c, M_{Z'})/9 - (1 + 6\eta)r_3(m_c, M_{Z'})/9|$.

In the above, we have fixed the slowly varying $r_1(m_c, M_{Z'})$ and $\kappa(m_c, M_{Z'})$ at the middle of their ranges. The results in Eqs. (53)–(55) which constrain combinations of the flavor-changing couplings and the Z' mass (see Fig. 7), can be applied to fit the needs of the NP model builder. For example, in Eq. (54) the choice $C_L = 1$, $C_R = 0$ implies $M_{Z'} > 8.9 \times 10^2$ TeV or alternatively taking $M_{Z'} = 1$ TeV yields the bound $C_L < 1.1 \times 10^{-3}$.

B. Family symmetries

One class of new physics possibilities to be explored in the TeV range is family (horizontal) symmetries. The gauge sector of the standard model Lagrangian,

$$\mathcal{L}_{SM} = \mathcal{L}_{QCD} + \mathcal{L}_{SU(2)\times U(1)} + \mathcal{L}_H, \tag{56}$$

actually exhibits a very large global symmetry viz. $SU(3)_L \times SU(3)_R \times U(1) \times U(3)_L \times U(3)_R$. The hope is then that some subgroup G of this large symmetry is shared by the Higgs sector $\mathcal{L}_H$ and the gauge symmetry of the full Lagrangian becomes $SU(3)_C \times SU(3)_L \times U(1)$. The group G acts on the families horizontally [53], and, of course, eventually G has to be broken, preferably spontaneously.

The symmetry G can be implemented locally, so there will be flavor-changing interactions mediated by new gauge bosons. The symmetry is broken spontaneously, making the gauge boson massive with new scalar fields being introduced in addition to the standard Higgs field.

As a prototype, let us consider a very simple model [54]. We consider the group $SU(2)_G$ acting only on the first two

left-handed families [it may be regarded as a subgroup of an $SU(3)_G$, which is broken]. Spontaneous breaking of $SU(2)_G$ makes the gauge bosons G_i massive. The LH doublets

$$\begin{pmatrix} u^0 \\ d^0 \end{pmatrix}_L \quad \text{and} \quad \begin{pmatrix} c^0 \\ s^0 \end{pmatrix}_L, \tag{57}$$

transform as $I_G = 1/2$ under $SU(2)_G$, as do the lepton doublets

$$\begin{pmatrix} \nu_e^0 \\ e^0 \end{pmatrix}_L \quad \text{and} \quad \begin{pmatrix} \nu_\mu^0 \\ \mu^0 \end{pmatrix}_L, \tag{58}$$

and the right-handed fermions are singlets under $SU(2)_G$. The superscript refers to the fact that these are weak eigenstates and not mass eigenstates. The couplings of fermions to the family gauge bosons G is given by

$$\mathcal{L} = f[\bar{\psi}_{d^0 L}\gamma_\mu \vec{\tau}\cdot\vec{G}_\mu \psi_{d^0 L} + \bar{\psi}_{u^0 L}\gamma_\mu \vec{\tau}\cdot\vec{G}_\mu \psi_{u^0 L} + \bar{\psi}_{\ell^0 L}\gamma_\mu \vec{\tau}\cdot\vec{G}_\mu \psi_{\ell^0 L}], \tag{59}$$

where f denotes the coupling strength and $\vec{\tau}$ are the generators of $SU(2)_G$. We define the mass basis by

$$\begin{pmatrix} d \\ s \end{pmatrix}_L = U_d \begin{pmatrix} d^0 \\ s^0 \end{pmatrix}_L, \qquad \begin{pmatrix} u \\ c \end{pmatrix}_L = U_u \begin{pmatrix} u^0 \\ c^0 \end{pmatrix}_L, \qquad \begin{pmatrix} e \\ \mu \end{pmatrix}_L = U_\ell \begin{pmatrix} e^0 \\ \mu^0 \end{pmatrix}_L. \tag{60}$$

In the limit of CP conservation each of the three 2×2 matrices U_d, U_u, and U_ℓ is characterized by one angle: θ_d, θ_u, and θ_ℓ (where the Cabibbo angle is $\theta_c = \theta_u - \theta_d$). One then finds for the couplings in the fermion mass basis:

$$\begin{aligned}\mathcal{L} = f[&G_{1\mu}\{\sin 2\theta_d(\bar{d}_L\gamma_\mu d_L - \bar{s}_L\gamma_\mu s_L) + \sin 2\theta_u(\bar{u}_L\gamma_\mu u_L - \bar{c}_L\gamma_\mu c_L) + \sin 2\theta_l(\bar{e}_L\gamma_\mu e_L - \bar{\mu}_L\gamma_\mu \mu_L)\\ &+ \cos 2\theta_d(\bar{d}_L\gamma_\mu s_L + \bar{s}_L\gamma_\mu d_L) + \cos 2\theta_u(\bar{u}_L\gamma_\mu c_L + \bar{c}_L\gamma_\mu u_L) + \cos 2\theta_l(\bar{e}_L\gamma_\mu \mu_L + \bar{\mu}_L\gamma_\mu e_L)\}\\ &+ iG_{2\mu}\{(\bar{s}_L\gamma_\mu d_L - \bar{d}_L\gamma_\mu s_L) + (\bar{c}_L\gamma_\mu u_L - \bar{u}_L\gamma_\mu c_L) + (\bar{\mu}_L\gamma_\mu e_L - \bar{e}_L\gamma_\mu \mu_L)\} + G_{3\mu}\{\cos 2\theta_d(\bar{d}_L\gamma_\mu d_L - \bar{s}_L\gamma_\mu s_L)\\ &+ \cos 2\theta_u(\bar{u}_L\gamma_\mu u_L - \bar{c}_L\gamma_\mu c_L) + \cos 2\theta_l(\bar{e}_L\gamma_\mu e_L - \bar{\mu}_L\gamma_\mu \mu_L) - \sin 2\theta_d(\bar{d}_L\gamma_\mu s_L + \bar{s}_L\gamma_\mu d_L)\\ &- \sin 2\theta_u(\bar{u}_L\gamma_\mu c_L + \bar{c}_L\gamma_\mu u_L) - \sin 2\theta_l(\bar{e}_L\gamma_\mu \mu_L + \bar{\mu}_L\gamma_\mu e_L)\}].\end{aligned} \tag{61}$$

For simplicity we assume that after symmetry breaking the gauge boson mass matrix is diagonal to a good approximation in which case $G_{i\mu}$ are physical eigenstates and any mixing between them is neglected. This Lagrangian clearly introduces tree-level FCNC interactions and gives a contribution to D^0-$\bar{D}^0$ mixing of

$$\mathcal{H}_{\rm FS}(m_i) = f^2\left(\frac{\cos^2 2\theta_u}{m_1^2} + \frac{\sin^2 2\theta_u}{m_3^2} - \frac{1}{m_2^2}\right)\bar{u}_L\gamma_\mu c_L \bar{u}_L\gamma^\mu c_L. \tag{62}$$

A simple symmetry-breaking pattern (see, e.g., [54]) leads to $m_1 = m_3 \neq m_2$. Since the effective Hamiltonian only involves the operator Q_1, the RG running is simple and leads to the following structure at the m_c scale,

$$\mathcal{H}_{\rm FS}(m_c) = f^2 r_1(m_c, M)\frac{m_2^2 - m_1^2}{m_1^2 m_2^2}\bar{u}_L\gamma_\mu c_L \bar{u}_L\gamma^\mu c_L, \tag{63}$$

where M is the smaller of the new gauge boson masses m_1 and m_2. This leads to a value for $x_{\rm D}^{\rm (FS)}$ of

$$x_{\rm D}^{\rm (FS)} = \frac{2 f_D^2 M_D B_D}{3\Gamma_D}\frac{f^2}{m_1^2}\left(1 - \frac{m_1^2}{m_2^2}\right) r_1(m_c, M). \tag{64}$$

Using the available experimental data on D^0-$\bar{D}^0$ mixing parameters, yields constraints on the masses of the family symmetry-mediating gauge bosons. They are presented in Fig. 8 for m_i/f.

C. Left-right symmetric model

A puzzling feature of the SM is the left-handed nature of the electroweak interactions. A long-standing possible remedy, known as the left-right symmetric model (LRM) [55], seeks to restore parity at high energies by enlarging the gauge symmetry to $SU(2)_L \times SU(2)_R \times U(1)_{B-L}$. This model can be embedded into an $SO(10)$ (or E_6) GUT structure which then provides a natural mechanism (see-saw) for generating light neutrino masses. A supersymmetric version of a left-right symmetric $SO(10)$ GUT model yields the correct prediction [56] for $x_w \equiv \sin^2\theta_w(M_Z)$ and $\alpha_s(M_Z)$, while allowing for the masses of the new gauge bosons (Z_R and $W_R^\pm$) associated with the $SU(2)_R$ symmetry to be of order a few TeV or less. Light masses for the new gauge bosons can also be obtained in models with a horizontal symmetry [57]. Manifest left-right symmetry dictates that the right-handed gauge coupling take on the same value as the left-handed SM coupling g_L and that the elements of the right-handed CKM matrix be equal to their left-handed counterparts. In this case, the direct search for new gauge bosons at the Tevatron places the bound [49] of $M_R > 788$ GeV on the mass of the charged right-handed gauge boson.

The Z_R has flavor-conserving couplings in this model, and thus does not mediate D^0-$\bar{D}^0$ mixing. The charged

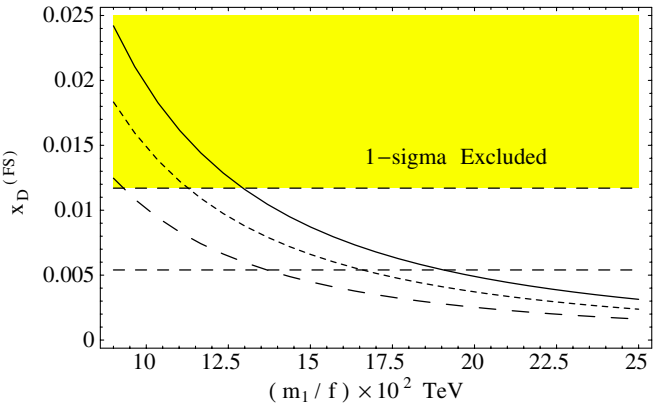

FIG. 8 (color online). $x_D^{(FS)}$ as a function of m_1/f for the gauge boson mass ratios $m_1/m_2 = 0.01, 0.5, 0.7$ corresponding to the solid, dotted, and dashed curves, respectively. The 1σ region for x_D is also shown, with the yellow shaded region depicting the excluded region.

right-handed gauge field, however, can participate in virtual exchange in a box diagram, in association with the SM $Q = -1/3$ quarks, and gives a contribution to meson mixing. In fact, the strongest bound on the mass of the W_R, which is $M_R \gtrsim 1.6$ TeV in the limit of manifest left-right symmetry, is derived from its contribution to K^0-$\bar{K}^0$ mixing [58].

However, there is no compelling theoretical reason to adopt manifest left-right symmetry and in more general models the elements of the right-handed analog of the CKM matrix can take on any values, while still respecting unitarity. In addition the ratio of gauge couplings can vary [59] between $x_w/(1-x_w) = 0.55 < g_R/g_L \equiv \kappa < 1$–2. In this case where manifest left-right symmetry is dropped, the bounds from Kaon mixing are softened to $M_{W_R} \gtrsim 300$ GeV [60] and the direct collider searches are significantly weakened [61].

The $|\Delta C| = 2$ Hamiltonian at the right-handed mass scale is given by

$$\mathcal{H}_{\rm LRM} = \frac{G_F^2 M_W^4}{4\pi^2 M_R^2}[\kappa^2 V_{ub}^R V_{cb}^{R*} V_{ub}^L V_{cb}^{L*} J(x_b^W, \beta) Q_2 + \kappa^4 (V_{ub}^R V_{cb}^{R*})^2 S(x_b^R) Q_6], \quad (65)$$

with $x_b^i = m_b^2/M_i^2$, $\beta = M_W^2/M_R^2$, $V^{L,R}$ denote the left- and right-handed CKM matrix, and the quantities $S(x)$ (an Inami-Lim function) and $J(x, \beta)$ are given in the appendix. The first term in this Hamiltonian corresponds to the exchange of one W_R and one standard model W boson in the box diagram, while the second term represents the contribution where only the W_R participates. Here, we ignore mixing between the left- and right-handed gauge bosons. The identification of the matching conditions at the high scale, $C_{2,6}(M_R)$, are obvious. The RG evolution to the charm scale yields the effective Hamiltonian at $\mu = m_c$

$$\mathcal{H}_{\rm LRM} = \frac{1}{2M_R^2}[C_2(m_c)Q_2 + C_3(m_c)Q_3 + C_6(m_c)Q_6], \quad (66)$$

where operator mixing has induced the dependence on Q_3 similar to the generic Z' case discussed above, with

$$C_2(m_c) = r_2(m_c, M_R)C_2(M_R),$$
$$C_3(m_c) = \frac{2}{3}[r_2(m_c, M_R) - r_3(m_c, M_R)]C_2(M_R), \quad (67)$$
$$C_6(m_c) = r_6(m_c, M_R)C_6(m_c, M_R).$$

Evaluating the hadronic matrix elements yields

$$x_D^{(\rm LRM)} = \frac{f_D^2 M_D B_D}{24 M_R^2 \Gamma_D}[-10C_2(m_c) + 7C_3(m_c) + 8C_6(m_c)] \quad (68)$$

upon employing the vacuum saturation approximation and taking $\eta = 1$ in Eq. (26).

It is clear that in the case of manifest left-right symmetry, the combination of the small $(V_{ub}^L V_{cb}^{L*})$ CKM elements and the M_R^{-2} suppression will result in a very small value for $x_D^{(\rm LRM)}$. However, it is possible that for nonmanifest left-right symmetry, where the right-handed CKM elements $(V_{ub}^R V_{cb}^{R*})$ may take on larger values, that a significant effect may be generated. We examine this scenario, taking $(V_{ub}^R V_{cb}^{R*})$ to lie in the range 0.001–0.5, where 0.5 is the maximum value that this quantity can attain while respect-

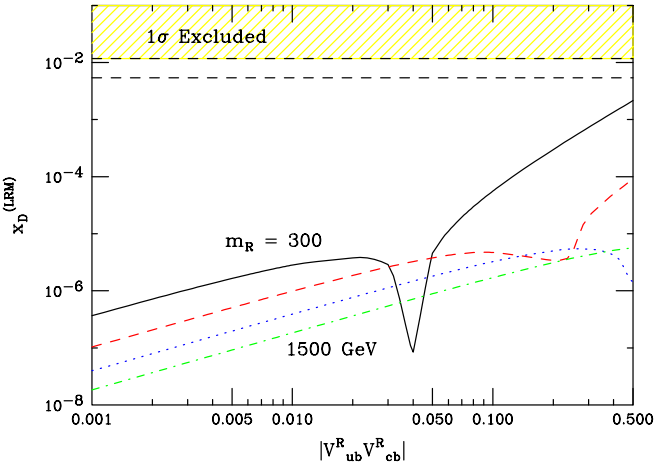

FIG. 9 (color online). x_D in the left-right symmetric model with nonmanifest left-right symmetry as a function of the right-handed CKM mixing factor $|V_{ub}^R V_{cb}^{R*}|$ for $M_R = 300$, 600, 1000, 1500 GeV from top to bottom. The 1σ experimental bounds are as indicated, with the yellow shaded area depicting the region that is excluded.

ing unitarity of the right-handed CKM matrix. Our results are shown in Fig. 9 for various values of M_R, taking $\kappa \equiv g_R/g_L = 1$. We see, that even for the most extreme values of the parameters, the LRM contribution to D^0-$\bar{D}^0$ mixing never reaches the experimentally determined value. Since both of the loop functions $J(x, \beta)$ and $S(x)$ go as m_b^2, the suppression from the small internal quark masses dominates this result. The dip in the curves results from interference due to operator mixing.

This exercise shows that a generic scenario with a new heavy charged gauge boson that participates in the box diagram for D mixing will not induce sizable contributions to the neutral D meson mass difference, unless it is accompanied by new heavy $Q = -1/3$ quarks. The recently proposed twin-Higgs models [62], which are based on a $SU(2)_R \times S(2)_L \times U(1)_{B-L}$ gauge symmetry, contain an extended top-quark sector with heavy $Q = +2/3$ quarks and would give significant contributions to K, $B_{d,s}$ mixing, but not to $\Delta M_{\rm D}$.

D. Alternate left-right model from E_6 theories

An alternative to the conventional left-right symmetric model discussed above is possible in supersymmetric E_6 grand unified theories [35]. This model is also based on the low-energy gauge group $SU(2)_L \times SU(2)_R \times U(1)$, but makes use of ambiguous fermion assignments within the fundamental representation of E_6 [63]. The additional right-handed charged and neutral gauge fields in this model have different properties than in the traditional scenario. A single generation in E_6 theories contains 27, 2-component fermions [in contrast to the 16 fermions per generation in $SO(10)$], and quantum number ambiguities arise that allow the $T_{3L(R)}$ assignments to differ from their customary values for the $\nu_{L,R}$, e_L, and d_R fields. In the quark sector, the right-handed up-quarks then form $SU(2)_R$ doublets with the exotic $Q = -1/3$ vector singlet quark, D_R, that is present in the **27** representation of E_6, while the $SU(2)_L$ doublet (u, d) remains unchanged. D_L and d_R are then singlet fields under all gauge symmetries. This allows, for example, the right-handed W boson to couple the right-handed up-quark sector to the singlet quark D_R. Examination of the superpotential for this model shows that the D_R takes on the quantum number assignment of a leptoquark, while the W_R carries negative R parity and nonzero lepton number, and thus cannot mix with the W_L of the SM or couple to the down-quark sector. The usual constraints on right-handed gauge bosons from the $K_L - K_S$ mass difference and polarized μ decay are thus evaded in this scenario.

These exotic particles can induce significant contributions to D^0-$\bar{D}^0$ mixing [64] via W_R and D_R exchange in a standard box diagram. Note that since the heavy D_R quarks are not kinematically accessible in charm-quark decay, there is no dispersive amplitude in this case. The interactions of the right-handed W boson take the form

$$\mathcal{L} = \frac{g_R}{\sqrt{2}} V_{ij}^R \bar{u}_i \gamma_\mu (1 + \gamma_5) D_j W_R^\mu, \tag{69}$$

where i, j are generational indices and V_{ij}^R is the right-handed analog of the CKM quark mixing matrix governing the right-handed charged currents. The effective $|\Delta C| = 2$ Hamiltonian at the scale of the right-handed interactions is

$$\mathcal{H}_{\rm ALRM} = \frac{g_R^4}{128\pi^2 M_R^2} \sum_{i,j} (V_{ui}^R V_{ci}^{R*})(V_{uj}^R V_{cj}^{R*}) S(x_i, x_j) Q_6, \tag{70}$$

where the sum over i, j extends over the three generations of D_R quarks, $S(x_i, x_j)$ are the standard Inami-Lim functions [32] (given in the appendix) and $x_i = m_{D_{R,i}}^2/M_R^2$ with M_R being the mass of the new right-handed gauge boson. Note that this expression mirrors that in Eq. (34) except for the presence of the right-handed operator Q_6. Matching at the scale M_R yields

$$C_6(M_R) = \frac{g_R^4}{64\pi^2} \sum_{i,j} (V_{ui}^R V_{ci}^{R*})(V_{uj}^R V_{cj}^{R*}) S(x_i, x_j). \tag{71}$$

Performing the RG evolution we obtain at the charm-quark scale

$$\mathcal{H}_{LR} = \frac{1}{2M_R^2} C_6(m_c) Q_6, \tag{72}$$

with $C_6(m_c) = r_6(m_c, M_R) C_6(M_R)$. This yields the contribution to the D meson mass difference

$$x_{\rm D}^{\rm (ALRM)} = \frac{g_R^4 f_D^2 B_D M_D}{192\pi^2 \Gamma_D M_R^2} r_6(m_c, M_R) \sum_{i,j} (V_{ui}^R V_{ci}^{R*}) \times (V_{uj}^R V_{cj}^{R*}) S(x_i, x_j). \tag{73}$$

The magnitude of these contributions is determined by the form of the right-handed quark mixing matrix, the degeneracy of the 3 generations of D_R quarks, as well as the right-handed mass scale. If the quarks are fully degenerate, then a right-handed GIM mechanism is operative due to the unitarity of V^R and this contribution to D mixing vanishes. If there are mass splittings between the three generations of $D_{R,i}$, then the observed value of D mixing can place bounds on the size of these splittings. Here, we will examine the case where V^R takes on the form of the left-handed quark mixing matrix, i.e., it displays the hierarchal structure of the CKM matrix, and derive constraints on this mass splitting as a function of the right-handed mass scale. Our results are presented in Fig. 10. The value of $x_{\rm D}^{\rm (ALRM)}$ as a function of M_R, the mass of the right-handed charged gauge boson is displayed for various mass splittings, $\Delta m/m_{D_1}$, where $\Delta m \equiv m_i - m_j$ is taken to be constant between the first and second as well as second and third generations. We also display the constraints the present 1σ experimental bound of $x_{\rm D} < 11.7 \times 10^{-3}$, as well as contours for future possible values of $x_{\rm D}$,

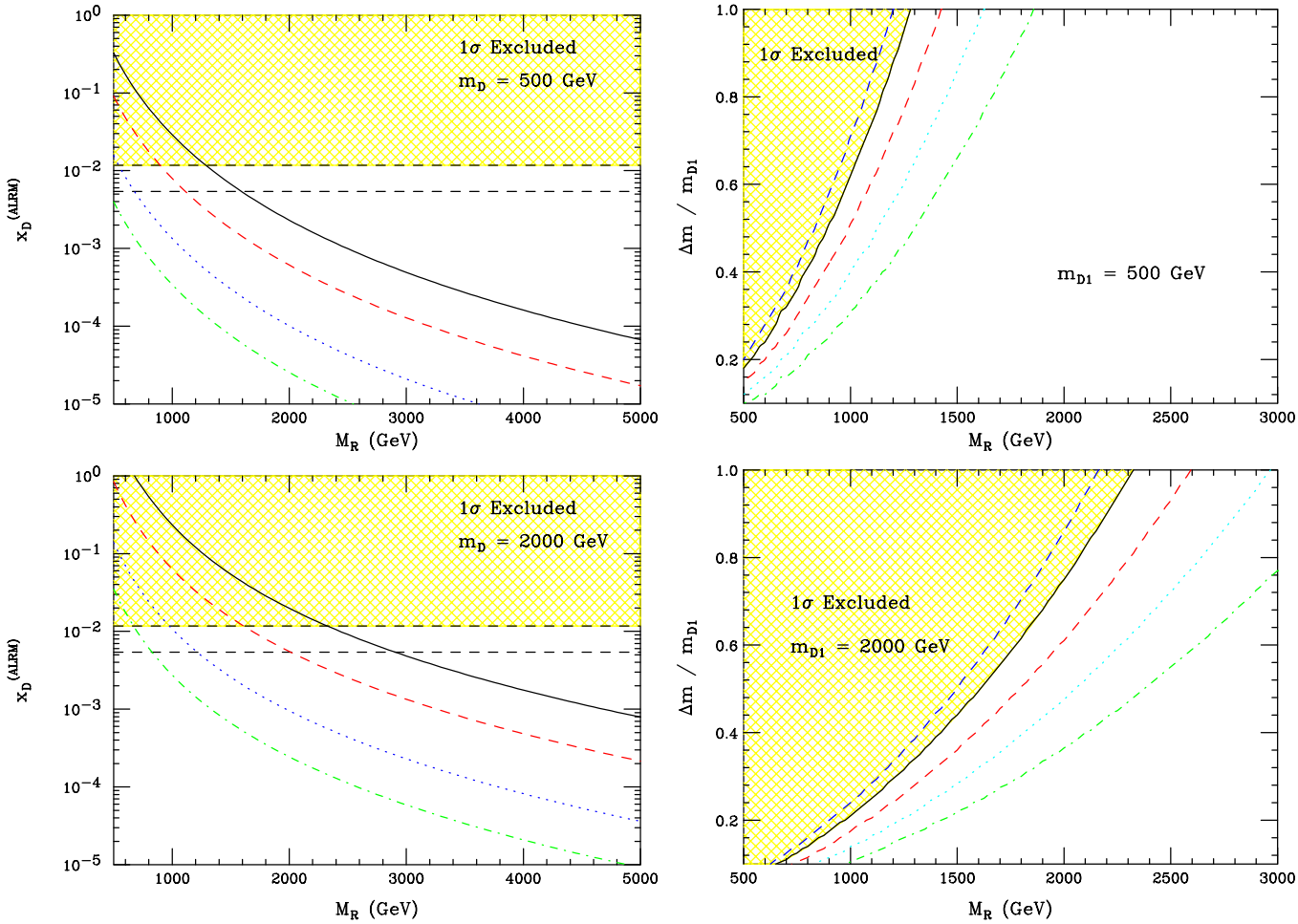

FIG. 10 (color online). Left: x_D in the alternate left-right model as a function of the mass of the W_R for various values of the singlet quark mass splittings, $\Delta/m = 0.1, 0.2, 0.5, 1.0$ from bottom to top. The 1σ experimental bounds are as indicated, with the yellow shaded area depicting the region that is excluded. Right: The present 1σ excluded region in the M_R—mass splitting parameter plane, as well as possible future contours taking $x_D < (15.0, 8.0, 5.0, 3.0) \times 10^{-3}$, corresponding to the blue (dark gray) dashed, red (gray) dashed, cyan (lightest gray) dotted, and green (light gray) dot-dashed curves, respectively. The mass of the first generation singlet quark D_1 is taken to be 500 and 2000 GeV as labeled.

places on the M_R—mass splitting parameter plane. The results are shown for two representative values of the first generation D-quark mass, $m_{D_1} = 500$ and 2000 TeV. We see that the mass of the W_R is restricted to be $M_R \gtrsim 1$–$5 = 2.0$ for large values of the quark mass splittings.

E. Vector leptoquark bosons

In most recent papers on the subject, scalar leptoquarks (particles with both quark and lepton quantum numbers) have usually been associated with R-parity-violating supersymmetry (SUSY) scalars (to be considered in Sec. VIII C). However, vector leptoquarks (VLQs) are also a possibility [65]. For example, they naturally arise in grand unified theories, where quarks and leptons belong to the same multiplet [66]. Many new physics models where leptoquarks are introduced as fundamental vector particles imply that they serve as gauge particles mediating quark and lepton-number-changing interactions resulting from GUT-model symmetry groups. Those symmetries are usually broken at a rather high scale, of order 10^{15} GeV, which implies that, barring fine-tuning, vector leptoquarks receive masses near the GUT symmetry-breaking scale. Yet, some models exist where leptoquarks receive masses at a lower scale. In addition, more exotic constructions, such as preon (composite) models, could also contain vector leptoquarks. In those models, however, leptoquarks are composite particles with masses that are of the order of compositeness scale. Thus, observations of effects of VLQs could potentially probe physics at a very high mass scale. It is for these reasons vector leptoquarks are searched for experimentally. Collider searches at the Tevatron for the direct production of vector leptoquark pairs yield the constraint $m_{\mathrm{VLQ}} > 290$ GeV [67] from run I data for second generation leptoquarks which decay into muons.

While there are a number of phenomenological studies of vector leptoquarks [68,69], a general problem exists with placing constraints on VLQs from indirect measurements, and, in particular, from D^0-$\bar{D}^0$ mixing. This is because their couplings are model dependent. In particular, loop calculations with massive composites, i.e. nongauge leptoquarks, receive contributions that are divergent and must be regulated by the compositeness scale. For the case of gauge leptoquarks, and in the absence of a GIM-like mechanism in the leptoquark box diagram, one can choose a gauge (such as the Feynman gauge) to unambiguously compute the effects of leptoquark interactions. In that gauge, however, one also must add contributions from unphysical states responsible for the generation of the VLQ masses. In a specific model, the interactions of the unphysical states are fixed and their contributions are readily computable. However, this then becomes a rather model-dependent procedure because VLQ masses can be generated by various means, including some version of the Higgs mechanism, or a Frogatt-Nielsen mechanism, etc. Rather than rely on a specific model, in what follows, for generality, we shall follow the approach of Ref. [68] and obtain bounds on the couplings of gauge VLQs by dropping the contributions from the unphysical states.

In general, a VLQ could couple to both left-handed and right-handed fermions, so we shall assume the general form of the coupling. We note, however, that there are stringent bounds [70] from low-energy data if leptoquarks couple to both left- and right-handed states, and it is generally assumed that their couplings are chiral. For a quark of flavor q and a lepton ℓ, we adopt the interaction vertex $i\gamma_\mu[\lambda_L^{\ell q} P_L + \lambda_R^{\ell q} P_R]$, which leads to the contribution to D meson mixing,

$$
\begin{aligned}
x_{\mathrm{D}}^{(\mathrm{VLQ})} &= \frac{1}{8\pi^2 m_{LQ}^2 \Gamma_D M_D}\Big[(\lambda_{LL}\langle Q_1\rangle + 2\lambda_{LR}\langle Q_2\rangle \\
&\quad + \lambda_{RR}\langle Q_6\rangle) + \frac{10}{9}\frac{m_c^2}{m_{LQ}^2}(\lambda_{LL}\langle Q_7\rangle + 2\lambda_{LR}\langle Q_3\rangle \\
&\quad + \lambda_{RR}\langle Q_4\rangle)\Big] \\
&= \frac{f_D^2 M_D B_D}{12\pi^2 m_{LQ}^2 \Gamma_D}\Big[(\lambda_{LL} + \lambda_{RR}) - \frac{3}{2}\lambda_{LR}\Big(1 + \frac{2}{3}\eta\Big)\Big],
\end{aligned}
\tag{74}
$$

where $\lambda_{PP'} \equiv \sum_{ij}(\lambda_P^{\ell_i c}\lambda_P^{\ell_i u})(\lambda_{P'}^{\ell_j c}\lambda_{P'}^{\ell_j u})$, and we neglect $\mathcal{O}(m_c/m_{LQ})$ corrections in the last line. The resulting bounds on VLQ interactions are displayed in Fig. 11.

VI. EXTRA SCALARS

No known physical principle restricts the number of Higgs multiplets that can participate in electroweak symmetry breaking. In fact, several theories beyond the SM, such as supersymmetry and those with extended gauge sectors, require an enlarged Higgs sector in order to break the additional symmetries. Here we examine the effect in D^0-$\bar{D}^0$ mixing of models with multiple Higgs doublets, with and without flavor conservation, Higgsless models and models with scalar leptoquarks.

A. Flavor-conserving two-Higgs-doublet models

A simple extension of the SM is to enlarge the Higgs sector by one additional $SU(2)$ doublet. We first examine two-Higgs-doublet models that naturally avoid tree-level FCNC by requiring that all fermions of a given charge receive their masses from only one Higgs doublet [39]. In

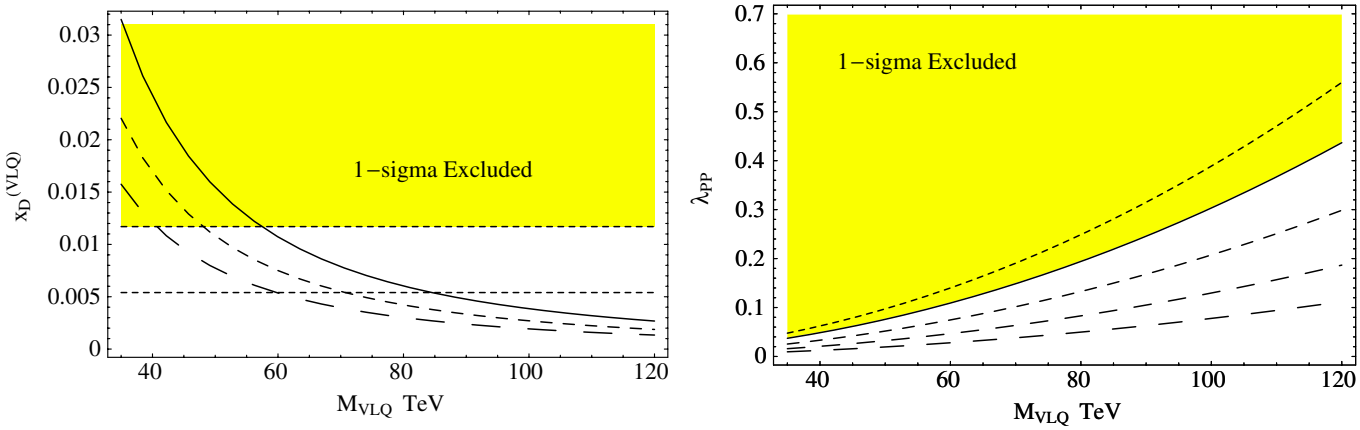

FIG. 11 (color online). Left: x_{D} in vector leptoquark models as a function of the vector leptoquark mass M_{VLQ}, with $\lambda_{PP} = 0.1$ (solid line), $\lambda_{PP} = 0.07$ (short dash), and $\lambda_{PP} = 0.05$ (long dash) for $P = L$ or R. The 1σ experimental bounds are as indicated, with the yellow shaded area depicting the region that is excluded. Right: The present 1σ excluded region in the vector leptoquark mass–coupling parameter plane, as well as possible future contours taking $x_{\mathrm{D}} < (15.0, 8.0, 5.0, 3.0) \times 10^{-3}$, corresponding to the blue (dark gray) dashed, red (gray) dashed, cyan (lightest gray) dotted, and green (light gray) dot-dashed curves, respectively.

one such model, known in the literature as model II, one doublet (ϕ_2) gives mass to the up-type quarks, while the down-type quarks and charged leptons receive their mass from the other doublet ϕ_1. This is the scenario that is present in supersymmetric theories and is in fact required by supersymmetry in order to generate masses for all the fermions. Another model, known as model I, imposes a discrete symmetry such that one doublet (ϕ_2) generates masses for all fermions and the second (ϕ_1) decouples from the fermion sector. In both cases, each doublet receives a vacuum expectation value v_i, subject to the constraint that $v_1^2 + v_2^2 = v_{\rm SM}^2$. There are five physical scalars in these models, h^0, H^0, A^0, and $H^\pm$. The charged Higgs boson can participate in the box diagram for ΔM_D in exchange with the SM $Q = -1/3$ quarks as shown in Fig. 12. The $H^\pm$ interactions with the quark sector are governed by the Lagrangian

$$\mathcal{L} = \frac{g}{2\sqrt{2}M_W} H^\pm [V_{ij} m_{u_i} A_u \bar{u}_i (1 - \gamma_5) d_j + V_{ij} m_{d_j} A_d \bar{u}_i (1 + \gamma_5) d_j] + \text{H.c.}, \tag{75}$$

with $A_u = \cot\beta$ in both models and $A_d = -\cot\beta(\tan\beta)$ in model I(II), where $\tan\beta \equiv v_2/v_1$. The $H^\pm$ can have a large contribution [71] to the rare decay $b \to s\gamma$, and in model II the branching fraction for this process sets the bound [72] $M_{H^\pm} \gtrsim 295$ GeV at 95% C.L. This constraint is relaxed when other sources of new physics also contribute to $b \to s\gamma$, such as in supersymmetry. In this case, the lower limit on the charged Higgs mass is 78.6 GeV from LEP II data [13].

It is clear that the contributions to ΔM_D from the first term in this Lagrangian (which are proportional to $m_{c,u}\cot\beta$) will only be sizable for extremely small values of $\tan\beta$; this region is, however, already excluded [73] from, e.g., $b \to s\gamma$ and B_d^0-$\bar{B}_d^0$ mixing. In addition, since the contributions in model I go as $\cot\beta$ multiplied by small mass factors, the effects in this case are also restricted to be small. However, the term proportional to $m_{b,s}\tan\beta$ in model II has the potential to generate a significant contribution to D mixing in the large $\tan\beta$ limit. We will thus work in this limit here. Restrictions on the size of $\tan\beta$ can be obtained by requiring that the $\bar{t}bH^+$ coupling remain perturbative. If we demand that this coupling not exceed the value of the strong coupling constant, g_s, we find that $\tan\beta \lesssim 100$.

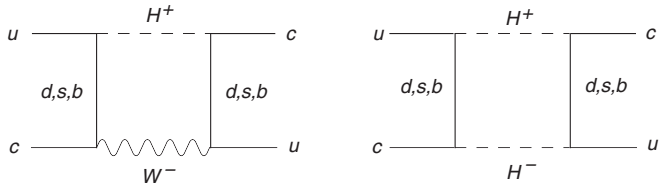

FIG. 12. Box diagrams with charged Higgs contributions to D meson mixing.

The effective Hamiltonian governing D meson mixing in the large $\tan\beta$ limit takes the form

$$\mathcal{H}_{\rm 2HDM} = \frac{G_F^2 M_W^2}{4\pi^2} \sum_{i,j} \lambda_i \lambda_j \{\tan^4\beta A_{HH}(x_i, x_j, x_H) + \tan^2\beta A_{WH}(x_i, x_j, x_H)\} Q_1, \tag{76}$$

where $\lambda_i = V_{ui} V_{ci}^*$ as usual, $x_i = m_i^2/M_W^2$, the sum extends over $i, j = s, b$, the loop functions can be found in Ref. [73] and are given in the appendix. The operator structure is the same as in Eq. (34); here, the Q_1 operator appears due to the presence of the fermion propagator. Note that this structure is quite different than for the case of $B_{d,s}$ mixing [74] in the large $\tan\beta$ limit. This is simply due to the helicity structure of the couplings when the charged $-1/3$ quarks are internal. The QCD evolution to the charm-quark scale is simple and results in the factor of $r_1(m_c, M_{H^\pm})$. The resulting contribution to the mass difference is

$$x_{\rm D}^{\rm (2HDM)} = \frac{G_F^2 M_W^2}{6\pi^2 \Gamma_D} f_D^2 M_D B_D r_1(m_c, M_{H^\pm}) \times \sum_{i,j} \lambda_i \lambda_j [\tan^4\beta A_{HH}(x_i, x_j, x_H) + \tan^2\beta A_{WH}(x_i, x_j, x_H)]. \tag{77}$$

Our results for $x_{\rm D}^{\rm (2HDM)}$ are displayed in Fig. 13 as a function of $\tan\beta$ for various values of the charged Higgs

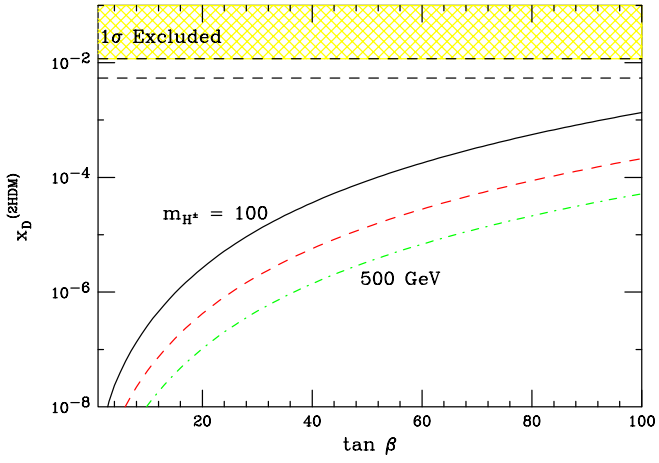

FIG. 13 (color online). $x_{\rm D}^{\rm (2HDM)}$ in the flavor-conserving two-Higgs-doublet model as a function of $\tan\beta$ for charged Higgs boson masses of $m_{H^\pm} = 100$, 250, and 500 GeV, corresponding to the solid, dashed red (gray), and dashed-dot green (light gray) curves, respectively. The 1σ experimental bounds are as indicated, with the yellow shaded region depicting the region that is excluded.

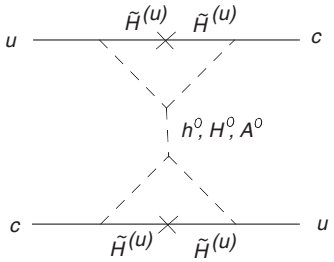

FIG. 14. The dipenguin diagram with neutral Higgs exchange.

mass. We see that the effect is quite small and even at large values of $\tan\beta$ the contributions from this model are at least an order of magnitude below the experimental observation.

In the down-quark sector, sizable effects in $B_{d,s}$ and K meson mixing are obtained in the large $\tan\beta$ limit from a double penguin contribution with neutral Higgs exchange [74] as depicted in Fig. 14. In this limit, an effective Yukawa interaction is induced for the down-type quarks which includes a contribution from the large Yukawa coupling of the top quark. This generates sizable one-loop FCNC couplings for the neutral Higgs in the down-quark sector. While the same effects occurs in the up-quark sector, the term that becomes significant at large $\tan\beta$ is now proportional to the down quark Yukawa coupling and hence does not generate a sizable effect in D^0-$\bar{D}^0$ mixing.

B. Flavor-changing neutral Higgs models

It is well known that the existence of multiple Higgs doublets can lead in general to tree-level FCNC transitions [39]. In the down-quark sector, there are severe constraints on such couplings from Kaon decays, but these do not necessarily lead to equally strong restrictions in the up-quark sector.

The phenomenological requirement that FCNC effects in the down-strange sector must be very small can be met in a variety of ways. For example, the imposition of global symmetries can make $\Delta S = 1$ FCNC vanish without affecting the $|\Delta C| = 1$ sector [75]. Another example is the Cheng-Sher ansatz [76], where the flavor-changing couplings of the neutral Higgs bosons are given by $\lambda_{h^0 f_i f_j} \simeq (\sqrt{2}G_F)^{1/2}\sqrt{m_i m_j}\Delta_{ij}$, with the $m_{i(j)}$ being the relevant fermion masses and Δ_{ij} representing a combination of mixing angles.

To keep our initial discussion general, we allow for N Higgs scalars, which have the interactions in the up-quark sector

$$\mathcal{L} \sim \lambda^u_{ijn}\bar{Q}_{Li}u_{Rj}\phi_n, \tag{78}$$

where Q_L represents the left-handed quark doublet and u_R is the singlet state. If $M_{\rm H}$ is the mass of the lightest physical Higgs with flavor-changing couplings, the most general effective four-fermion Hamiltonian just below the $M_{\rm H}$ scale is

$$\mathcal{H}_H = -\frac{1}{2M_{H^2}}[2G_1Q_3 + G_2Q_7 + G_3Q_4], \tag{79}$$

where the couplings $G_{1,2,3}$ are model-dependent parameters. As shown in Ref. [77],

$$G_1 = \sum_{nmN}\lambda^{u*}_{12n}\lambda^u_{21m}A_{nN}A^*_{mN},$$
$$G_2 = G_3 = \frac{1}{2}\sum_{nmN}[\lambda^u_{21n}\lambda^u_{21m}A_{nN}A_{mN} + \lambda^{u*}_{12n}\lambda^{u*}_{12m}A^*_{nN}A^*_{mN}], \tag{80}$$

at the $M_{\rm H}$ scale. Here, A_{nN} refers to the mixing matrix which rotates the Higgs doublets Φ_n to their N neutral physical eigenstates. Matching at the Higgs mass scale relates the Wilson coefficients to the three couplings $G_{1,2,3}$ via

$$C_3(M_H) = -2G_1, \qquad C_7(M_H) = -G_2, \qquad C_4(M_H) = -G_3, \tag{81}$$

with all other Wilson coefficients being zero. Assuming that $M_{H_N} > m_t$ for all N and computing the evolution of Eq. (79) to $\mu = m_c$ we obtain

$$\mathcal{H}_H = \frac{1}{2M_{H^2}}[C_3(m_c)Q_3 + C_4(m_c)Q_4 + C_5(m_c)Q_5 + C_7(m_c)Q_7 + C_8(m_c)Q_8], \tag{82}$$

with

$$\begin{aligned}
C_3(m_c) &= r_3(m_c, M_H)C_3(M_H),\\
C_4(m_c) &= \left[\left(\frac{1}{2} - \frac{8}{\sqrt{241}}\right)r_4(m_c, M_H) + \left(\frac{1}{2} + \frac{8}{\sqrt{241}}\right)r_5(m_c, M_H)\right]C_4(M_H),\\
C_5(m_c) &= \frac{1}{8\sqrt{241}}[r_4(m_c, M_H) - r_5(m_c, M_H)]C_4(M_H),\\
C_7(m_c) &= \left[\left(\frac{1}{2} - \frac{8}{\sqrt{241}}\right)r_7(m_c, M_H) + \left(\frac{1}{2} + \frac{8}{\sqrt{241}}\right)r_8(m_c, M_H)\right]C_7(M_H),\\
C_8(m_c) &= \frac{1}{8\sqrt{241}}[r_7(m_c, M_H) - r_8(m_c, M_H)]C_7(M_H).
\end{aligned} \tag{83}$$

The Higgs tree-level contribution to $x_{\rm D}$ is found by evaluating the D^0-to-$\bar{D}^0$ matrix element, which gives

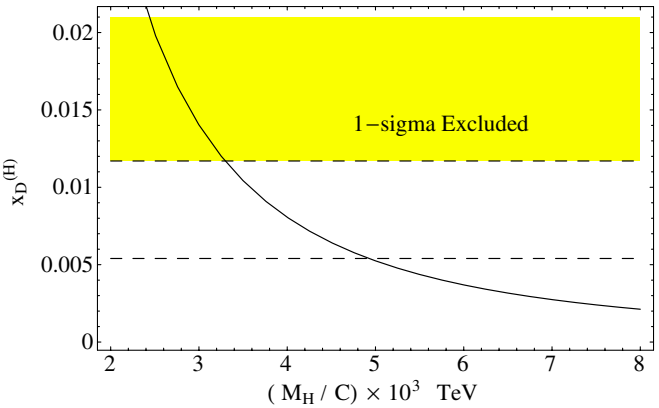

FIG. 15 (color online). x_D as a function of M_H/C in models with no natural flavor conservation in the Higgs sector. The 1σ experimental bounds are as indicated, with the yellow shaded area depicting the region that is excluded.

$$x_D^{(H)} = \frac{5 f_D^2 M_D B_D}{24 \Gamma_D M_H^2}\left[\frac{1+6\eta}{5} C_3(m_c) - \eta(C_4(m_c) + C_7(m_c)) + \frac{12\eta}{5}(C_5(m_c) + C_8(m_c))\right]. \quad (84)$$

where, again, we have used Eqs. (24) and (26). Together with Eqs. (81) and (83), the above can be used to constrain the lightest Higgs mass and associated couplings. As an example, let us assume that $|G_1| = |G_2| = C^2$ at the Higgs mass scale in Eq. (79) and M_H is the effective mass of the N Higgs scalars. In that case, the restriction on possible values of the effective Higgs mass are presented in Fig. 15.

We now return to the specific case of the Cheng-Sher ansatz. Here, the neutral Higgs bosons can contribute to ΔM_D through tree-level exchange as well as mediating D meson mixing by H^0 and t-quark virtual exchange in a box diagram. The restrictions placed on the parameter space of this model from the tree-level contribution are computed as described above, and are presented for an effective Higgs mass M_H as a function of the coupling parameter Δ_{uc} in Fig. 16. We see that the form of the couplings, being proportional to the light quark masses, results in reduced limits compared to those in Fig. 15 for the general case. The box contribution with H^0, t-quark exchange is described by the effective Hamiltonian just below the M_H scale of

$$\mathcal{H}_{\rm CS} = \frac{G_F^2 m_u m_c m_t^2 \Delta_{ut}^2 \Delta_{ct}^2}{8\pi^2 M_H^2} F_{tH}(x)[Q_1 + Q_6], \quad (85)$$

where $x = m_t^2/M_H^2$, $F_{tH}(x)$ is given in the appendix, and the vector operators $Q_{1.6}$ are generated from the fermion propagators. The RG evolution and evaluation of the matrix elements yields

$$x_D^{(CS)} = \frac{G_F^2 m_u m_c m_t^2 \Delta_{ut}^2 \Delta_{ct}^2}{6\pi^2 M_H^2 \Gamma_D} f_D^2 M_D B_D F_{tH}(x) r_1(m_c, M_H). \quad (86)$$

The resulting constraints from this contribution are displayed in Fig. 16 in the effective Higgs mass–coupling parameter plane. We see that this box contribution only competes with those from the tree-level process for large values of Δ_{ij}.

C. Scalar leptoquark bosons

Leptoquarks are color triplet particles which couple to a lepton-quark pair and are naturally present in many theo-

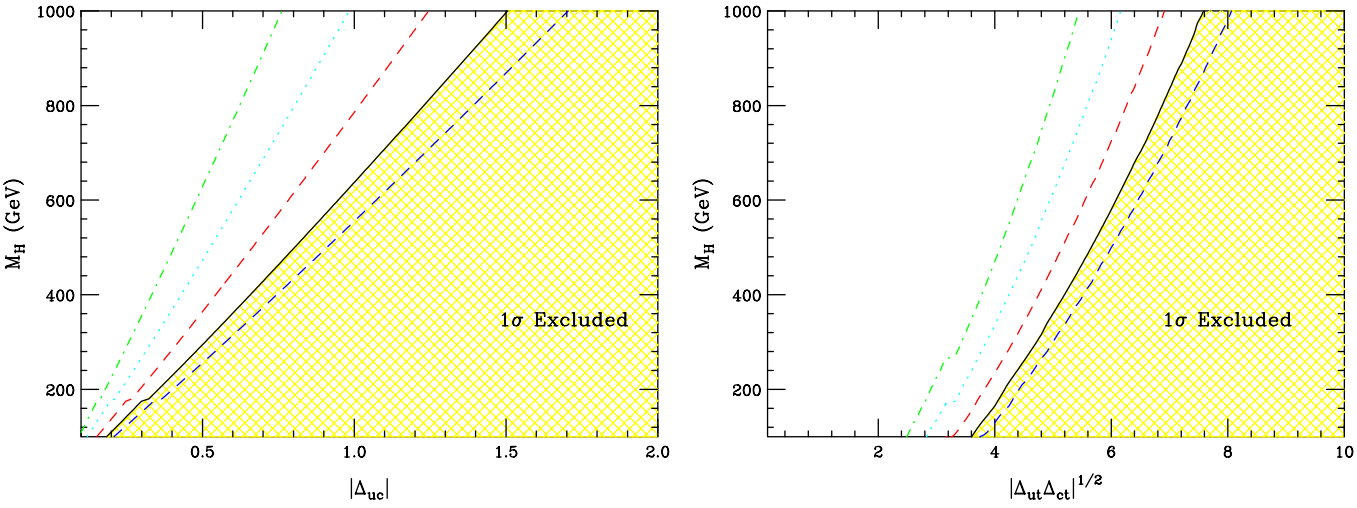

FIG. 16 (color online). Left: 1σ excluded region in the effective neutral Higgs mass–coupling plane for the tree-level contribution to D^0-$\bar{D}^0$ mixing in the Cheng-Sher ansatz. Right: 1σ excluded region in the effective neutral Higgs mass–coupling plane for the box diagram contribution to D^0-$\bar{D}^0$ mixing in the Cheng-Sher ansatz. In both figures, possible future contours taking $x_D <$ $(15.0, 8.0, 5.0, 3.0) \times 10^{-3}$, corresponding to the blue (dark gray) dashed, red (gray) dashed, cyan (lightest gray) dotted, and green (light gray) dot-dashed curves, respectively, are also displayed.

ries beyond the SM which relate leptons and quarks at a more fundamental level. Their *a priori* unknown couplings can be parametrized as $\lambda^2_{\ell q}/4\pi = F_{\ell q}\alpha$. Searches for the pair production of scalar leptoquarks at the Tevatron run II yield the bounds [78] $m_{LQ} \gtrsim 225$ GeV, which are independent of the coupling strength $F_{\ell q}$

Scalar leptoquarks participate in D meson mixing via virtual exchange inside a box diagram [68], together with a charged lepton or neutrino. Their interactions are analogous to those of R-parity violating supersymmetric models with the terms in the superpotential proportional to λ'. We thus refer to Sec. VIII C for the details of the analysis for these contributions. The resulting constraints on scalar leptoquark are governed by the translation

$$F_{\ell u}F_{\ell c} = \frac{\lambda'_{R_p(i2k)}\lambda'_{R_p(i2k)}}{4\pi\alpha} \quad \text{with} \quad m_{\tilde{d}} = m_{LQ}. \tag{87}$$

D. Composite Higgs models

A class of composite Higgs models which has been developed recently to generate a naturally light Higgs, employs chiral symmetries of "theory space" [79] (see also Refs. [40,80]). Such models involve the "deconstruction" of higher-dimensional field theories such that the low-energy effective field theory resembles the standard model but has nice features such as the absence of quadratic divergences of the Higgs mass. Here, the Higgs can be interpreted as a Goldstone boson of some interaction occurring at higher energies. This approach allows for the construction of realistic theories of electroweak symmetry breaking in four spacetime dimensions without any higher-dimensional interpretation.

This picture emerges from the AdS/CFT correspondence of the 5D Higgsless model of Csaki *et al.* [81]. In the 5D framework, there is no physical Higgs boson and electroweak symmetry breaking is generated via the boundary conditions for the 5th dimension. The gauge symmetry in the higher-dimensional space is $SU(2)_L \times SU(2)_R \times U(1)_{B-L}$ and the right-handed gauge fields receive Planck scale masses. The Kaluza-Klein towers of the γ and Z bosons unitarize the WW high energy scattering amplitude [82], although there is some tension with precision electroweak data as to the precise energy scale that the Kaluza-Klein states populate [83]. The standard model fermion fields are localized within the 5th dimension and also receive their masses from the boundary conditions, with the exact value being dependent on their position in the extra dimension [84]. The effects on D mixing from this 5D picture are presented below in Sec. VII C. Here, we present our results for the AdS/CFT related framework with a composite Higgs.

The key idea in the composite Higgs picture is that the flavor physics responsible for generation of the Yukawa couplings can induce flavor-changing neutral currents [79]. Applied to charm physics they generically lead to the following effective Hamiltonian,

$$\begin{aligned}\mathcal{H}_{\not H} = \sum_{\mathcal{C}=1,T^a}\Big[& (c^c_L s^c_L)^2 \frac{g^2}{M^2}(\bar{u}_L\gamma_\mu \mathcal{C} c_L)(\bar{u}_L\gamma^\mu \mathcal{C} c_L) \\ & + 2(c^c_L s^c_L)(c^c_R s^c_R)\frac{g^2}{M^2}(\bar{u}_L\gamma_\mu \mathcal{C} c_L)(\bar{u}_R\gamma^\mu \mathcal{C} c_R) \\ & + (c^c_R s^c_R)^2 \frac{g^2}{M^2}(\bar{u}_R\gamma_\mu \mathcal{C} c_R)(\bar{u}_R\gamma^\mu \mathcal{C} c_R)\Big],\end{aligned} \tag{88}$$

where g, M are, respectively, the gauge coupling and gauge boson mass of new flavor gauge interactions, and the mixing angles generate different strengths for the gauge coupling. In the sum over the color label $\mathcal{C}$, the case $\mathcal{C} = 1$ corresponds to color-singlet interactions, whereas $\mathcal{C} = T^a$ refers to color-octet interactions for which $T^a \equiv \lambda^a/2$ are the generators of $SU(3)_C$. In addition, the angles $\theta^c_{L,R}$ that relate the gauge and mass eigenstates [79] appear in factors of $c^c_{L,R} \equiv \cos\theta^c_{L,R}$, $s^c_{L,R} \equiv \sin\theta^c_{L,R}$, where we take $\theta^c_{L,R} \sim \theta_C$, with θ_C being the Cabibbo angle.

The Hamiltonian of Eq. (88) can be easily transformed to contain the operators from the general basis of Eq. (16),

$$\mathcal{H}_{\not H} = (c^c_L s^c_L)^2 \frac{g^2}{M^2}(C^{\not H}_1 Q_1 + C^{\not H}_2 Q_2 + C^{\not H}_3 Q_3 + C^{\not H}_6 Q_6), \tag{89}$$

where $C^{\not H}_1 = (3N_c - 1)/(2N_c)$, $C^{\not H}_2 = r_{LR}(2N_c - 1)/(2N_c)$, $C^{\not H}_3 = -r_{LR}$, $C^{\not H}_6 = r^2_{LR}C^{\not H}_1$, and $r_{LR} = (c^c_R s^c_R)/(c^c_L s^c_L)$. Performing the RG running, we obtain the effective Hamiltonian at the scale m_c with the Wilson coefficients

$$\begin{aligned}\mathrm{C}_1(m_c) &= r_1(m_c, M)\mathrm{C}_1(M), \\ \mathrm{C}_2(m_c) &= r_2(m_c, M)\mathrm{C}_2(M), \\ \mathrm{C}_3(m_c) &= \frac{2}{3}[r_2(m_c, M) - r_3(m_c, M)]\mathrm{C}_2(M) \\ &\quad + r_3(m_c, M)C_3(M), \\ \mathrm{C}_6(m_c) &= r_6(m_c, M)\mathrm{C}_6(M).\end{aligned} \tag{90}$$

This, in turn, implies for the mixing amplitude,

$$\begin{aligned}x^{(\not H)}_{\mathrm{D}} = \frac{f^2_D M_D B_D}{\Gamma_D}(c^c_L s^c_L)^2 \frac{g^2}{M^2}\Big[& \frac{2}{3}(C_1(m_c) + C_6(m_c)) \\ & + -C_2(m_c)\Big(\frac{1}{2} + \frac{\eta}{3}\Big) + \frac{1}{12}C_3(m_c)(1 + 6\eta)\Big],\end{aligned} \tag{91}$$

where η is as in Eq. (26). The available experimental data can be used to constrain the mass of the gauge boson M for different values of the coupling constant g, as shown in Fig. 17. It is clear that unless g is very small, it is unlikely that any of the gauge bosons of the new flavor interactions of Higgsless models will be directly seen at the LHC.

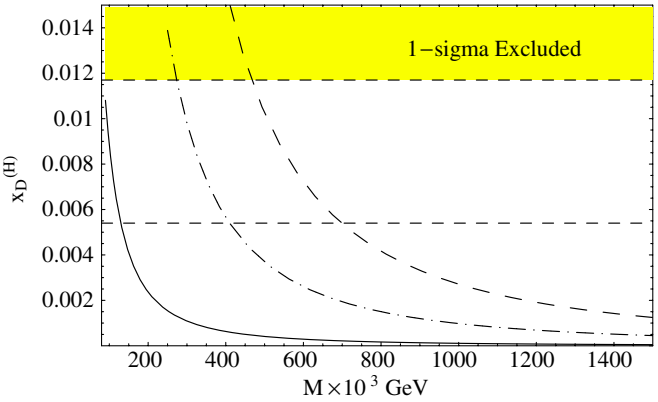

FIG. 17 (color online). x_D as a function of the new gauge boson mass M in composite Higgs models for $g = 0.1$ (solid line), $g = 0.3$ (dash-dotted line), and $g = 0.5$ (dashed line). The 1σ experimental bounds are as indicated, with the yellow shaded area depicting the region that is excluded.

VII. EXTRA SPACE DIMENSIONS

Recent speculation that the geometry of spacetime could resolve the hierarchy problem have led to theories with extra spatial dimensions that have verifiable consequences at the TeV scale. There are several such models [85] and the size and geometry of the additional spatial dimensions, as well as the field content that is allowed to propagate within them, varies between the different scenarios. When the extra dimensions are compactified, the fields that reside in the higher-dimensional space (known as the bulk) expand into Kaluza-Klein (KK) towers of states. The masses of these KK states correspond to the extra dimensional components of the bulk field momentum and are related to the bulk geometry. The observation, either directly or by indirect effects, of these KK states signals the existence of extra dimensions. The properties of the KK states reveal the underlying geometry of the higher-dimensional spacetime.

The extra dimensional theories which yield contributions to $\Delta F = 2$ processes are those in which the SM fermion fields reside in the bulk. Here, we consider three such scenarios: (i) universal extra dimensions, (ii) localized fermions in a flat extra dimension, and (iii) warped extra dimensions.

A. Universal extra dimensions

The possibility of TeV^{-1}-sized extra dimensions naturally arises in braneworld theories [86]. By themselves, they do not allow for a reformulation of the hierarchy problem, but they may be incorporated into a larger structure in which this problem is solved. The scenario which places all standard model fields in the bulk is known as universal extra dimensions [87]. The simplest model of this type contains a single extra dimension compactified on an S_1/Z_2 orbifold. Since branes are not present in this case, translational invariance in the higher-dimensional space would be preserved without the presence of the orbifolding. This leads to the tree-level conservation of the extra dimensional momentum of the bulk fields, which in turn implies that KK number is conserved at tree-level while KK parity, $(-1)^n$ where n denotes the KK level, is conserved to all orders in interactions involving the KK states. Two immediate consequences of KK number and parity conservation are that the KK states must be produced in pairs, and the lightest KK particle is stable and is a dark matter candidate [88]. The former results in a substantial reduction of the sensitivity to such states in precision electroweak and collider data. The present bound from run I at the Tevatron on the mass of the first KK excitation is of order 250 GeV [89].

Since all SM fields reside in the bulk in this model, every SM field expands into a KK tower of states. The KK reduction of the 5D fermion fields leaves a chiral zero-mode and a vectorlike tower of KK states for each flavor. There is one KK tower for each SM gauge boson, as well as the Higgs, and additional towers of KK scalars, $a^0_{(n)}$ and $a^\pm_{(n)}$, which correspond to the physical eigenstates of the mixing between the KK towers associated with the SM Goldstone fields and the W_5, Z_5 remnants from the electroweak gauge KK reduction. This mixing also generates scalar KK towers which behave as Goldstone fields, which are eaten by the gauge boson KK towers and provide masses for the gauge KK states. The additional physical scalar KK towers $a^{0,\pm}_{(n)}$ do not have zero modes. The masses of the KK states are roughly degenerate and are given at tree level by

$$m_n = (m_0^2 + n^2/R_c^2)^{1/2}, \tag{92}$$

where R_c represents the compactification radius of the extra dimension and m_0 is the zero-mode mass. The KK states clearly become more degenerate with increasing KK level (increasing n). These masses are modified [90] by loop-induced localized kinetic terms and nonlocal radiative corrections. Given that the effect of these mass corrections occurs at two-loop order in D meson mixing, one would expect them to have a small effect. We thus neglect them in our initial analysis, but will return to this issue at the end of this section.

The contributions to D mixing in this model are box diagrams with the $W^\pm$ boson KK tower, its associated KK Goldstone modes $G^\pm_{(n)}$, and the $a^\pm_{(n)}$, all in exchange with the KK towers associated with the d, s, and b quarks; the zero-mode analogues of these diagrams are shown in Fig. 12. Note that the conservation of KK parity restricts the KK levels of the KK quark and boson being exchanged. In addition, only the quark KK towers that are even under the Z_2 symmetry (and thus have a zero mode) couple to the external zero-mode quarks in the box diagram. The relevant Hamiltonian at the compactification scale is then

$$\mathcal{H}_{\rm UED} = \frac{G_F^2 M_W^2}{4\pi^2} \sum_{n=1}^{\infty} \sum_{i,j} \lambda_i \lambda_j S(x_i^{(n)}, x_j^{(n)}) Q_1, \qquad (93)$$

which has the same structure as that occurring in Eq. (34). Here, i, j run over d, s, b. Note that at all KK levels, the CKM structure is the same as that in the SM. Using unitarity of the CKM matrix, the function $S(x_i^{(n)}, x_j^{(n)})$ becomes

$$S(x_i^{(n)}, x_j^{(n)}) = \sum_{XY} (F_{XY}(x_i^{(n)}, x_j^{(n)}) + F_{XY}(x_d^{(n)}, x_d^{(n)}) - F_{XY}(x_i^{(n)}, x_d^{(n)}) - F_{XY}(x_j^{(n)}, x_d^{(n)})), \qquad (94)$$

with $x_i^{(n)} = (m_n^i)^2/(m_n^W)^2$ where now $i, j = s, b$, and the sum extends over the bosons $X, Y = W_{(n)}^{\pm}, G_{(n)}^{\pm}, a_{(n)}^{\pm}$. The functions $F_{XY}(x_i^{(n)}, x_j^{(n)})$ are given in the appendix of Ref. [91], with the appropriate substitutions of quark flavors relevant for D mixing. After the RG evolution of the Hamiltonian to the charm-quark scale, this leads to

$$x_{\rm D}^{\rm (UED)} = \frac{G_F^2 M_W^2}{6\pi^2 \Gamma_D} f_D^2 M_D B_D r_1(m_c, m_1) \times \sum_{n=1}^{\infty} \sum_{i,j} \lambda_i \lambda_j S(x_i^{(n)}, x_j^{(n)}). \qquad (95)$$

Looking at the expression in Eq. (92) for the KK masses, we see that the d- and s-quark KK towers are degenerate and the mass splittings between the b- and d-, s-quark towers are nonzero, yet small, for the first couple of KK levels and then effectively vanish for higher KK excitations. The GIM cancellation is thus exact in the case of the s-quark KK tower contributions, level by level in the KK tower, and leaves a tiny contribution from the first few b-quark KK states. However, factoring in that $\lambda_b \sim \mathcal{O}(10^{-4})$, we see that the contributions to D mixing from the b-quark KK states are numerically negligible. Hence, this model is not probed by D^0-$\bar{D}^0$ mixing.

We now return to the case where mass splittings are generated for the KK states via localized boundary terms or loop-induced gauge interactions. Since the above one-loop contributions to D mixing essentially vanish due to the degeneracy of the KK towers, perhaps a non-negligible effect is obtained once the KK degeneracy is lifted. Examining the latter effect first, we see from Ref. [90] that the nonlocal radiative corrections yield two classes of mass splittings for the fermion fields: (i) a term which is dependent on the gauge couplings and is flavor independent, and (ii) a term which depends on the fermion's Yukawa couplings. The latter term takes the form

$$\delta m_n^f = m_n^f \left(\frac{-3h_f^2}{16\pi^2 X} \ln \frac{\Lambda^2}{\mu^2} \right), \qquad (96)$$

where $X = (2, 4)$ for fermion (singlets, doublets), respectively, h_f is the fermion Yukawa coupling, Λ represents a cutoff scale which absorbs the logarithmic divergences and μ is the renormalization scale. If $1/R_c$ is of order a few hundred GeV, the third generation quark doublet and top-quark singlet thus receives a correction from the Yukawa term of order 10–20 GeV for the first KK state, while the b-quark singlet KK excitation remains essentially unaffected. Given the small CKM factor for the b-quark KK contributions to D meson mixing, and the effectiveness of the GIM mechanism, we find that this mass splitting is not enough to generate a sizable contribution to $x_{\rm D}$. The second possibility of including the localized boundary terms holds the promise of inducing large mass splittings between the KK states associated with the various quark flavors. However, these boundary terms may take on essentially any value with no predictivity, leaving a virtual continuum of possible contributions to D^0-$\bar{D}^0$ mixing.

B. Split fermion models

In this scenario, the standard model fermions are localized at specific points, y_i, where $0 \leq y_i \leq R_c$, in extra TeV^{-1}-sized flat dimensions. The fermions have narrow Gaussian-like wave functions in the extra dimensions with the width of their wave function being much smaller than the compactification radius R_c of the additional dimensions. The placement of the different fermions at distinct locations in the additional dimensions, along with the narrowness of their wave functions, can then naturally suppress [92] operators mediating dangerous processes such as proton decay and also provide a mechanism for generating the fermion mass hierarchy [93].

This split fermion scenario is capable of generating large flavor-changing neutral currents [94,95]. In contrast to the fermion sector, the gauge bosons are free to propagate throughout the extra dimensions. The gauge KK states have cosine profiles which have different heights at the various distinct fermion locations, generating nonuniversal couplings to different fermion species. This leads to tree-level FCNC as depicted in Fig. 18, with the gluon KK states clearly giving the largest contributions.

With one extra dimension, the coupling of the nth KK gluon to a quark localized at the scaled position y_q is determined by the overlap of wave functions in the additional dimension

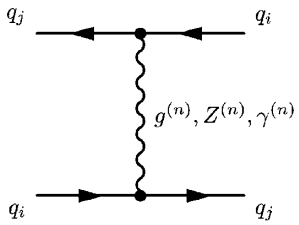

FIG. 18. Tree-level gauge KK exchange that mediates neutral meson oscillations.

$$\int_0^1 dy\bar{\psi}(y)\psi(y)G^{(n)}(y) \sim \int_0^1 dy\cos(n\pi y)e^{-(y-y_q)^2R_c^2/\sigma^2} \sim \cos\left(\frac{n\pi y_q}{R_c}\right)e^{-n^2\sigma^2/R_c^2}, \quad (97)$$

where σ represents the width of the quark's localized wave function with $\sigma/R_c \ll 1$, and y_q has been normalized to R_c so that it lies in the range $0 \leq y_q \leq 1$. The interaction Lagrangian in the quark mass eigenstate basis is then

$$\mathcal{L} = \sum_{n=1}^{\infty}[\sqrt{2}g_s G_\mu^{A(n)}(\bar{\mathbf{u}}_L\gamma^\mu T^A V_L^u C_L^{(n)} V_L^{u\dagger}\mathbf{u}_L + \bar{\mathbf{u}}_R\gamma^\mu T^A V_R^u C_R^{(n)} V_R^{u\dagger}\mathbf{u}_R + (\mathbf{u}\to\mathbf{d})], \quad (98)$$

where the product $V_L^{u\dagger}V_L^d$ is the usual CKM matrix, the diagonal matrices $C_{L,R}^{(n)}$ are the wave function overlaps given above in Eq. (97), and the factor of $\sqrt{2}$ arises from the renormalization of the KK gauge kinetic terms to the canonical value. $\mathbf{u_i}$ refers to the set $(u_i, c_i.t_i)$.

The effective Hamiltonian mediating D meson mixing is given by (taking the contributions from the first two generations to be dominant)

$$\mathcal{H}_{\text{split}} = \frac{2}{3}g_s^2\sum_{\tilde{n}=1}^{\infty}\frac{1}{M_n^2}(U_{L(cu)}^{u(n)\dagger}U_{L(uc)}^{u(n)}Q_1 + 2U_{L(cu)}^{u(n)\dagger}U_{R(uc)}^{u(n)}Q_2 + U_{R(cu)}^{u(n)\dagger}U_{R(uc)}^{u(n)}Q_6), \quad (99)$$

where $U_i^{u(n)} \equiv V_i^{u\dagger}C_i^{(n)}V_i^u$ with $i = L$, R, and M_n is the mass of the nth gluon KK state with $M_n = n/R_c$. For the case of one additional dimension, the sum over the gluon KK tower converges, and for the scenario with numbers of extra dimensions >1, the sum is naturally cut off from the finite width of the fermion wave function. Performing this sum [95] and making use of the unitarity properties of the $V_{L,R}^q$, we can write the effective Hamiltonian at the compactification scale as

$$\mathcal{H}_{\text{split}} = \frac{2}{3}g_s^2R_c^2(|V_{L11}^uV_{L12}^{u*}|^2F(y_{u_L}, y_{c_L})Q_1 + 2|V_{L11}^uV_{L12}^{u*}V_{R11}^uV_{R12}^{u*}|G(y_{u_L}, y_{c_L}, y_{u_R}, y_{c_R})Q_2 + |V_{R11}^uV_{R12}^{u*}|^2F(y_{u_R}, y_{c_R})Q_6), \quad (100)$$

with y_{u_i,c_i} being the positions of the up- and charm-quark fields, and

$$F(x,y) = \frac{\pi^2}{2}|x-y|,$$
$$G(x_1,y_1,x_2,y_2) = \frac{-\pi^2}{4}(|x_1-x_2| + |y_1-y_2| - |x_1-y_2| - |x_2-y_1|). \quad (101)$$

Although some cancellations could occur between the $Q_{1,6}$ and Q_2 terms by finely tuning the quark positions, and thus decreasing the KK gluon contribution to D meson mixing, operator mixing from QCD renormalization would spoil this possibility. The RG running of the above effective Hamiltonian is the same as that performed for the case of flavor-changing Z' bosons in Sec. V A, with the appropriate replacement of the Wilson coefficients, since the same operator basis of $Q_{1,2,6}$ is present.

In order to explore the magnitude of the KK gluon FCNC effects we examine a single term in the above Hamiltonian. This will reduce the number of parameters in the computation without significantly changing the results. Choosing the term proportional to Q_1 yields an effective Hamiltonian at the charm scale of

$$\mathcal{H}_{\text{split}} = \frac{g_s^2R_c^2\pi^2\Delta y}{3}r_1(m_c, M)|V_{L11}^uV_{L12}^{u*}|^2Q_1. \quad (102)$$

Here, $\Delta y \equiv |y_{u_L} - y_{c_L}|$ is the separation between the localized u_L and c_L quarks, scaled to the compactification radius. This leads to a contribution to x_{D} of

$$x_{\text{D}}^{(\text{split})} = \frac{2}{9\Gamma_D}g_s^2R_c^2\pi^2\Delta y r_1(m_c, M)|V_{L11}^uV_{L12}^{u*}|^2f_D^2M_DB_1. \quad (103)$$

Figure 19 shows the range of values for $x_{\text{D}}^{(\text{split})}$ as a function of the separation between the u_L and c_L states for various values of the compactification scale, where $M_c = 1/R_c$. In our numerical work we have used the natural assumption that $(V_L)_{ij} = (V_{\text{CKM}})_{ij}$. We see that $x_{\text{D}}^{(\text{split})}$ vanishes as the separation of the 2 fermions tends to zero as expected. However, for most of the range of Δy, we find that compactification scales of order 100–500 TeV are excluded by the observation of D^0-$\bar{D}^0$ mixing and hence D mixing provides severe constraints on the localization of the up-type fermions within this model. Note that these constraints are dependent on the choice of values for the elements of the quark diagonalization matrices $V_{L,R}$, which are *a priori* unknown, and could be reduced if quark mixing is tiny in the up-quark sector. The worst case scenario would be if the $V_{L,R}^u$ are diagonal and all quark mixing occurs in the down-quark sector.[8] In this case, strong bounds on the compactification scale, similar to those presented here, would be obtained from K meson mixing [94,95].

C. Warped geometries

In the simplest scenario with warped extra dimensions [96], known as the Randall-Sundrum (RS) model, the

[8]This is frequently the case in models of quark mass matrices where the up-quark mass matrix is taken to be diagonal and all mixing is assigned to the down-quark sector. A rationale for this is given, for example, in Ref. [38].

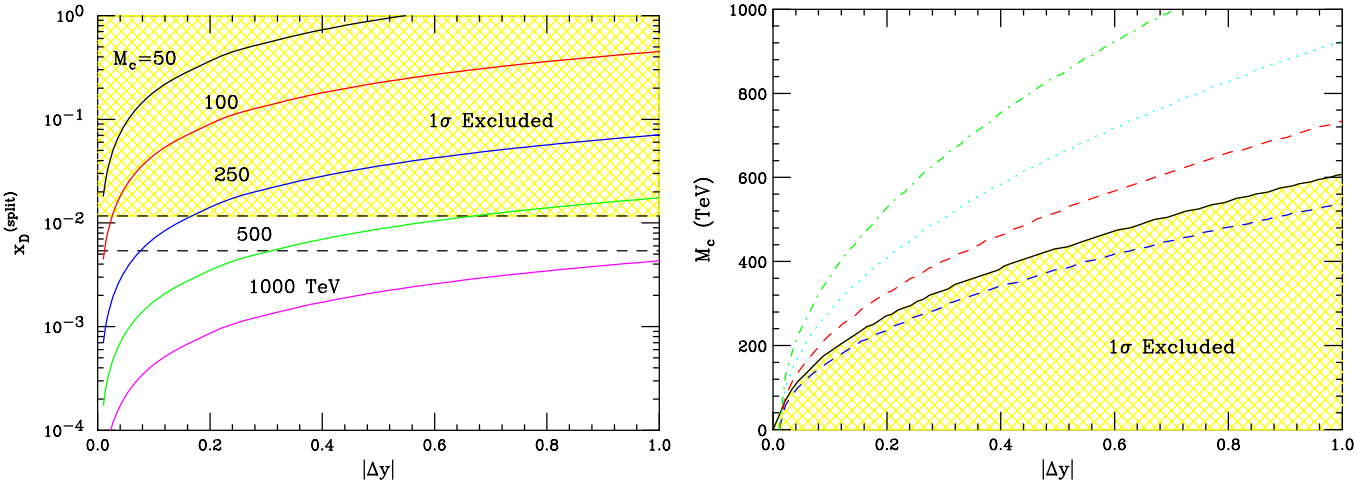

FIG. 19 (color online). Left: x_D in the split fermion model as a function of the separation between the left-handed u and c quark states in the extra dimension for various values of the compactification scale. The 1σ experimental bounds are as indicated, with the yellow shaded region depicting the region that is excluded. Right: 1σ excluded region in the $u_L - c_L$ separation and compactification scale parameter plane, as well as possible future contours taking $x_D < (15.0, 8.0, 5.0, 3.0) \times 10^{-3}$, corresponding to the blue (dark gray) dashed, red (gray) dashed, cyan (lightest gray) dotted, and green (light gray) dot-dashed curves, respectively.

hierarchy between the electroweak and Planck scales is generated geometrically via a large curvature of a single extra dimension. The geometry is that of a 5D anti–de Sitter space (AdS_5), where the extent of the 5th dimension is $y = \pi r_c$ (r_c is the compactification radius), and every slice of the additional dimension corresponds to a 4D Minkowski metric. Two 3-branes reside at the boundaries of the AdS_5 slice, with the 3-brane located at the fixed point $y = \pi r_c$ being known as the TeV brane, while the opposite brane at the other boundary $y = 0$ is referred to as the Planck brane. Within this framework, gravity is localized about the Planck brane, and electroweak symmetry breaking can take place either with the Higgs field being localized on or near the TeV brane, or via boundary conditions imposed at the fixed points as in the Higgsless models discussed above. The FCNC effects considered here are independent of this choice.

FCNC effects are induced [97,98] when the SM fermions and gauge bosons are localized in the warped 5th dimension [99–101]. As in the case of flat TeV^{-1}-sized extra dimensions with split fermions discussed above, the observed fermion masses and mixings are automatically explained by the geometry, with the 5D Yukawa couplings all being of order unity. Localizing the light fermions near the Planck brane results in small 4D Yukawa couplings for these fields, whereas if the top-quark field is localized near the TeV brane a large 4D top Yukawa coupling is induced. This localization scheme also naturally suppresses higher-dimensional flavor-changing operators that are problematic when the SM is confined to the TeV brane. This flavor breaking fermion localization leads to FCNC interactions via nonuniversal couplings of the zero-mode fermions to the gauge boson KK states. Since the SM gauge bosons are localized near the TeV brane (in order to acquire their masses) and have exponentially decaying wave functions towards the Planck brane, we expect FCNC in the light-quark sector to be suppressed.

The action for fermion fields in the RS bulk is given by [100]

$$S = \int d^4x dy \sqrt{G}\left(\frac{i}{2}\bar{\Psi}\gamma^M D_M \Psi + \mathrm{sgn}(y) M_f \bar{\Psi}\Psi + \mathrm{H.c.}\right), \tag{104}$$

where G represents the determinant of the 5D metric, D_M is the covariant derivative in curved space, and $\gamma^M \equiv V_\mu^M \gamma^\mu$ with V_μ^M being the inverse vierbein. The parameter of importance to us here is M_f which is the 5D bulk mass for the fermion f. It is given by $M_f = kc_f$, where k is the parameter describing the curvature of the AdS_5 space and is of order of the 5D Planck scale. The constants c_f indicate the position of the fermion's localized wave function in the bulk, with $c_f > 1/2$ ($c_f < 1/2$) corresponding to the fermion being localized near the Planck (TeV) brane. These constants determine the flavor structure of the theory.

The KK decomposition of the bulk fermion fields yields the normalized zero-mode wave function (a discrete symmetry ensures that the zero-mode fields are chiral),

$$f^{(0)} = \sqrt{\frac{kr_c(1-2c_f)}{e^{\pi kr_c(1-2c_f)} - 1}} e^{-c_f k y} \equiv \sqrt{kr_c} Y_f e^{-c_f k y}. \tag{105}$$

The asymptotic behavior of the Y_f on the localization parameters c_f are listed in Table IV. We see that these factors become exponentially small when the fermions are localized near the Planck brane. In the basis where the 5D bulk masses, M_f, are diagonal the fermion Higgs interactions yield the 4D Yukawa couplings,

TABLE IV. The asymptotic behavior of the square of the parameter Y_f for various localization points $\{c_f\}$ of the fermion's wave function.

Y_f^2	Range of c_f
$\frac{1}{2} - c_f$	$c_f < \frac{1}{2} - \epsilon$
$\frac{1}{2\pi k r_c}$	$c_f \to \frac{1}{2}$
$(c_f - \frac{1}{2}) e^{\pi k r_c (1-2c_f)}$	$c_f > \frac{1}{2} + \epsilon$

$$\lambda^f_{4(ij)} = \lambda^f_{5(ij)} Y_{f_{Li}} Y_{f_{Rj}} e^{\pi k r_c (1 - c_{f_{Li}} - c_{f_{Rj}})}, \tag{106}$$

for the zero-mode fermions in terms of the 5D Yukawa couplings λ^f_5. We take the elements of λ^f_5 to be complex and of order unity. Note that $kr_c \approx 11.3$ in order to resolve the gauge hierarchy problem. The elements of the matrices that diagonalize the up and down quark fields to their 4D mass eigenstates have magnitude

$$|V^{u,d}_L|_{ij} \simeq \frac{Y_{f_{Li}}}{Y_{f_{Lj}}} \simeq |V_{\rm CKM}|_{ij} \qquad (i < j), \tag{107}$$

with $L \to R$ for the matrices that diagonalize the right-handed fields. For the elements with $j \leq i$ one should interchange $i \leftrightarrow j$.

The wave functions for the gauge KK states are given by the first order Bessel functions J_1, Y_1, and the mass of the nth gauge KK mode is $M_n = x_n k e^{-\pi k r_c}$ where x_n is related to the roots of Bessel functions [99]. The first few values of x_n are 2.45, 5.57, 8.70, and 11.84. Precision electroweak data places severe bounds on the masses of the gauge KK states [99,102]. However these bounds can be reduced to $M_1 \gtrsim 3$ TeV if the gauge symmetry in the bulk is expanded to $SU(2)_L \times SU(2)_R \times U(1)_{B-L}$, which restores custodial symmetry [103]. The couplings of these states to the zero-mode fermions, $\{C^{(n)}_f\}$, are determined by the overlap of their wave functions in the additional dimension. They are given (as a ratio to the SM coupling) by

$$C^{(n)}_f = \frac{g^{(n)}}{g_{\rm SM}} = \sqrt{2\pi k r_c} Y_f^2 I^{(n)}_f, \tag{108}$$

where $I^{(n)}_f$ is an integral over J_1 Bessel functions, and are given explicitly in Ref. [101] and in the appendix. As displayed in Fig. 20, this coupling weakens substantially as the gauge KK level, n, increases for $c_f < 1/2$, while for $c_f > 1/2$ the couplings tend to a small fixed value for all KK levels. The interaction Lagrangian for the gluon KK states in the quark mass eigenstate basis is as given in Eq. (98) with the substitution of the prefactor $\sqrt{2} \to \sqrt{2\pi k r_c}$, which arises from the renormalization of the KK gauge kinetic terms to the canonical value.

D^0-$\bar{D}^0$ mixing is then mediated via tree-level flavor-changing interactions of the KK gauge boson states as depicted in Fig. 18. In analogy to the previous section, the effective Hamiltonian for this process is given by (for

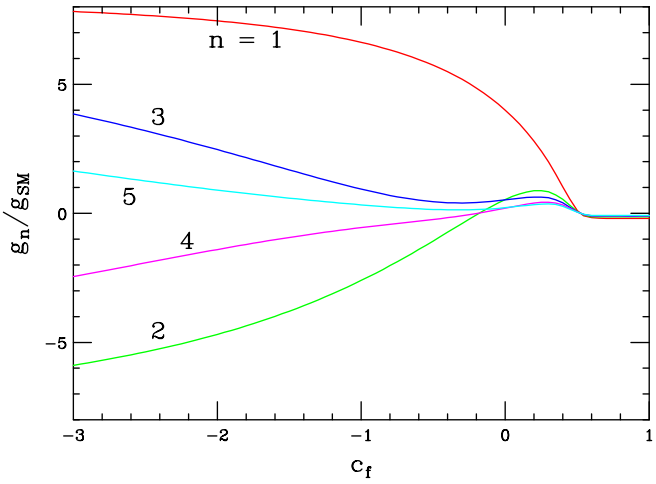

FIG. 20 (color online). The coupling strength, scaled to the SM strong coupling constant, of the zero-mode fermions to the first five gluon KK excitations (as labeled) as a function of the fermion bulk mass parameter c_f.

the exchange of gluon KK states which yield the largest contribution)

$$\mathcal{H}_{\rm RS} = \frac{2\pi k r_c}{3} g_s^2 \sum_{\vec{n}=1}^{\infty} \frac{1}{M_n^2} (U^{u(n)\dagger}_{L(cu)} U^{u(n)}_{L(uc)} Q_1 + 2 U^{u(n)\dagger}_{L(cu)} U^{u(n)}_{R(uc)} Q_2 + U^{u(n)\dagger}_{R(cu)} U^{u(n)}_{R(uc)} Q_6), \tag{109}$$

where $U^{u(n)}_{L,R} \equiv V^{u\dagger}_{L,R} C^{(n)}_f V^u_{L,R}$. Writing this explicitly for $U^{u(n)}_L$ yields,

$$U^{u(n)}_{L(uc)} = V^{u\dagger}_{L(uj)} C^{(n)}_{jk} V^u_{L(kc)} \delta_{jk} = V^{u\dagger}_{L(uj)} Y^2_{f_j} V^u_{L(jc)} I^{(n)_{f_j}}, \tag{110}$$

since the $C^{(n)}_f$ are diagonal, and where the index j sums over the generations. Looking at the asymptotic values of Y_f in Table IV, we see that $U^{u(n)}_{L(uc)}$ is only sizable when the fermion is localized towards the TeV brane. Unitarity of the $V^u_{L,R}$ results in

$$\mathcal{H}_{\rm RS} = \frac{2\pi k r_c}{3 M_1^2} g_s^2 (C_1(M_n) Q_1 + C_2(M_n) Q_2 + C_6(M_n) Q_6), \tag{111}$$

where M_1 is the mass of the first gluon KK excitation, and with the Wilson coefficients being given by

$$
\begin{aligned}
C_1(M_1) &= 2\pi k r_c \sum_{n=1}^{\infty} \frac{M_1^2}{M_n^2} (V^{u\dagger}_{L(13)} V^{u}_{L(32)} [Y^2_{t_L} (I^{(n)}_{t_L})^2 \\
&\quad - Y^2_{u_L} (I^{(n)}_{u_L})^2] + V^{u\dagger}_{L(12)} V^{u}_{L(22)} [Y^2_{c_L} (I^{(n)}_{c_L})^2 \\
&\quad - Y^2_{u_L} (I^{(n)}_{u_L})^2])^2, \\
C_2(M_1) &= 4\pi k r_c \sum_{n=1}^{\infty} \frac{M_1^2}{M_n^2} (V^{u\dagger}_{L(13)} V^{u}_{L(32)} [Y^2_{t_L} (I^{(n)}_{t_L})^2 \\
&\quad - Y^2_{u_L} (I^{(n)}_{u_L})^2] + V^{u\dagger}_{L(12)} V^{u}_{L(22)} [Y^2_{c_L} (I^{(n)}_{c_L})^2 \\
&\quad - Y^2_{u_L} (I^{(n)}_{u_L})^2]) (V^{u\dagger}_{R(13)} V^{u}_{R(32)} [Y^2_{t_R} (I^{(n)}_{t_R})^2 \\
&\quad - Y^2_{u_R} (I^{(n)}_{u_R})^2] + V^{u\dagger}_{R(12)} V^{u}_{R(22)} [Y^2_{c_R} (I^{(n)}_{c_R})^2 \\
&\quad - Y^2_{u_R} (I^{(n)}_{u_R})^2]), \\
C_6(M_1) &= 2\pi k r_c \sum_{n=1}^{\infty} \frac{M_1^2}{M_n^2} (V^{u\dagger}_{R(13)} V^{u}_{R(32)} [Y^2_{t_R} (I^{(n)}_{t_R})^2 \\
&\quad - Y^2_{u_R} (I^{(n)}_{u_R})^2] + V^{u\dagger}_{R(12)} V^{u}_{R(22)} [Y^2_{c_R} (I^{(n)}_{c_R})^2 \\
&\quad - Y^2_{u_R} (I^{(n)}_{u_R})^2])^2,
\end{aligned}
\tag{112}
$$

with $M_1^2/M_n^2 = x_1^2/x_n^2$ where x_n are the Bessel function roots described above.

The RG evolution proceeds as in Sec. II A and results in the effective Hamiltonian at the charm-quark scale

$$
\begin{aligned}
\mathcal{H}_{\rm RS} &= \frac{g_s^2}{3M_1^2} (C_1(m_c) Q_1 + C_2(m_c) Q_2 + C_3(m_c) Q_3 \\
&\quad + C_6(m_c) Q_6),
\end{aligned}
\tag{113}
$$

where additional operators have been generated due to mixing in the RG evolution. The evolved Wilson coefficients at the charm scale are as given in Eq. (52) with the appropriate substitution of $M_{Z'} \to M_1$. Upon evaluating the matrix elements we obtain the contribution to $x_{\rm D}$ from warped extra dimensions

$$
\begin{aligned}
x_{\rm D}^{\rm (RS)} &= \frac{g_s^2}{3M_1^2} \frac{f_D^2 B_D M_D}{\Gamma_D} \left(\frac{2}{3} [C_1(m_c) + C_6(m_c)] \right. \\
&\quad \left. - \frac{5}{6} C_2(m_c) + \frac{7}{12} C_3(m_c) \right)
\end{aligned}
\tag{114}
$$

in the modified vacuum saturation approximation. Here, we have taken the factor η of Eq. (26) to be unity.

To obtain numerical results, we need to specify the fermion locations in the warped dimension. We examine three popular scenarios in the literature that correctly generate the 4D Yukawa hierarchy for the SM fermions. As mentioned above, localizing the fields near the uv (ultraviolet or Planck) brane generates an exponentially small 4D Yukawa coupling. In all three models, all of the light quarks are localized such that their bulk mass parameters take on values with $c_f > 1/2$. Special attention must be paid to the localization of the third generation quarks; in order to generate a large top-quark mass, the corresponding $SU(2)$ singlet field is usually taken to reside close to the TeV brane. The third generation $SU(2)$ doublet fields and b-quark $SU(2)$ singlet field are located as close to the IR (infrared, or TeV) brane while maintaining consistency with the experimentally determined $Zb\bar{b}$ coupling. The three scenarios that we follow are fairly uniform in their treatment of the third generation, differing only slightly in the location of the $SU(2)$ top-quark singlet. The scenarios are: (I) a study of flavor physics in the Randall-Sundrum model [104], (II) a scenario that has been constructed in order to generate fermion masses within the 5D picture of Higgsless models [84], (III) the up-quark singlet field is taken to lie even closer to the uv brane [105] in order to solve the strong CP problem with warped geometries. The numerical values of the bulk mass parameters are summarized in Table V for the three cases.

TABLE V. The values of the bulk mass parameters for the three models described in the text.

	Model I	Model II	Model III
c_{u_L}	$>1/2$	0.6	0.5
c_{u_R}	$>1/2$	0.6	1.4
c_{c_L}	$>1/2$	0.52	0.5
c_{c_R}	$>1/2$	0.52	0.53
c_{t_L}	0.45	0.4	0.46
c_{t_R}	0	0.3	On the IR brane

Our results for $x_{\rm D}^{\rm RS}$ for these three models are presented in Fig. 21, where as above, we assume the quark diagonalization matrices take on CKM-like values. In the figure, the

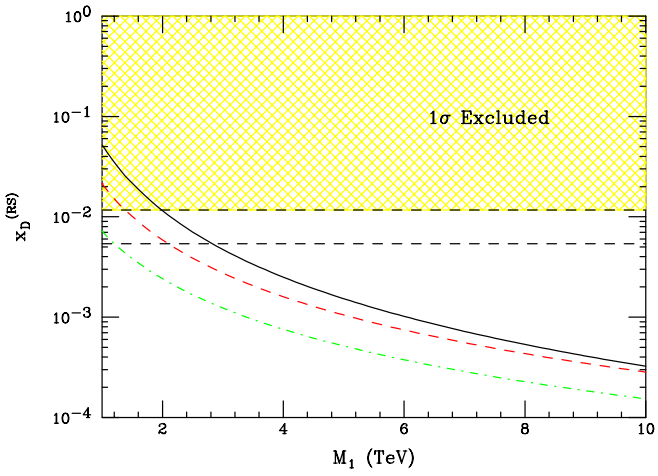

FIG. 21 (color online). The contribution to $x_{\rm D}$ from a warped extra dimension with the SM fields in the bulk as a function of the mass for the first gluon KK excitation. The 1σ experimental bounds are as indicated, with the yellow shaded region depicting the region that is excluded. The curves correspond to model I [dash-dotted, green (light gray)], model II [dashed, red (gray)], and model III (solid) as described in the text.

dot-dashed green (light gray), dashed red (gray), and solid black curves correspond to the bulk mass parameters of model I, II, and III, respectively. We see from Fig. 20 that fermions localized towards the Planck brane have very small couplings to the KK gluon states and thus do not substantially contribute to x_D^{RS}. This simplifies the expressions in Eq. (112) in this case, as only the $t_{L,R}$ terms have sizable contributions. Looking at the figure we see the mass of the first gluon KK excitation is constrained to lie $\gtrsim$ 1–2 TeV, which is essentially the same value as the bound obtained from the precision electroweak data in warped models with bulk custodial symmetry [103]. Last, we recall from discussion in the previous section, that these constraints can be evaded if the matrix which diagonalizes the up-quark sector is essentially diagonal.

VIII. EXTRA SYMMETRIES

In this section, we focus on supersymmetry. Weak-scale supersymmetry is a possible solution to the gauge hierarchy problem, leads to the unification of the gauge couplings at high energies, and provides a natural dark matter candidate. It is thus a very well motivated theory of physics beyond the SM. Supersymmetry is an extension of the Poincaré symmetry, relating fermions and bosons at a fundamental level. All SM particles have supersymmetric partners (''sparticles'') with the same mass and gauge interactions, but with spin differing by one-half unit. Since the supersymmetric particles have yet to be discovered, we know that supersymmetry is broken; in this section, we will be agnostic as to which supersymmetry breaking mechanism nature may have chosen. We note that in nonbroken supersymmetry the rates for all loop-induced processes would vanish due to an exact cancellation between the SM and supersymmetric contributions. It is thus due to the breaking of supersymmetry that contributions to FCNC are generated in these theories.

Here, we examine the contributions to D^0-$\bar{D}^0$ mixing in four supersymmetric scenarios: the minimal supersymmetric standard model (MSSM), models with alignment in the quark-squark mass matrices, models with R-parity violating couplings, and split supersymmetry. Other scenarios with extended nonsupersymmetric symmetries have been considered elsewhere in this paper.

A. Minimal supersymmetric standard model

As the name implies, the MSSM is the simplest version of supersymmetry as it contains the minimal number of new particles. The SM fermions are placed in chiral supermultiplets, the SM gauge bosons lie in vector supermultiplets, and the Higgs sector takes the form of the flavor-conserving two-Higgs-doublet model II discussed above. A discrete symmetry, R parity, is imposed to forbid unwanted terms in the superpotential that would mediate proton decay at a dangerous level. Conservation of R parity implies that only pairs of sparticles can be produced or exchanged in loops. Collider searches for direct squark and gluino pair production place the bound $m_{\tilde{q},g} \gtrsim$ 330 GeV [13] in the MSSM with gravity mediated supersymmetry breaking.

As mentioned above, we will not assume any particular supersymmetry breaking mechanism in our discussion, and so we employ a model-independent parametrization of all possible soft supersymmetry breaking terms. This soft supersymmetry breaking sector generally includes three gaugino masses, trilinear scalar interactions, as well as Higgs and sfermion masses, and thus contains many potential sources of flavor violation. Here, we are interested in the flavor violating sources that arise in the up-squark sector. In what is known as the super-CKM basis, the squark fields are rotated by the same matrices that diagonalize the quark masses, giving rise to nondiagonal squark mass matrices. The squark propagators are then expanded such that the nondiagonal mass terms result in mass insertions that change the squark flavor [106–109]. This source of flavor violation differs from that of the SM and many NP models discussed earlier. Here, the quark-squark-gaugino neutral couplings are flavor conserving, while flavor violation arises from the nondiagonality of the squark mass propagators. The 6×6 mass matrix for the $Q = +2/3$ squarks can be divided into 3×3 submatrices,

$$\tilde{M}^2 = \begin{pmatrix} \tilde{M}^2_{LL} & \tilde{M}^2_{LR} \\ \tilde{M}^{2T}_{LR} & \tilde{M}^2_{RR} \end{pmatrix}, \tag{115}$$

and the mass insertions can be parametrized in a model-independent fashion as

$$(\delta_{ij})_{MN} = \frac{(V_M \tilde{M}^2 V_N^\dagger)_{ij}}{m^2_{\tilde{q}}}. \tag{116}$$

Here, i, j are flavor indices, M, N refers to the helicity choices LL, LR, RR, and $m_{\tilde{q}}$ represents the average squark mass. Although this source of flavor violation is present in general, and, in particular, in models with gravity mediated supersymmetry breaking, it can be avoided if supersymmetry is broken by gauge or anomaly mediation. These mass insertions are thought to be small in the MSSM, but can be large in nonminimal supersymmetric models.

In this scenario, the virtual exchange of squarks and gluinos in the box diagrams depicted in Fig. 22 can have a strong contribution to D^0-$\bar{D}^0$ mixing. Note that the

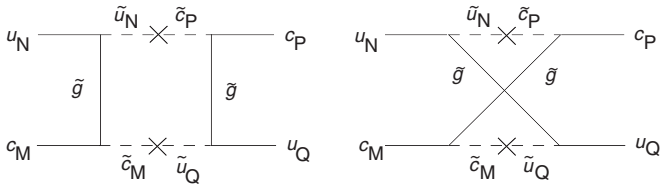

FIG. 22. Contributions to D mixing from mass insertions in the squark propagator in MSSM. N, M, P, and Q label the helicity (L, R).

second diagram in the figure is due to the Majorana nature of the gluino. The effective Hamiltonian at the supersymmetric scale is given by

$$\mathcal{H}_{\rm MSSM} = \frac{\alpha_s^2}{2m_{\tilde{q}}^2}\sum_{i=1}^{8} C_i(m_{\tilde{q}})Q_i, \tag{117}$$

where all eight operators in the independent basis contribute. The matching conditions at the supersymmetric mass scale are [110]

$$\begin{aligned}
&C_1(m_{\tilde{q}}^2) = \frac{1}{18}(\delta^u_{12})^2_{LL}[4xf_1(x) + 11f_2(x)], \qquad C_2(m_{\tilde{q}}^2) = \frac{1}{18}\{(\delta^u_{12})_{LR}(\delta^u_{12})_{RL}15f_2(x) - (\delta^u_{12})_{LL}(\delta^u_{12})_{RR}[2xf_1(x) + 10f_2(x)]\},\\
&C_3(m_{\tilde{q}}^2) = \frac{1}{9}\{(\delta^u_{12})_{LL}(\delta^u_{12})_{RR}[42xf_1(x) - 6f_2(x)] - (\delta^u_{12})_{LR}(\delta^u_{12})_{RL}11f_2(x)\}, \qquad C_4(m_{\tilde{q}}^2) = \frac{1}{18}(\delta^u_{12})^2_{RL}37xf_1(x),\\
&C_5(m_{\tilde{q}}^2) = \frac{1}{24}(\delta^u_{12})^2_{RL}xf_1(x), \qquad C_6(m_{\tilde{q}}^2) = \frac{1}{18}(\delta^u_{12})^2_{RR}[4xf_1(x) + 11f_2(x)],\\
&C_7(m_{\tilde{q}}^2) = \frac{1}{18}(\delta^u_{12})^2_{LR}37xf_1(x), \qquad C_8(m_{\tilde{q}}^2) = \frac{1}{24}(\delta^u_{12})^2_{LR}xf_1(x),
\end{aligned} \tag{118}$$

where $x \equiv m_{\tilde{g}}^2/m_{\tilde{q}}^2$, with $m_{\tilde{g}}$ being the mass of the gluino. The functions $f_1(x)$ and $f_2(x)$ are given in the appendix. Note that these conditions are symmetric under the interchange $L \leftrightarrow R$. We also note that the NLO expressions for these matching conditions have been computed in Ref. [111].

The RG evolution to the charm-quark scale results in

$$\begin{aligned}
C_1(m_c) &= r_1(m_c, m_{\tilde{q}})C_1(m_{\tilde{q}}), \qquad C_2(m_c) = r_2(m_c, m_{\tilde{q}})C_2(m_{\tilde{q}}),\\
C_3(m_c) &= \frac{2}{3}[r_2(m_c, m_{\tilde{q}}) - r_3(m_c, m_{\tilde{q}})]C_2(m_{\tilde{q}}) + r_3(m_c, m_{\tilde{q}})C_3(m_{\tilde{q}}),\\
C_4(m_c) &= \frac{8}{\sqrt{241}}[r_5(m_c, m_{\tilde{q}}) - r_4(m_c, m_{\tilde{q}})]\left[C_4(m_{\tilde{q}}) + \frac{15}{4}C_5(m_{\tilde{q}})\right] + \frac{1}{2}[r_4(m_c, m_{\tilde{q}}) + r_5(m_c, m_{\tilde{q}})]C_4(m_{\tilde{q}}),\\
C_5(m_c) &= \frac{1}{8\sqrt{241}}[r_4(m_c, m_{\tilde{q}}) - r_5(m_c, m_{\tilde{q}})][C_4(m_{\tilde{q}}) + 64C_5(m_{\tilde{q}})] + \frac{1}{2}[r_4(m_c, m_{\tilde{q}}) + r_5(m_c, m_{\tilde{q}})]C_5(m_{\tilde{q}}),\\
C_6(m_c) &= r_6(m_c, m_{\tilde{q}})C_6(m_{\tilde{q}}),\\
C_7(m_c) &= \frac{8}{\sqrt{241}}[r_8(m_c, m_{\tilde{q}}) - r_7(m_c, m_{\tilde{q}})]\left[C_7(m_{\tilde{q}}) + \frac{15}{4}C_8(m_{\tilde{q}})\right] + \frac{1}{2}[r_7(m_c, m_{\tilde{q}}) + r_8(m_c, m_{\tilde{q}})]C_7(m_{\tilde{q}}),\\
C_8(m_c) &= \frac{1}{8\sqrt{241}}[r_7(m_c, m_{\tilde{q}}) - r_8(m_c, m_{\tilde{q}})][C_7(m_{\tilde{q}}) + 64C_8(m_{\tilde{q}})] + \frac{1}{2}[r_7(m_c, m_{\tilde{q}}) + r_8(m_c, m_{\tilde{q}})]C_8(m_{\tilde{q}}),
\end{aligned} \tag{119}$$

which agrees in form with that in Ref. [112]. Here, we have assumed that the squarks and gluinos are integrated out at roughly the same scale. Upon evaluating the matrix elements in the modified vacuum saturation approximation we obtain the MSSM contribution to $x_{\rm D}$,

$$\begin{aligned}
x_{\rm D}^{\rm (MSSM)} = \frac{\alpha_s}{2m_{\tilde{q}}^2}\frac{f_D^2 B_D m_D}{\Gamma_D}\Bigg[&\frac{2}{3}[C_1(m_c) + C_6(m_c)]\\
&- \frac{5}{12}[C_4(m_c) + C_7(m_c)] + \frac{7}{12}C_3(m_c)\\
&- \frac{5C_2(m_c)}{6} + [C_5(m_c) + C_8(m_c)]\Bigg].
\end{aligned} \tag{120}$$

Here, we have taken the factor η of Eq. (26) to be unity.

Our results for $x_{\rm D}^{\rm (MSSM)}$ are presented in Figs. 23–25. In these figures, we show contours for the absolute value of the up-charm squark mass insertions for various helicities as a function of the ratio $m_{\tilde{g}}/m_{\tilde{q}}$ for different average squark masses. These contours correspond to $x_{\rm D} = (11.7, 15.0, 3.0) \times 10^{-3}$ in the three figures. In Fig. 23, the region above the contours represents the current 1σ excluded region. In these figures we take one or two of the mass insertions to be nonvanishing, as indicated. Because of the $L \leftrightarrow R$ symmetry of the matching conditions, the constraints on $|\delta^u_{12}|_{LL}$ and $|\delta^u_{12}|_{RR}$, as well as $|\delta^u_{12}|_{LR}$ and $|\delta^u_{12}|_{RL}$ are identical. We see that D meson mixing restricts the up and charm squark masses to be degenerate at the (1–10)% level for most of the parameter space. We note that our results numerically agree with those recently computed by Ciuchini *et al.* [113].

There are several other contributions to D meson mixing within the MSSM. These are all mediated via box diagrams with internal sparticle exchange and we now discuss each

one in turn. (i) The exchange of any of the 4 neutralinos χ_i^0 ($i = 1, 4$) with the up and charm squarks. This contribution proceeds via mass insertions in the squark propagators with flavor diagonal quark-squark-neutralino couplings as in the case of internal squark-gluino exchange discussed above. Since the couplings are of weak interaction strength in this case, the magnitude of this contribution is suppressed by the ratio g^4/g_s^4 compared to the squark-gluino results and is thus numerically insignificant. (ii) The exchange of one of the neutralinos and one gluino with the up and charm squarks. This again proceeds via the nondiagonal squark mass insertions at a rate of g^2/g_s^2 compared to the pure gluino-squark contribution. Although larger than the pure neutralino-squark contribution, it is still a subleading effect. (iii) The exchange of charginos $\chi_i^{\pm}$ ($i = 1, 2$) and all three down-type squarks inside the box diagram. Here, the squark propagators are diagonal (mass insertions do not contribute in this case since the internal squarks are $Q = -1/3$) and the flavor violation is given by the CKM structure of the quark-squark-chargino vertices. However, the $Q = -1/3$ squarks are constrained to be highly degenerate from their contributions (with gluino exchange) to K, B_d, B_s meson mixing. Thus a supersymmetric-GIM mechanism is in effect, yielding nearly exact cancellations, and rendering this contribution negligible. This is in contrast to the chargino-squark contributions to K, B_d, B_s meson mixing, where the potentially nondegenerate stop squark participates and can induce large contributions. (iv) The charged Higgs contribution of the two-Higgs-Doublet model of type II discussed in Sec. VI A. As shown in that section, these contributions are numerically small, even in the case of large $\tan\beta$. In summary, we see that all other supersymmetric contributions to D^0-$\bar{D}^0$ mixing are numerically insignificant compared to the squark-gluino exchange. It is interesting to note that stop-squarks do not contribute to D meson mixing.

B. Quark-squark alignment models

As we saw in the previous section, in the MSSM there is a new "flavor problem," namely, how to keep the contributions from the supersymmetric particles to FCNC as small as the observations. The conventional solution is to impose constraints, such as those derived above, of (i) degeneracy in the squark sector (except for the special case of stop squarks), i.e. the diagonal submatrices M_{LL} and M_{RR} in Eq. (116) should be proportional to the unit matrix, and (ii) the nondiagonal submatrices M_{LR} should be proportional to the corresponding quark matrix.

Nir and Seiberg [114] have proposed an alternative to this picture where the quark and squark mass matrices are approximately aligned with each other. Their proposal is as follows: if for some symmetry reason the matrices corresponding to the squark mass insertions, δ_{MN}, are themselves diagonal, then the squark contributions to FCNC vanish, regardless of the mass spectrum of the squarks. Corrections to this approximation are expected to remain tolerably small and it should be possible to simultaneously diagonalize the quark mass matrices and the squark mass-squared matrices while essentially preserving flavor diagonal gluino interactions.

Within this framework, it is somewhat problematic to satisfy the constraints from K^0–$\bar{K}^0$ mixing. Specific implementations of this proposal, based on Abelian horizontal symmetries, restrict the supersymmetric contributions to Kaon mixing via a unique structure for the down-quark mass matrix using holomorphic zeros [115]. This implies that Cabibbo mixing between the first and second generation quarks must be induced by mixing in the up-quark sector, which in turn leads to sizable supersymmetric contributions to D^0-$\bar{D}^0$ mixing. In this case, mixing in the up-charm squark sector gives

$$(\delta_{LL})_{uc} = \frac{(V_L^u \tilde{M}^2 V_L^{u\dagger})_{uc}}{\tilde{m}^2} \approx \theta_c \frac{\Delta \tilde{m}_{uc}^2}{\tilde{m}_q^2}, \tag{121}$$

where θ_c is the Cabibbo angle, while the $(\delta_{LR})_{uc}$ mass insertions can naturally remain small. Mirroring the above discussion for MSSM, this leads to the effective Hamiltonian that mediates D mixing

$$\mathcal{H}_A = \frac{\alpha_s^2}{2m_{\tilde{q}}^2} C_1(m_{\tilde{q}}) Q_1, \tag{122}$$

with

$$C_1(m_{\tilde{q}}) = \frac{1}{18}(\delta_{12}^u)_{LL}^2 [4x f_1(x) + 11 f_2(x)], \tag{123}$$

where $f_{1,2}(x)$ with $x \equiv m_{\tilde{g}}^2/m_{\tilde{q}}^2$ are again given in the appendix. The RG evolution is simple and yields

$$x_{\mathrm{D}}^{(A)} = \frac{\alpha_s}{3m_{\tilde{q}}^2} \frac{f_D^2 B_D m_D}{\Gamma_D} r_1(m_c, m_{\tilde{q}}) C_1(m_{\tilde{q}}). \tag{124}$$

The bounds on $(\delta_{12}^u)_{LL}$ from the current measurement of D meson mixing are given in the upper left-hand panel of Fig. 23. Using Eq. (121) above, this results in the constraint on squark and gluino masses of (assuming $m_{\tilde{q}} \approx m_{\tilde{g}}$ for simplicity) $m_{\tilde{g},\tilde{q}} \gtrsim 2$ TeV, which agrees with the results in Refs. [12,113]. This would exclude early discovery of supersymmetry at the LHC, but leaves a discovery window with higher luminosities as the LHC detectors are expected to have a search reach of $m_{\tilde{g},\tilde{q}}$ up to 2.5–3.0 TeV with 300 fb^{-1} of integrated luminosity.

C. Supersymmetry with R-parity violation

The conventional gauge symmetries of supersymmetry allow for the existence of additional terms in the superpotential that violate baryon and lepton number. The assumption of R-parity conservation in the MSSM prohibits these terms, ensuring that baryon and lepton number are conserved, and forbids related dangerous operators, e.g.,

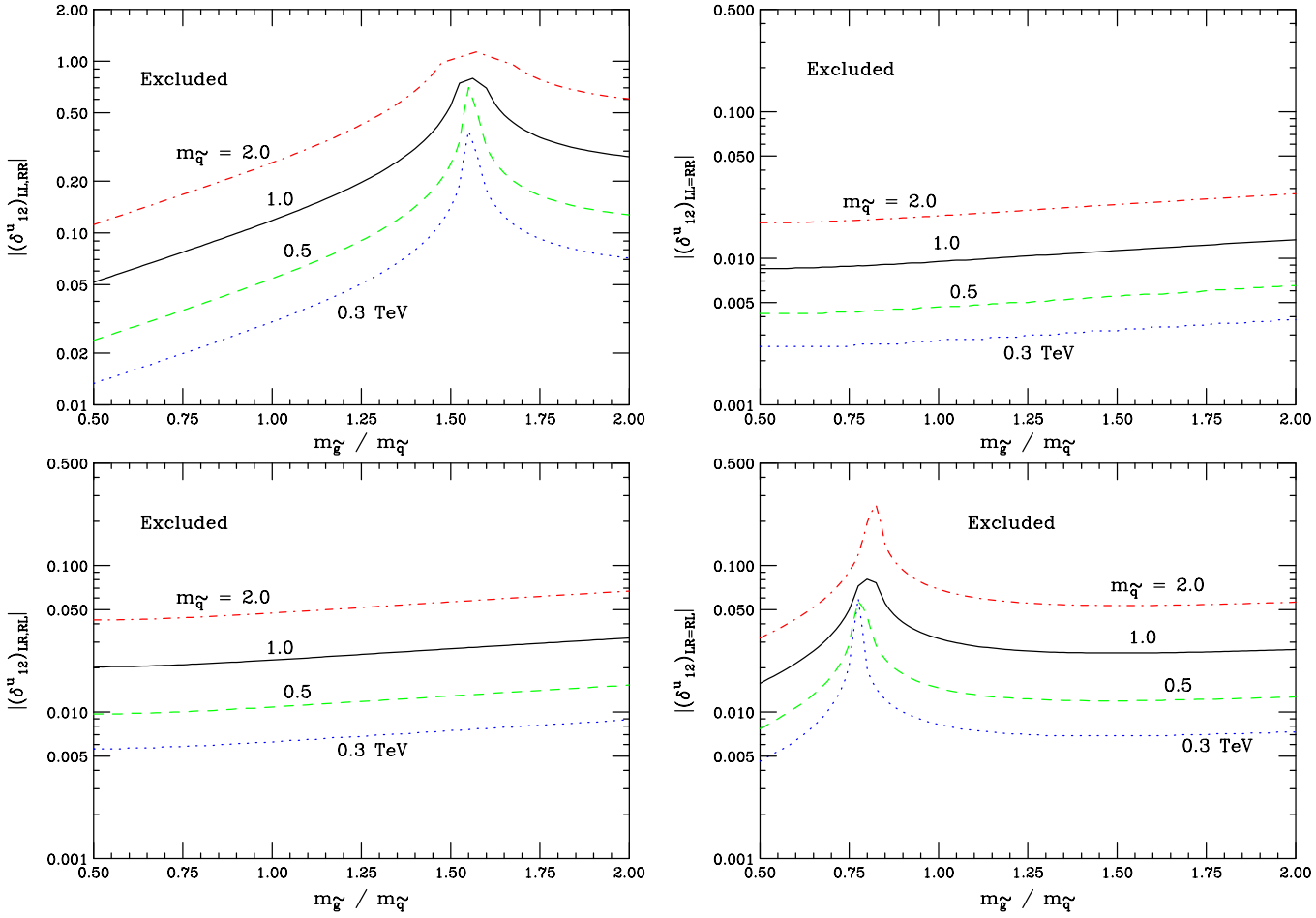

FIG. 23 (color online). The constraints on the absolute value of the mass insertions with different helicities as a function of the mass ratio $m_{\tilde{g}}/m_{\tilde{q}}$ for various values of the average squark mass. The 1σ excluded region, corresponding to $x_D < 11.7 \times 10^{-3}$, lies above the curves.

those that mediate proton decay. However, it is possible to construct alternative discrete symmetries [116], such as baryon-parity or lepton-parity, that allow terms which violate either baryon or lepton number, but not both. These symmetries also forbid unwanted operators, and there is no strong theoretical motivation to prefer R parity over these alternative scenarios. The R-parity violating terms in the superpotential can be written as

$$W_{R_p} = \frac{1}{2}\lambda_{ijk} L_i L_j \bar{E}_k + \lambda'_{ijk} L_i Q_j \bar{D}_k + \frac{1}{2}\lambda''_{ijk} \bar{U}_i \bar{D}_j \bar{D}_k. \tag{125}$$

i, j, k are generation indices and symmetry demands $i \neq j$ $(j \neq k)$ in the terms proportional to λ (λ''). The quantities L, E, Q, D, U in Eq. (125) are the chiral superfields in the MSSM, and the $SU(2)_L$, $SU(3)_C$ indices have been suppressed. A bilinear term may also be present, but it can be rotated away and will not be considered here. The lepton number violating terms, λ and λ', cannot exist simultaneously with the $\Delta B \neq 0$ term containing λ''. The λ' terms have the same structure as the couplings for scalar leptoquarks, as discussed in Sec. VI C. This model still contains the minimal superfield content, but leads to a markedly different supersymmetric phenomenology as sparticles can now be produced singly and can mediate FCNC at tree level.

The superfields are in the weak basis and should be rotated to their mass eigenstates. The $\Delta L \neq 0$ λ' term becomes [117]

$$W_{R_p} = \tilde{\lambda}'_{ijk}[N_i V_{jl} D_l - E_i U_j]\bar{D}_k, \tag{126}$$

with the definition

$$\tilde{\lambda}'_{ijk} \equiv \lambda'_{irs} \mathcal{U}^L_{rj} \mathcal{D}^{*R}_{sk}. \tag{127}$$

Here, $\mathcal{U}^L$ and $\mathcal{D}^R$ are the matrices which rotate the left-handed up- and right-handed down-quark fields to their mass basis. Written in terms of component fields, the second term in this superpotential contains the interactions

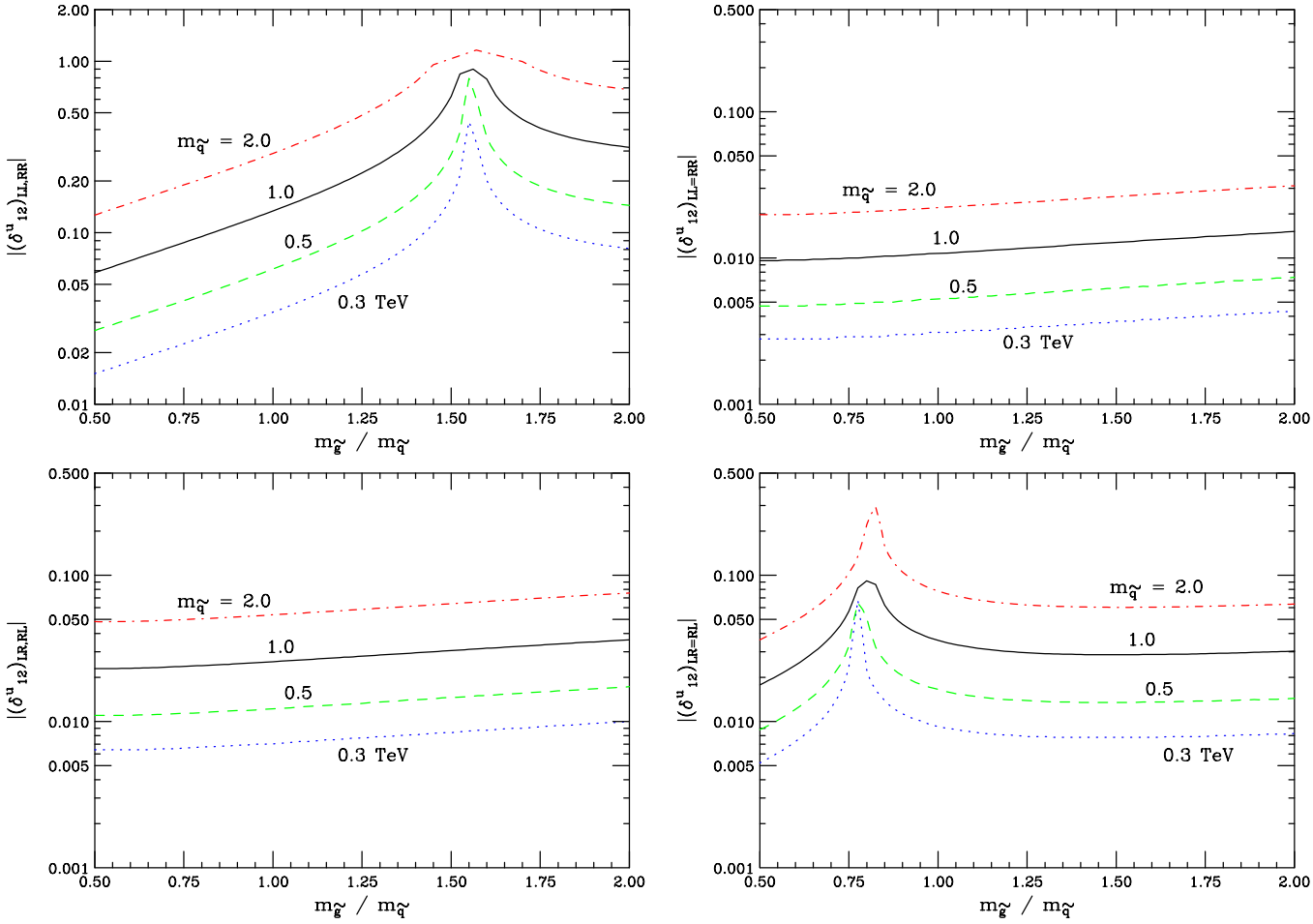

FIG. 24 (color online). Contours, corresponding to $x_D = 15.0 \times 10^{-3}$, for the absolute value of the mass insertions with different helicities as a function of the mass ratio $m_{\tilde{g}}/m_{\tilde{q}}$ for various values of the average squark mass. The region above the curves corresponds to larger values of x_D.

$$W_{\lambda'} = \tilde{\lambda}'_{ijk}\{V_{jl}[\tilde{\nu}^i_L \bar{d}^k_R d^l_L + \tilde{d}^l_L \bar{d}^k_R \nu^i_L + (\tilde{d}^k_R)^*(\bar{\nu}^i_L)^c d^l_L] - \tilde{e}^i_L \bar{d}^k_R u^j_L - \tilde{u}^j_L \bar{d}^k_R e^i_L - (\tilde{d}^k_R)^*(\bar{e}^i_L)^c u^j_L\}, \quad (128)$$

where the second line involving the up-quark sector is relevant for D^0-$\bar{D}^0$ mixing.

Constraints on the size of these R-parity violating couplings have been obtained in the literature. These limits are derived from considerations of various processes [118] such as charged current universality, semileptonic meson decays, rare meson decays, atomic parity violation, double nucleon decay, neutron oscillations, and Z boson decays. A compilation of the 2σ bounds on the couplings relevant for D^0-$\bar{D}^0$ mixing are given in Table VI. In addition, the recently improved upper bound on the branching fraction for the process $D^+ \to \pi^+ e^+ e^-$ of $\mathcal{B} < 7.4 \times 10^{-6}$ from CLEO-c [119] yields the stringent restriction [7] on the product of couplings $\tilde{\lambda}'_{12k}\tilde{\lambda}'_{11k} < 0.003\,(m_{\tilde{d}_{R,k}}/(100\ \text{GeV}))^2$.

It is possible for the quark flavor rotations to generate flavor violation in the down- or up-quark sectors, but not both. In the case where the flavor rotations occur in the up-quark sector only, large flavor-changing effects are expected in the D meson system and the limits on the R-parity violating couplings shown in Table VI become modified [118]. However, this scenario is rather model dependent, we will adopt a more conservative, model-independent formalism in the following.

For the lepton number violating coupling $\tilde{\lambda}'$, the first and third terms in the second line of Eq. (128) mediate D^0-$\bar{D}^0$ mixing via box diagrams where either the pair $(\tilde{\ell}_{L,i} - d_{R,k})$ or $(\ell_{L,i} - \tilde{d}_{R,k})$ are exchanged internally with the assignment of the generational index $j = 1, 2$ [117]. The corresponding Feyman diagrams are depicted in Fig. 26. Note that there are no tree-level contributions as in the case of meson mixing in the down-quark sector. This is described at the high mass scale by the effective Hamiltonian

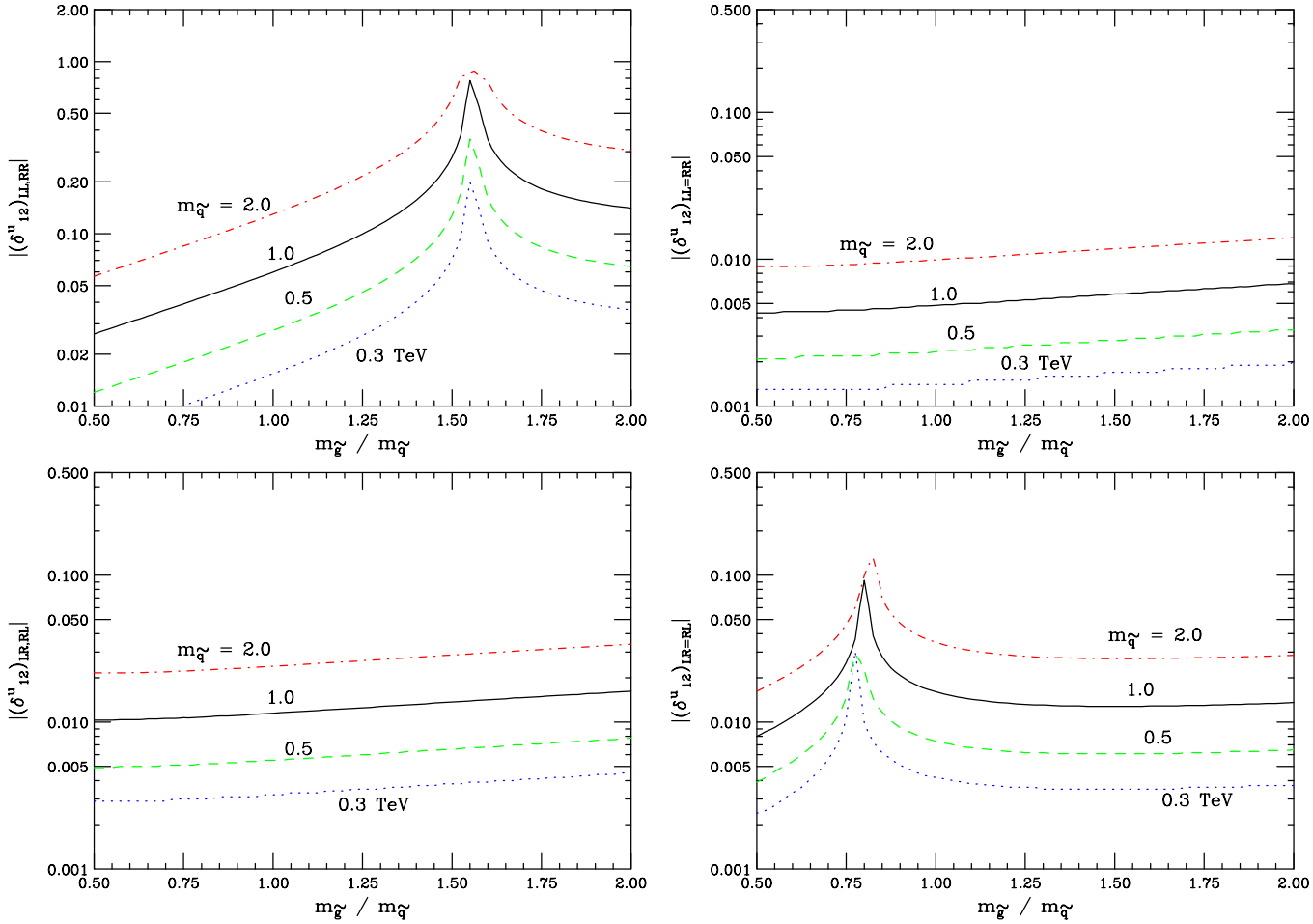

FIG. 25 (color online). Contours, corresponding to $x_D = 3.0 \times 10^{-3}$, for the absolute value of the mass insertions with different helicities as a function of the mass ratio $m_{\tilde{g}}/m_{\tilde{q}}$ for various values of the average squark mass. The region above the curves corresponds to larger values of x_D.

$$\mathcal{H}_{R_p} = \frac{1}{128\pi^2}(\tilde{\lambda}'_{i2k}\tilde{\lambda}'_{i1k})^2\left[\frac{1}{m^2_{\tilde{\ell}_{L,i}}} + \frac{1}{m^2_{\tilde{d}_{R,k}}}\right]Q_1, \quad (129)$$

where the dependence on the operator Q_1 is induced due to the fermion propagator. This interaction will yield constraints on the product of couplings $\tilde{\lambda}'_{i2k}\tilde{\lambda}'_{i1k}$. Here, we have assumed that only one set of the R-parity violating couplings $\tilde{\lambda}'_{i2k}\tilde{\lambda}'_{i1k}$ (i.e., only one value of i and k) is large and dominant. This is equivalent to saying that, e.g., both sleptons and both down-type quarks being exchanged in the first box diagram shown in Fig. 26 are from the same generation. In general, this need not be the case and, for example, the coupling factor would then be the product $\tilde{\lambda}'_{i2k}\tilde{\lambda}'_{m1k}\tilde{\lambda}'_{m2n}\tilde{\lambda}'_{i1n}$, with, e.g., the set of $\tilde{\ell}_{L,i}$, $d_{R,k}$, $\tilde{\ell}_{L,m}$, $d_{R,n}$ being exchanged.

TABLE VI. 2σ constraints on the R-parity violating couplings which participate in D mixing. Here, $k = 1, 2, 3$ with the exception that $k \neq j$, where j represents the middle index, for the λ'' couplings. All numbers are scaled by the factor $(m_{\tilde{d}_{R,k}}/100$ GeV). Details of the derivation of these restrictions are given in Refs. [7,118].

$\tilde{\lambda}'_{11k}$	$\tilde{\lambda}'_{12k}$	$\tilde{\lambda}'_{21k}$	$\tilde{\lambda}'_{22k}$	$\tilde{\lambda}'_{31k}$	$\tilde{\lambda}'_{32k}$
5×10^{-4}–0.021	0.043	0.021–0.059	0.18–0.21	0.11	0.52
$\tilde{\lambda}''_{11k}$	$\tilde{\lambda}''_{21k}$	$\tilde{\lambda}''_{12k}$	$\tilde{\lambda}''_{22k}$	$\tilde{\lambda}''_{13k}$	$\tilde{\lambda}''_{23k}$
10^{-15}–10^{-4}	1.23	10^{-15}–1.23	1.23	10^{-4}–1.23	1.23

Matching at the SUSY scale yields the Wilson coefficient

$$C_1(m_{\tilde{q}}) = \frac{1}{64\pi^2}(\tilde{\lambda}'_{i2k}\tilde{\lambda}'_{i1k})^2\left(1 + \frac{m^2_{\tilde{d}_{R,k}}}{m^2_{\tilde{\ell}_{L,i}}}\right). \quad (130)$$

Computing the evolution to the charm-quark scale yields

$$\mathcal{H}_{R_p} = \frac{1}{2m^2_{\tilde{d}_{R,k}}}C_1(m_c)Q_1, \quad (131)$$

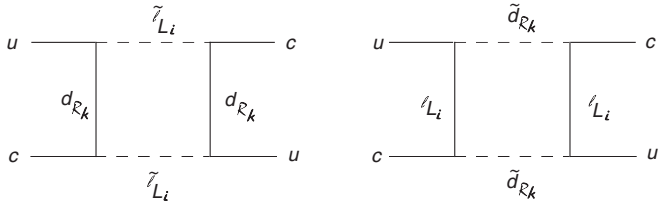

FIG. 26. Contributions to D^0-$\bar{D}^0$ mixing from the λ' superpotential terms in supersymmetric models with R-parity violation.

with

$$C_1(m_c) = r_1(m_c, m_{\tilde{q}}) C_1(m_{\tilde{q}}). \tag{132}$$

Evaluating the appropriate matrix element gives the D mixing contribution for the R-parity violating λ' terms,

$$x_{\rm D}^{(R_p)} = \frac{f_D^2 B_D M_D}{3\Gamma_D m_{\tilde{d}_R}^2} C_1(m_c). \tag{133}$$

Taking $m_{\tilde{\ell}_{L,i}} \simeq m_{\tilde{d}_{R,k}}$ for simplicity, we obtain the constraint

$$\frac{(\tilde{\lambda}'_{i2k}\tilde{\lambda}'_{i1k})^2}{m_{\tilde{d}_{R,k}}^2} \leq x_{\rm D}^{(\rm expt)} \frac{96\pi^2\Gamma_D}{f_D^2 B_D M_D r_1(m_c, m_{\tilde{q}})}, \tag{134}$$

which yields numerically

$$\tilde{\lambda}'_{i2k}\tilde{\lambda}'_{i1k} \leq 0.085\sqrt{x_{\rm D}^{(\rm expt)}}\left(\frac{m_{\tilde{d}_{R,k}}}{500\ \text{GeV}}\right). \tag{135}$$

We find that relaxing our assumption on the slepton mass and taking $m_{\tilde{\ell}_{L,i}} \leq m_{\tilde{d}_{R,k}}$ strengthens this bound at most by a factor of 3.7 when $m_{\tilde{\ell}_{L,i}} = 100$ GeV. In computing the renormalization group equation (RGE) evolution we used the value $m_{\tilde{q}} = 500$ GeV and find little sensitivity in the evolution on the squark mass once it is above the current experimental limit from HERA of $\sim$300 GeV [13]. It is trivial to scale our result in Eq. (135) to compare to the limits in Table VI which are based on setting $m_{\tilde{d}_{R,k}} = 100$ GeV. Taking, $m_{\tilde{d}_{R,k}} = 500$ GeV, we see that the bounds on $\tilde{\lambda}'_{i2k}\tilde{\lambda}'_{i1k}$ from D^0-$\bar{D}^0$ mixing are a factor of 50 (250) times stronger than those in the table for $i = 2$ ($i = 3$).

The full numerical results for $x_{\rm D}$ and the constraints obtained in the R-parity violating coupling, squark mass parameter plane are presented in Fig. 27 in the limit $m_{\tilde{\ell}_{L,i}} \simeq m_{\tilde{d}_{R,k}}$. We see that D meson mixing provides stringent constraints on R-parity violating couplings. These bounds can be directly translated to constraints on the couplings of scalar leptoquarks as discussed in a previous section.

The baryon number violating λ'' couplings can also contribute to D^0-$\bar{D}^0$ mixing. We remind the reader that they cannot exist simultaneously with the lepton number violating terms in the superpotential. They participate in D mixing via d_R-quark and $\tilde{d}_R$ exchange in the box diagram. The formalism is analogous to the $\Delta L \neq 0$ case above. The

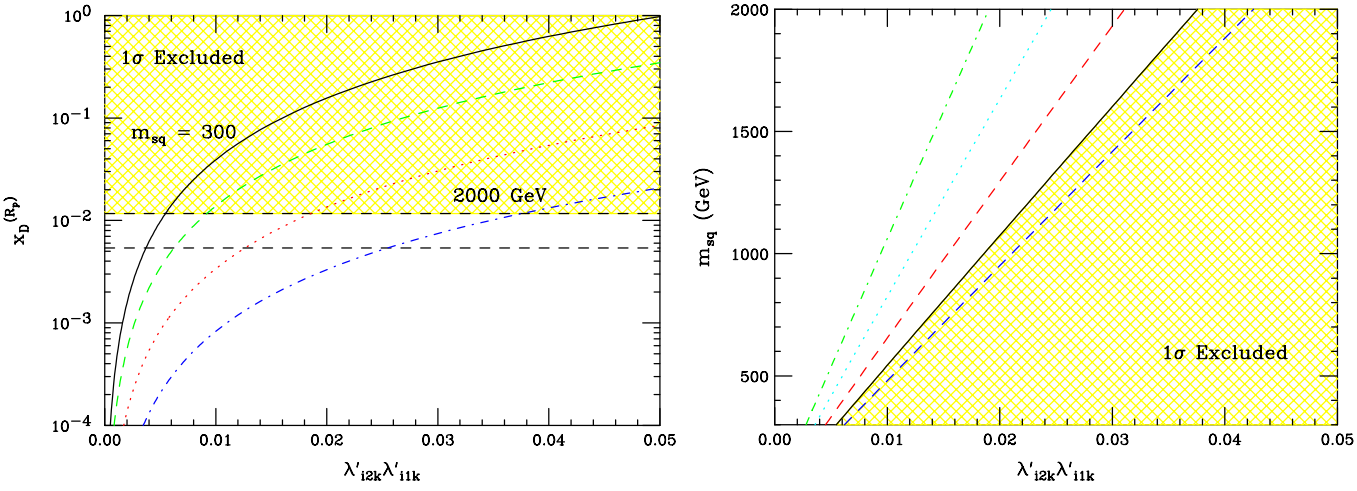

FIG. 27 (color online). Left: $x_{\rm D}$ in supersymmetry with R-parity violation as a function of the product of R-parity violating couplings $\tilde{\lambda}'_{i2k}\tilde{\lambda}'_{i1k}$ taking $m_{\tilde{d}_{R,k}} = m_{\tilde{\ell}_{L,i}}$, with $m_{\tilde{d}_{R,k}} = 300$, 500, 1000, and 2000 GeV corresponding to the solid, green (light gray) dashed, red (gray) dotted, and blue (dark gray) dash-dotted curves, respectively. The 1σ experimental bounds are as indicated, with the yellow shaded region depicting the region that is excluded. Right: 1σ excluded region in the R-parity violating coupling–squark mass plane, as well as possible future contours taking $x_{\rm D} < (15.0, 8.0, 5.0, 3.0) \times 10^{-3}$, corresponding to the blue (dark gray) dashed, red (gray) dashed, cyan (lightest gray) dotted, and green (light gray) dot-dashed curves, respectively.

effective Hamiltonian at the SUSY mass scale is

$$\mathcal{H}_{R_p} = \frac{1}{128\pi^2}(\tilde{\lambda}''_{1jk}\tilde{\lambda}''_{2jk})^2\left[\frac{1}{m^2_{\tilde{d}_{R,j}}} + \frac{1}{m^2_{\tilde{d}_{R,k}}}\right]Q_1. \quad (136)$$

Recall that symmetry dictates $j \neq k$. After completing the RGE evolution as described above, and assuming the charged $-1/3$ squarks are degenerate, we have

$$x_{\rm D}^{(R_p)} = \frac{f_D^2 B_D M_D}{96\pi^2 m^2_{\tilde{d}_R}\Gamma_D} r_1(m_c, m_{\tilde{d}_R})(\tilde{\lambda}''_{1jk}\tilde{\lambda}''_{2jk})^2. \quad (137)$$

This yields the constraint

$$\tilde{\lambda}''_{1jk}\tilde{\lambda}''_{2jk} \leq 0.085\sqrt{x_{\rm D}^{(\rm expt)}}\left(\frac{m_{\tilde{d}_R}}{500\ \text{GeV}}\right), \quad (138)$$

which mirrors that for the lepton number violating scenario.

D. Split supersymmetry

Lastly, for completeness, we briefly discuss the case of split supersymmetry [120]. This scenario postulates that supersymmetry breaking occurs at a very high scale, $m_S \gg 1000$ TeV. The scalar particles all acquire masses at this high scale, except for a single neutral Higgs boson, whose mass is either finely tuned or is preserved by some other mechanism. Split supersymmetry proponents argue that this tuning may, indeed, be present in nature, perhaps being related to the cosmological constant problem (which suffers an even greater degree of fine-tuning). The fermions in this theory, including the gauginos, are assumed to be protected by chiral symmetries and thus can have weak-scale masses. This feature preserves the gauge coupling unification found in supersymmetric models, and provides a natural dark matter candidate in the lightest neutralino. One important consequence of this scenario is that since all the scalar fields are present at only a very high scale, they decouple from physics at the TeV scale and their contributions to FCNC in the flavor sector are negligible. Since all contributions to D^0-$\bar{D}^0$ mixing in supersymmetry involve the internal exchange of scalar quarks, we expect these effects to essentially vanish in this scenario.

IX. CONCLUSIONS

The recent *BABAR* and Belle findings on D^0-$\bar{D}^0$ mixing have brought the long-standing search for this phenomenon to a successful conclusion, although much remains to be done. Compared to mixing in the other flavor sectors, the

TABLE VII. Approximate constraints on np models from D^0 mixing.

Model	Approximate constraint
Fourth generation (Fig. 2)	$\lvert V_{ub'}V_{cb'}\rvert \cdot m_{b'} < 0.5$ (GeV)
$Q = -1/3$ singlet quark (Fig. 4)	$s_2 \cdot m_S < 0.27$ (GeV)
$Q = +2/3$ singlet quark (Fig. 6)	$\lvert\lambda_{uc}\rvert < 2.4 \times 10^{-4}$
Little Higgs	Tree: see entry for $Q = +2/3$ singlet quark
	Box: region of parameter space can reach observed $x_{\rm D}$
Generic Z' (Fig. 7)	$M_{Z'}/C > 2.2 \times 10^3$ TeV
Family symmetries (Fig. 8)	$m_1/f > 1.2 \times 10^3$ TeV (with $m_1/m_2 = 0.5$)
Left-right symmetric (Fig. 9)	No constraint
Alternate left-right symmetric (Fig. 10)	$M_R > 1.2$ TeV ($m_{D_1} = 0.5$ TeV)
	$(\Delta m/m_{D_1})/M_R > 0.4$ TeV^{-1}
Vector leptoquark bosons (Fig. 11)	$M_{\rm VLQ} > 55(\lambda_{PP}/0.1)$ TeV
Flavor conserving two-Higgs doublet (Fig. 13)	No constraint
Flavor-changing neutral Higgs (Fig. 15)	$m_H/C > 2.4 \times 10^3$ TeV
FC neutral Higgs (Cheng-Sher ansatz) (Fig. 16)	$m_H/\lvert\Delta_{uc}\rvert > 600$ GeV
Scalar leptoquark bosons	See entry for RPV SUSY
Composite Higgs (Fig. 17)	$M > 100$ TeV
Universal extra dimensions	No constraint
Split fermion (Fig. 19)	$M/\lvert\Delta y\rvert > (6 \times 10^2$ GeV)
Warped geometries (Fig. 21)	$M_1 > 3.5$ TeV
Minimal supersymmetric standard (Fig. 23)	$\lvert(\delta^u_{12})_{\rm LR,RL}\rvert < 3.5 \times 10^{-2}$ for $\tilde{m} \sim 1$ TeV
	$\lvert(\delta^u_{12})_{\rm LL,RR}\rvert < 0.25$ for $\tilde{m} \sim 1$ TeV
Supersymmetric alignment	$\tilde{m} > 2$ TeV
Supersymmetry with RPV (Fig. 27)	$\lambda'_{12k}\lambda'_{11k}/m_{\tilde{d}_{R,k}} < 1.8 \times 10^{-3}/100$ GeV
Split supersymmetry	No constraint

observed value for charm [cf. Eq. (4)] is by far the smallest,

$$x_{\rm K} \simeq 0.47, \qquad x_{\rm B_d} \simeq 0.776, \qquad x_{\rm B_s} \simeq 26, \qquad x_{\rm D} \simeq 0.009. \tag{139}$$

In our opinion, the measured value for $x_{\rm D}$ is in accord with expectations of the standard model, with the proviso that hadronic (rather than quark-level) effects are the dominating influence (cf. Sec. III). We have argued that the relatively small magnitude of charm mixing could afford new physics an enhanced chance to compete successfully with the standard model. It should be kept in mind, however, that the current experimental value of $x_{\rm D}$ is relatively imprecise and that the SM theoretical determination contains hadronic uncertainties. These facts tend to frustrate the attempt to disentangle any potentially large NP contribution from that of the SM.

By design, our study of NP contributions has addressed a rather broad spectrum of possibilities. We have avoided playing favorites among the NP models contained in this paper, letting the results speak for themselves. Since the average reader is unlikely to be conversant with the details of such a large array of NP models, our presentation has been pedagogical in nature. We have tried to precede any formula for $x_{\rm D}^{\rm (NP)}$ with a summary of the relevant background.

A work such as this is meant to constrain the parameter spaces of NP models. The case of D^0 mixing is especially interesting because the intermediate states which generate the D^0-to-$\bar{D}^0$ transitions are distinct from those occurring in K, B_d, and B_s mixing. Typically, NP parameters will involve the masses of yet-to-be-discovered particles and their coupling strengths to ordinary matter. In some cases (left-right symmetric model, split supersymmetry, universal extra dimensions, flavor conserving two-Higgs doublets) we have found that the NP model will not generate a D^0-$\bar{D}^0$ signal at the observed level for any values of its parameters. More often, however, this is not the case and for some models (split fermions, flavor-changing neutral Higgs) the constraints can be strong.

The main quantitative conclusions for this work appear in the set of figures which appear throughout the paper. For convenience, we have compiled a summary of our results in Table VII, using the 1σ value $x_{\rm D} < 11.7 \times 10^{-3}$ to mark the boundary between allowed and excluded regions. Such a list is by nature approximate, and we refer the reader to the body of the paper for a more precise presentation of our results.

We recommend further experimental study of this subject on two fronts. First, of course, is the need to reduce error bars in the measured values of $y_{\rm D}$ and especially $x_{\rm D}$. Equally important is continuing the search for evidence of CP violation in mixing for the D^0 system. CP violation provides an interesting contrast with D^0 mixing because it provides an independent arena for competition between the SM and NP signals. There is especially room for improvement in the SM analysis of charm CP violation, and work on this is under way.

ACKNOWLEDGMENTS

The work of E. G. was supported in part by the U.S. National Science Foundation under Grant PHY–0555304, J. H. was supported by the U.S. Department of Energy under Contract DE-AC02-76SF00515, S. P. was supported by the U.S. Department of Energy under Contract DE-FG02-04ER41291 and A. P. was supported in part by the U.S. National Science Foundation PHY–0547794, and by the U.S. Department of Energy under Contract DE-FG02-96ER41005. J. H. would like to thank the theoretical physics group at Fermilab for their hospitality and E. G., J. H., and A. P. thank the High Energy Physics Group at the University of Hawaii for their hospitality while part of this work was performed. We would like to thank C. F. Berger, S. Chivukula, B. Dobrescu, J. Donoghue, K. C. Kong, B. Lillie, E. Lunghi, E. Simmons, and T. Tait for discussions related to this work and especially T. Browder, T. Rizzo, and X. Tata for a careful reading of the manuscript.

Note added.—After the work described in Sec. V was completed, we received Ref. [121] in which similar results were discussed.

APPENDIX: COLLECTED FORMULAS

Here, we collect the formulas used throughout the manuscript to compute the contributions to D^0-$\bar{D}^0$ mixing in the various new physics models.

Inami-Lim: (from Ref. [32])

The loop functions, first calculated by Inami-Lim, apply for several NP scenarios discussed in the text. For a contribution from two internal quarks of the same flavor in the box diagram, the loop function is

$$S(x) = x\left[\frac{1}{4} + \frac{9}{4(1-x)} - \frac{3}{2(1-x)^2}\right] - \frac{3x^3}{2(1-x)^3}\ln x, \tag{A1}$$

and for two quarks of different flavors,

$$S(x_i, x_j) = x_i x_j\left(\frac{\ln x_i}{x_i - x_j}\left[\frac{1}{4} + \frac{3}{2(1-x_i)} - \frac{3}{4(1-x_i)^2}\right] + (x_i \leftrightarrow x_j) - \frac{3}{4(1-x_i)(1-x_j)}\right). \tag{A2}$$

Little Higgs: (from Ref. [47])

The loop function for the case where the mirror fermions and heavy gauge bosons are exchanged in the box diagram is given by

$$F_{LH}(z_i, z_j) = \frac{1}{(1-z_i)(1-z_j)}\left(1 - \frac{7}{4}z_i z_j\right) + \frac{z_i^2 \log z_i)}{(z_i - z_j)(1-z_i)^2}\left(1 - 2z_j + \frac{z_i z_j}{4}\right) - \frac{z_j^2 \log z_j}{(z_i - z_j)(1-z_j)^2}\left(1 - 2z_i + \frac{z_i z_j}{4}\right)$$
$$- \frac{3}{4}\left(\frac{1}{(1-z_i)(1-z_j)} + \frac{z_i^2 \log z_i}{(z_i - z_j)(1-z_i)^2} - \frac{z_j^2 \log z_j}{(z_i - z_j)(1-z_j)^2}\right)$$
$$- \frac{3}{100a}\left(\frac{1}{(1-z_i')(1-z_j')} + \frac{z_i' z_i \log z_i'}{(z - I - z_j)(1-z_i')^2)} - \frac{z_j' z_j \log z_j'}{(z_i - z_j)(1-z_j')^2}\right)$$
$$- \frac{3}{10}\left(\frac{\log a}{(a-1)(1-z_i')(1-z_j')} + \frac{z_i^2 \log z_i}{(z_i - z_j)(1-z_i)(1-z_i')} - \frac{z_j^2 \log z_j}{(z_i - z_j)(1-z_j)(1-z_j')}\right), \quad \text{(A3)}$$

with

$$z_i = \frac{m_{M_i}^2}{M_{W_H}^2} \qquad z_i' = \frac{m_{M_i}^2}{M_{A_H}^2} \qquad a = \frac{5}{\tan^2\theta_w}. \quad \text{(A4)}$$

Left-right symmetric model:

The loop function with one W_L and one W_R boson being exchanged in the box diagram is

$$J(x, \beta) = \frac{x\beta \ln\beta}{(1-\beta)(1-\beta x)^2} - \frac{x + x\ln x}{(1-x)(1-\beta x)}. \quad \text{(A5)}$$

Charged Higgs: (from Ref. [73])

The loop functions with one $H^\pm$ and one SM W boson and with two $H^\pm$ being exchanged in the box diagram are

$$A_{\rm HH}(x, y) = \frac{x^2}{4}\left[\frac{x+y}{(x-y)^2} - \frac{2xy}{(x-y)^3}\ln\frac{x}{y}\right],$$
$$A_{\rm WH}(x, y) = 2x^2\left[\frac{1}{(x-y)(1-x)} + \frac{y\ln y}{(x-y)^2(1-y)} + \frac{(x^2-y)\ln x}{(x-y)^2(1-x)^2} - \frac{1}{4}\left(\frac{x}{(x-y)(1-x)} + \frac{y^2\ln y}{(1-y)(x-y)^2} + \frac{x(x+xy-2y)\ln x}{(x-y)^2(1-x)^2}\right)\right]. \quad \text{(A6)}$$

Cheng-Sher box:

The loop function in the Cheng-Sher ansatz with flavor-changing neutral Higgs bosons for a top-quark and neutral Higgs being exchanged in a box diagram is

$$F_{tH}(x) = \frac{-1}{1-x} - \frac{\ln x}{(1-x)^2} + \frac{x^2 - 4x + 3 + 2\ln x}{2(1-x)^3}. \quad \text{(A7)}$$

Universal extra dimensions:

The expressions for the case of Universal Extra Dimenions are given in full in Ref. [91].

Warped extra dimensions: (from Ref. [101])

The coupling of two zero-mode fermions to the nth gauge boson KK state, $A^{(n)}$, relative to the SM coupling strength is

$$C_{oon}^{f\bar{f}A} = \frac{g^{(n)}}{g_{\rm SM}} = \sqrt{2\pi k r_c}\left[\frac{1-2c_f}{1 - e^{-\pi k r_c(1-2c_f)}}\right] \times \int_{e^{-\pi k r_c}}^1 dz z^{(1-2c_f)} \frac{J_1(x_n z) + \alpha_n Y_1(x_n z)}{|J_1(x_n) + \alpha_n Y_1(x_n)|}, \quad \text{(A8)}$$

where the roots x_n for the gauge boson KK spectrum are given by

$$J_1(x_n) + x_n J_1'(x_n) + \alpha_n[Y_1(x_n) + x_n Y_1'(x_n)] = 0, \quad \text{(A9)}$$

and α_n is defined by

$$\alpha_n = \frac{J_1(m_n/k) + (m_n/k)J_1'(m_n/k)}{Y_1(m_n/k) + (m_n/k)Y_1'(m_n/k)}. \quad \text{(A10)}$$

Supersymmetry: (from Ref. [110])

The loop functions from squark and gluino exchange in a box diagram with squark mass insertions are given by

$$f_1(x) = \frac{6(1+3x)\ln x + x^3 - 9x^2 - 9x + 17}{6(1-x)^5},$$
$$f_2(x) = \frac{6x(1+x)\ln x - x^3 - 9x^2 + 9x + 1}{3(1-x)^5}. \quad \text{(A11)}$$

[1] A. Datta and D. Kumbhakar, Z. Phys. C **27**, 515 (1985); for an early work on NP contributions to D0 mixing, see A. Datta, Phys. Lett. B **154**, 287 (1985).

[2] B. Aubert *et al.* (*BABAR* Collaboration), Phys. Rev. Lett. **98**, 211802 (2007).

[3] M. Staric *et al.* (Belle Collaboration), Phys. Rev. Lett. **98**,

211803 (2007).
[4] K. Abe *et al.* (Belle Collaboration), arXiv:hep-ex/0704.1000.
[5] B. Aubert *et al.* (*BABAR* Collaboration), Phys. Rev. D **76**, 014018 (2007).
[6] G. Burdman and I. Shipsey, Annu. Rev. Nucl. Part. Sci. **53**, 431 (2003); G. Burdman, E. Golowich, J. L. Hewett, and S. Pakvasa, Phys. Rev. D **52**, 6383 (1995); J. L. Hewett, T. Takeuchi, and S. D. Thomas, in *Electroweak Symmetry Breaking and New Physics at the TeV Scale*, edited by T. Barklow *et al.* (World Scientific, Singapore, 1997), p. 549; S. Bianco, F. L. Fabbri, D. Benson, and I. Bigi, Riv. Nuovo Cimento **26N7**, 1 (2003); A. A. Petrov, Int. J. Mod. Phys. A **21**, 5686 (2006); arXiv:hep-ph/0311371; H. N. Nelson, arXiv:hep-ex/9908021.
[7] G. Burdman, E. Golowich, J. Hewett, and S. Pakvasa, Phys. Rev. D **66**, 014009 (2002).
[8] Heavy Flavor Averaging Group, http://www.slac.stanford.edu/xorg/hfag/charm/index.html; D. Asner, Workshop on Flavor in the Era of the LHC (CERN Report No. 3/26-28/07); B. Peterson, in Proceedings of the Charm 2007 Workshop, Cornell University, Ithaca, NY, 2007 (unpublished).
[9] E. Golowich and A. A. Petrov, Phys. Lett. B **625**, 53 (2005).
[10] A. F. Falk, Y. Nir, and A. A. Petrov, J. High Energy Phys. 12 (1999) 019.
[11] S. Bergmann, Y. Grossman, Z. Ligeti, Y. Nir, and A. A. Petrov, Phys. Lett. B **486**, 418 (2000).
[12] Y. Nir, J. High Energy Phys. 05 (2007) 102.
[13] W.-M. Yao *et al.* (Particle Data Group), J. Phys. G **33**, 1 (2006).
[14] E. Golowich, S. Pakvasa, and A. A. Petrov, Phys. Rev. Lett. **98**, 181801 (2007).
[15] M. Ciuchini, E. Franco, V. Lubicz, G. Martinelli, I. Scimemi, and L. Silvestrini, Nucl. Phys. **B523**, 501 (1998).
[16] R. Gupta, T. Bhattacharya, and S. R. Sharpe, Phys. Rev. D **55**, 4036 (1997).
[17] M. Artuso *et al.* (CLEO Collaboration), Phys. Rev. Lett. **95**, 251801 (2005).
[18] A. A. Petrov, Phys. Rev. D **56**, 1685 (1997); H. Georgi, Phys. Lett. B **297**, 353 (1992); T. Ohl *et al.*, Nucl. Phys. **B403**, 605 (1993).
[19] I. I. Y. Bigi and N. G. Uraltsev, Nucl. Phys. **B592**, 92 (2001).
[20] A. F. Falk, Y. Grossman, Z. Ligeti, and A. A. Petrov, Phys. Rev. D **65**, 054034 (2002).
[21] E. Golowich, A. A. Petrov, and G. Yeghiyan (unpublished).
[22] E. Golowich and A. A. Petrov, Phys. Lett. B **427**, 172 (1998).
[23] J. F. Donoghue, E. Golowich, B. R. Holstein, and J. Trampetic, Phys. Rev. D **33**, 179 (1986).
[24] L. Wolfenstein, Phys. Lett. B **164**, 170 (1985).
[25] F. Buccella, M. Lusignoli, G. Miele, A. Pugliese, and P. Santorelli, Phys. Rev. D **51**, 3478 (1995).
[26] A. F. Falk, Y. Grossman, Z. Ligeti, Y. Nir, and A. A. Petrov, Phys. Rev. D **69**, 114021 (2004).
[27] M. E. Peskin and T. Takeuchi, Phys. Rev. D **46**, 381 (1992).
[28] LEP Electroweak Working Group, Phys. Rep. **427**, 257 (2006).
[29] See, for example, H. J. He, N. Polonsky, and S. F. Su, Phys. Rev. D **64**, 053004 (2001).
[30] M. S. Chanowitz, M. A. Furman, and I. Hinchliffe, Phys. Lett. B **78**, 285 (1978); Nucl. Phys. **B153**, 402 (1979).
[31] K. S. Babu, X. G. He, X. Li, and S. Pakvasa, Phys. Lett. B **205**, 540 (1988).
[32] T. Inami and C. S. Lim, Prog. Theor. Phys. **65**, 297 (1981); **65**, 1772(E) (1981).
[33] G. C. Branco, P. A. Parada, and M. N. Rebelo, Phys. Rev. D **52**, 4217 (1995).
[34] F. Gursey, P. Ramond, and P. Sikivie, Phys. Lett. B **60**, 177 (1976).
[35] J. L. Hewett and T. G. Rizzo, Phys. Rep. **183**, 193 (1989).
[36] N. Arkani-Hamed, A. G. Cohen, E. Katz, and A. E. Nelson, J. High Energy Phys. 07 (2002) 034.
[37] N. Arkani-Hamed, A. G. Cohen, E. Katz, A. E. Nelson, T. Gregoire, and J. G. Wacker, J. High Energy Phys. 08 (2002) 021.
[38] J. D. Bjorken, S. Pakvasa, and S. F. Tuan, Phys. Rev. D **66**, 053008 (2002).
[39] S. L. Glashow and S. Weinberg, Phys. Rev. D **15**, 1958 (1977); E. Paschos, Phys. Rev. D **15**, 1966 (1977).
[40] N. Arkani-Hamed, A. G. Cohen, and H. Georgi, Phys. Lett. B **513**, 232 (2001). For a review, see, M. Perelstein, Prog. Part. Nucl. Phys. **58**, 247 (2007).
[41] J. Y. Lee, J. High Energy Phys. 12 (2004) 065.
[42] C. H. Chen, C. Q. Geng, and T. C. Yuan, arXiv:0704.0601 [Phys. Lett. B (to be published)].
[43] C. Csaki, J. Hubisz, G. D. Kribs, P. Meade, and J. Terning, Phys. Rev. D **67**, 115002 (2003); J. L. Hewett, F. J. Petriello, and T. G. Rizzo, J. High Energy Phys. 10 (2003) 062; M. C. Chen and S. Dawson, Phys. Rev. D **70**, 015003 (2004).
[44] C. Csaki, J. Hubisz, G. D. Kribs, P. Meade, and J. Terning, Phys. Rev. D **68**, 035009 (2003).
[45] H. C. Cheng and I. Low, J. High Energy Phys. 09 (2003) 051; 08 (2004) 061.
[46] C. T. Hill and R. J. Hill, Phys. Rev. D **75**, 115009 (2007); arXiv:0705.0697.
[47] J. Hubisz, S. J. Lee, and G. Paz, J. High Energy Phys. 06 (2006) 041; M. Blanke, A. J. Buras, A. Poschenrieder, C. Tarantino, S. Uhlig, and A. Weiler, J. High Energy Phys. 12 (2006) 003.
[48] M. Blanke, A. J. Buras, S. Recksiegel, C. Tarantino, and S. Uhlig, arXiv:hep-ph/0703254.
[49] See, for example, P. Savard, in Proceedings of the XXXIII International Conference on High Energy Physics, Moscow, Russia, 2006 (unpublished); T. Adams, ''Searches for New Phenomena with Lepton Final States at the Tevatron,'' in Rencontres de Moriond Electroweak Interactions and Unified Theories 2007, La Thuile, Italy, 2007 (unpublished); A. Abulencia *et al.* (CDF Collaboration), Phys. Rev. D **75**, 091101 (2007).
[50] T. G. Rizzo, arXiv:hep-ph/0610104.
[51] P. Langacker and M. Plumacher, Phys. Rev. D **62**, 013006 (2000).
[52] A. Arhrib, K. Cheung, C. W. Chiang, and T. C. Yuan, Phys. Rev. D **73**, 075015 (2006).

[53] F. Wilczek and A. Zee, Phys. Rev. Lett. **42**, 421 (1979).
[54] V. A. Monich, B. V. Struminsky, and G. G. Volkov, Phys. Lett. B **104**, 382 (1981) [JETP Lett. **34**, 213 (1981); Zh. Eksp. Teor. Fiz. **34**, 222 (1981); **34**, 222 (1981)].
[55] R. N. Mohapatra and J. C. Pati, Phys. Rev. D **11**, 2558 (1975). For a review and complete set of original references, see R. N. Mohapatra, *Unification and Supersymemtry* (Springer, New York, 1986).
[56] N. G. Deshpande, E. Keith, and T. G. Rizzo, Phys. Rev. Lett. **70**, 3189 (1993).
[57] K. Kiers, M. Assis, and A. A. Petrov, Phys. Rev. D **71**, 115015 (2005).
[58] G. Beall, M. Bander, and A. Soni, Phys. Rev. Lett. **48**, 848 (1982).
[59] D. Chang, R. N. Mohapatra, and M. K. Parida, Phys. Rev. D **30**, 1052 (1984).
[60] F. I. Olness and M. E. Ebel, Phys. Rev. D **30**, 1034 (1984); P. Langacker and S. Uma Sankar, Phys. Rev. D **40**, 1569 (1989).
[61] T. G. Rizzo, Phys. Rev. D **50**, 325 (1994).
[62] Z. Chacko, H. S. Goh, and R. Harnik, Phys. Rev. Lett. **96**, 231802 (2006); H. S. Goh and S. Su, Phys. Rev. D **75**, 075010 (2007).
[63] K. S. Babu, X. G. He, and E. Ma, Phys. Rev. D **36**, 878 (1987).
[64] E. Ma, Mod. Phys. Lett. A **3**, 319 (1988).
[65] W. Buchmuller, R. Ruckl, and D. Wyler, Phys. Lett. B **191**, 442 (1987); **448**, 320(E) (1999).
[66] G. G. Ross, *Grand Unified Theories* (Benjamin/Cummings Publishing Company, Menlo Park, CA, 1984).
[67] B. Abbott *et al.* (D0 Collaboration), Phys. Rev. Lett. **83**, 2896 (1999).
[68] S. Davidson, D. C. Bailey, and B. A. Campbell, Z. Phys. C **61**, 613 (1994).
[69] M. Leurer, Phys. Rev. D **50**, 536 (1994).
[70] For a summary, see, J. L. Hewett and T. G. Rizzo, Phys. Rev. D **56**, 5709 (1997).
[71] See, for example, B. Grinstein and M. B. Wise, Phys. Lett. B **201**, 274 (1988); T. G. Rizzo, Phys. Rev. D **38**, 820 (1988); J. L. Hewett, Phys. Rev. Lett. **70**, 1045 (1993); V. D. Barger, M. S. Berger, and R. J. N. Phillips, Phys. Rev. Lett. **70**, 1368 (1993).
[72] M. Misiak *et al.*, Phys. Rev. Lett. **98**, 022002 (2007).
[73] V. D. Barger, J. L. Hewett, and R. J. N. Phillips, Phys. Rev. D **41**, 3421 (1990).
[74] G. Isidori and A. Retico, J. High Energy Phys. 11 (2001) 001; A. J. Buras, P. H. Chankowski, J. Rosiek, and L. Slawianowska, Nucl. Phys. **B619**, 434 (2001).
[75] S. Pakvasa and H. Sugawara, Phys. Lett. B **73**, 61 (1978).
[76] T. P. Cheng and M. Sher, Phys. Rev. D **35**, 3484 (1987).
[77] L. J. Hall and S. Weinberg, Phys. Rev. D **48**, R979 (1993).
[78] D. Acosta *et al.* (CDF Collaboration), Phys. Rev. D **72**, 051107 (2005); A. Abulencia *et al.* (CDF Collaboration), Phys. Rev. D **73**, 051102 (2006).
[79] R. S. Chivukula, N. J. Evans, and E. H. Simmons, Phys. Rev. D **66**, 035008 (2002).
[80] N. Arkani-Hamed, A. G. Cohen, T. Gregoire, and J. G. Wacker, J. High Energy Phys. 08 (2002) 020.
[81] C. Csaki, C. Grojean, L. Pilo, and J. Terning, Phys. Rev. Lett. **92**, 101802 (2004).
[82] C. Csaki, C. Grojean, H. Murayama, L. Pilo, and J. Terning, Phys. Rev. D **69**, 055006 (2004).
[83] Y. Nomura, J. High Energy Phys. 11 (2003) 050; R. Barbieri, A. Pomarol, and R. Rattazzi, Phys. Lett. B **591**, 141 (2004); H. Davoudiasl, J. L. Hewett, B. Lillie, and T. G. Rizzo, Phys. Rev. D **70**, 015006 (2004); G. Burdman and Y. Nomura, Phys. Rev. D **69**, 115013 (2004); G. Cacciapaglia, C. Csaki, C. Grojean, and J. Terning, Phys. Rev. D **70**, 075014 (2004); H. Davoudiasl, J. L. Hewett, B. Lillie, and T. G. Rizzo, J. High Energy Phys. 05 (2004) 015.
[84] C. Csaki, C. Grojean, J. Hubisz, Y. Shirman, and J. Terning, Phys. Rev. D **70**, 015012 (2004).
[85] For a review of TeV-scale extra dimensional models and their experimental consequences, see, for example, J. Hewett and M. Spiropulu, Annu. Rev. Nucl. Part. Sci. **52**, 397 (2002); T. G. Rizzo, arXiv:hep-ph/0409309).
[86] I. Antoniadis, Phys. Lett. B **246**, 377 (1990); J. D. Lykken, Phys. Rev. D **54**, R3693 (1996); I. Antoniadis and M. Quiros, Phys. Lett. B **392**, 61 (1997).
[87] T. Appelquist, H. C. Cheng, and B. A. Dobrescu, Phys. Rev. D **64**, 035002 (2001).
[88] G. Servant and T. M. P. Tait, Nucl. Phys. **B650**, 391 (2003); New J. Phys. **4**, 99 (2002); H. C. Cheng, J. L. Feng, and K. T. Matchev, Phys. Rev. Lett. **89**, 211301 (2002).
[89] C. Lin, CDF thesis [FERMILAB Report No. FERMILAB-PUB-05-572-E].
[90] H. C. Cheng, K. T. Matchev, and M. Schmaltz, Phys. Rev. D **66**, 036005 (2002).
[91] A. J. Buras, M. Spranger, and A. Weiler, Nucl. Phys. **B660**, 225 (2003).
[92] N. Arkani-Hamed, Y. Grossman, and M. Schmaltz, Phys. Rev. D **61**, 115004 (2000).
[93] E. A. Mirabelli and M. Schmaltz, Phys. Rev. D **61**, 113011 (2000); G. C. Branco, A. de Gouvea, and M. N. Rebelo, Phys. Lett. B **506**, 115 (2001); D. E. Kaplan and T. M. P. Tait, J. High Energy Phys. 11 (2001) 051; Y. Grossman and G. Perez, Phys. Rev. D **67**, 015011 (2003); C. Biggio, F. Feruglio, I. Masina, and M. Perez-Victoria, Nucl. Phys. **B677**, 451 (2004); B. Lillie, J. High Energy Phys. 12 (2003) 030; Y. Grossman, R. Harnik, G. Perez, M. D. Schwartz, and Z. Surujon, Phys. Rev. D **71**, 056007 (2005); G. Perez and T. Volansky, Phys. Rev. D **72**, 103522 (2005).
[94] A. Delgado, A. Pomarol, and M. Quiros, J. High Energy Phys. 01 (2000) 030; W. F. Chang and J. N. Ng, J. High Energy Phys. 12 (2002) 077.
[95] B. Lillie and J. L. Hewett, Phys. Rev. D **68**, 116002 (2003).
[96] L. Randall and R. Sundrum, Phys. Rev. Lett. **83**, 3370 (1999).
[97] S. J. Huber and Q. Shafi, Phys. Lett. B **498**, 256 (2001); S. J. Huber, Nucl. Phys. **B666**, 269 (2003); G. Burdman, Phys. Lett. B **590**, 86 (2004); K. Agashe, G. Perez, and A. Soni, Phys. Rev. Lett. **93**, 201804 (2004).
[98] K. Agashe, G. Perez, and A. Soni, Phys. Rev. D **71**, 016002 (2005).
[99] H. Davoudiasl, J. L. Hewett, and T. G. Rizzo, Phys. Lett. B **473**, 43 (2000); A. Pomarol, Phys. Lett. B **486**, 153 (2000).

[100] Y. Grossman and M. Neubert, Phys. Lett. B **474**, 361 (2000); T. Gherghetta and A. Pomarol, Nucl. Phys. **B586**, 141 (2000).
[101] H. Davoudiasl, J. L. Hewett, and T. G. Rizzo, Phys. Rev. D **63**, 075004 (2001).
[102] S. J. Huber and Q. Shafi, Phys. Rev. D **63**, 045010 (2001); S. J. Huber, C. A. Lee, and Q. Shafi, Phys. Lett. B **531**, 112 (2002); C. Csaki, J. Erlich, and J. Terning, Phys. Rev. D **66**, 064021 (2002); J. L. Hewett, F. J. Petriello, and T. G. Rizzo, J. High Energy Phys. 09 (2002) 030.
[103] K. Agashe, A. Delgado, M. J. May, and R. Sundrum, J. High Energy Phys. 08 (2003) 050.
[104] K. Agashe, R. Contino, and A. Pomarol, Nucl. Phys. **B719**, 165 (2005); K. Agashe, A. E. Blechman, and F. Petriello, Phys. Rev. D **74**, 053011 (2006).
[105] H. Davoudiasl and A. Soni, arXiv:0705.0151.
[106] J. R. Ellis and D. V. Nanopoulos, Phys. Lett. B **110**, 44 (1982).
[107] H. P. Nilles, Phys. Rep. **110**, 1 (1984).
[108] H. Georgi, Phys. Lett. B **169**, 231 (1986).
[109] L. J. Hall, V. A. Kostelecky, and S. Raby, Nucl. Phys. **B267**, 415 (1986).
[110] For a comprehensive study of FCNC effects in supersymmetry see, S. Bertolini, F. Borzumati, A. Masiero, and G. Ridolfi, Nucl. Phys. **B353**, 591 (1991); F. Gabbiani, E. Gabrielli, A. Masiero, and L. Silvestrini, Nucl. Phys. **B477**, 321 (1996); I. I. Y. Bigi, F. Gabbiani, and A. Masiero, Z. Phys. C **48**, 633 (1990).
[111] M. Ciuchini, E. Franco, D. Guadagnoli, V. Lubicz, V. Porretti, and L. Silvestrini, J. High Energy Phys. 09 (2006) 013.
[112] J. A. Bagger, K. T. Matchev, and R. J. Zhang, Phys. Lett. B **412**, 77 (1997).
[113] M. Ciuchini, E. Franco, D. Guadagnoli, V. Lubicz, M. Pierini, V. Porretti, and L. Silvestrini, arXiv:hep-ph/0703204.
[114] Y. Nir and N. Seiberg, Phys. Lett. B **309**, 337 (1993).
[115] Y. Nir and G. Raz, Phys. Rev. D **66**, 035007 (2002).
[116] See, for example, L. E. Ibanez and G. G. Ross, Nucl. Phys. **B368**, 3 (1992).
[117] K. Agashe and M. Graesser, Phys. Rev. D **54**, 4445 (1996).
[118] For a recent summary of constraints on the R-parity violating couplings, see, H. Baer and X. Tata, *Weak Scale Supersymmetry: From Superfields to Scattering Events* (Cambridge University Press, Cambridge, U.K., 2006). See, also, B. C. Allanach, A. Dedes, and H. K. Dreiner, Phys. Rev. D **60**, 075014 (1999); G. Bhattacharyya, arXiv:hep-ph/9709395, and references therein.
[119] Q. He *et al.* (CLEO Collaboration), Phys. Rev. Lett. **95**, 221802 (2005).
[120] N. Arkani-Hamed and S. Dimopoulos, J. High Energy Phys. 06 (2005) 073; G. F. Giudice and A. Romanino, Nucl. Phys. **B699**, 65 (2004); **B706**, 65(E) (2005).
[121] X.-G. He and G. Valencia, arXiv:hep-ph/0703270.